

ISSN: 2220-9506 (Print)
ISSN: 2414-0473 (Online)

ПРИБОРЫ И МЕТОДЫ ИЗМЕРЕНИЙ

**DEVICES AND METHODS
OF MEASUREMENTS**

Том 11

№ 2

Vol. 11

2020

ПРИБОРЫ И МЕТОДЫ ИЗМЕРЕНИЙ

Научно-технический журнал

Основан в 2010 г.

Учредитель

Белорусский национальный технический университет

Выходит 4 раза в год

Журнал включен в базы данных:

Web of Science Core Collection (ESCI),
EBSCO, DOAJ, WorldCat, OpenAIRE, Google Scholar, РИНЦ,
ЭБС «Лань», НЭБ «КиберЛенинка», Соционет

Том 11

№ 2

2020

ГЛАВНЫЙ РЕДАКТОР

Гусев О.К., д.т.н., профессор, проректор Белорусского национального технического университета
(г. Минск, Беларусь)

ЗАМЕСТИТЕЛЬ ГЛАВНОГО РЕДАКТОРА

Маляревич А.М., член-корреспондент НАН Беларуси, д.ф.-м.н., профессор, проректор Белорусского национального технического университета (г. Минск, Беларусь)

РЕДАКЦИОННАЯ КОЛЛЕГИЯ

Алексеев В.А., д.т.н., профессор, ученый секретарь Ижевского государственного технического университета имени М.Т. Калашникова (г. Ижевск, Россия)

Анищик В.М., д.ф.-м.н., профессор, профессор кафедры физики твёрдого тела Белорусского государственного университета (г. Минск, Беларусь)

Бубулис А., д.т.н., профессор, главный научный сотрудник Научного центра мехатроники Каунасского технологического университета (г. Каунас, Литва)

Вайн А.А., д.т.н., профессор Тартуского университета (г. Тарту, Эстония)

Виба Я., д.т.н., профессор, директор Института механики Рижского технического университета (г. Рига, Латвия)

Гуттен М., д.т.н., заведующий кафедрой метрологии и прикладной электротехники Жилинского университета (г. Жилина, Словакия)

Дмитриев С.М., д.т.н., профессор, ректор Нижегородского государственного технического университета имени Р.Е. Алексеева (г. Нижний Новгород, Россия)

Дэнилак С., профессор Производственно-исследовательского центра Технологического института штата Джорджия (г. Атланта, США)

Жарин А.Л., д.т.н., профессор, профессор кафедры «Информационно-измерительная техника и технологии» Белорусского национального технического университета (г. Минск, Беларусь)

Жуковский П., д.т.н., профессор, заведующий кафедрой электрических аппаратов и техники высоких напряжений Люблинского технического университета (г. Люблин, Польша)

Колтунович Т.Н., д.т.н., профессор, Люблинский технический университет (г. Люблин, Польша)

Комаров Ф.Ф., член-корреспондент НАН Беларуси, д.ф.-м.н., профессор, заведующий лабораторией элионики Института прикладных физических проблем имени А.Н. Севченко Белорусского государственного университета (г. Минск, Беларусь)

Кулешов Н.В., д.ф.-м.н., профессор, заведующий кафедрой «Лазерная техника и технология» Белорусского национального технического университета (г. Минск, Беларусь)
Кучинский П.В., д.ф.-м.н., доцент, директор Института прикладных физических проблем имени А.Н. Севченко Белорусского государственного университета (г. Минск, Беларусь)
Кэмп А., профессор Института фотоники Страсклайдского университета (г. Глазго, Великобритания)
Матеос Х., к.ф.-м.н., доцент, университет Ровира и Вирхилий (г. Таррагона, Испания)
Пилипенко В.А., член-корреспондент НАН Беларуси, д.т.н., профессор, заместитель директора ГЦ «Белмикрoанализ» НТЦ «Белмикросистемы» ОАО «ИНТЕГРАЛ» – управляющая компания холдинга «ИНТЕГРАЛ» (г. Минск, Беларусь)
Плескачевский Ю.М., член-корреспондент НАН Беларуси, д.т.н., профессор, заведующий кафедрой «Микро- и нанотехника» Белорусского национального технического университета (г. Минск, Беларусь)
Погребняк А.Д., д.ф.-м.н., профессор, заведующий кафедрой нанoeлектроники Сумского государственного университета (г. Сумы, Украина)
Распопов В.Я., д.т.н., профессор, заведующий кафедрой «Приборы управления» Тульского государственного университета (г. Тула, Россия)
Тимчик Г.С., д.т.н., профессор, декан приборостроительного факультета, Национальный технический университет Украины «Киевский политехнический институт имени Игоря Сикорского» (г. Киев, Украина)
Це Ли, заместитель директора Северо-Восточного НИИ техники датчиков (г. Харбин, КНР)
Чижик С.А., академик НАН Беларуси, д.т.н., профессор, Первый заместитель Председателя Президиума НАН Беларуси (г. Минск, Беларусь)
Шкадаревич А.П., академик НАН Беларуси, д.ф.-м.н., профессор, директор НТЦ «ЛЭМТ» Белорусского оптико-механического объединения (г. Минск, Беларусь)
Юмашев К.В., д.ф.-м.н., профессор, заведующий кафедрой «Экспериментальная и теоретическая физика» Белорусского национального технического университета (г. Минск, Беларусь)

Издание зарегистрировано в Министерстве информации Республики Беларусь 25 июня 2010 г.

Регистрационный номер 1372

В соответствии с решением ВАК от 8 июля 2011 г. №13/1 журнал включен в Перечень научных изданий для опубликования результатов диссертационных исследований; научное направление: «Средства и методы измерений, контроля, диагностики и оценки качества объектов и процессов» (технические и физико-математические науки)

ISSN 2220-9506

Подписка осуществляется через почтовые отделения связи по «Каталогу газет и журналов Республики Беларусь».

Подписные индексы – 74835; 748352.

Ответственный секретарь редакции: Шахлевич Л.Н.

Редактор: Чабарова О.Л.

Набор и верстка выполнены в редакции журнала «Приборы и методы измерений».

Подписано в печать 10.06.2020. Формат бумаги 60×84 1/8. Бумага мелованная.

Гарнитура Times New Roman. Печать цифровая. Усл. печ. л. 9,30. Уч.-изд. л. 3,64. Тираж 120 экз.

Дата выхода в свет 18.06.2020. Заказ № 352.

Отпечатано в Белорусском национальном техническом университете. ЛП № 02330/74 от 03.03.2014. Пр. Независимости, 65, 220013, г. Минск

АДРЕС РЕДАКЦИИ:

Белорусский национальный технический университет
пр. Независимости, 65, 220013, г. Минск, Республика Беларусь,
тел.: +375 (17) 293 96 67, факс: +375 (17) 292 67 94
e-mail: pimi@bntu.by
<http://pimi.bntu.by>

DEVICES AND METHODS OF MEASUREMENTS

Scientific and Engineering Journal

Founded in 2010

Founder
Belarusian National Technical University

Issued four times a year

The Journal is included in the following databases:
Web of Science Core Collection (ESCI),
EBSCO, DOAJ, WorldCat, OpenAIRE, Google Scholar,
RISC, Lan, CyberLeninka, Socionet

Volume 11

№ 2

2020

EDITOR-IN-CHIEF

Oleg K. Gusev, *Doctor of Science (Engineering), Professor, Vice-Rector of Belarusian National Technical University (Minsk, Belarus)*

DEPUTY EDITOR-IN-CHIEF

Aliaksandr M. Malyarevich, *Corresponding Member of the National Academy of Sciences of Belarus, Doctor of Science (Physics and Mathematics), Professor, Vice-Rector of Belarusian National Technical University (Minsk, Belarus)*

EDITORIAL BOARD

Vladimir A. Alekseev, *Doctor of Science (Engineering), Professor, Scientific Secretary of M.T. Kalashnikov Izhevsk State Technical University (Izhevsk, Russia)*

Victor M. Anishchik, *Doctor of Science (Physics and Mathematics), Professor, Department of Solid State Physics, Belarusian State University (Minsk, Belarus)*

Algimantas Bubulis, *Doctor of Science (Engineering), Professor, Kaunas University of Technology (Kaunas, Lithuania)*

Arvid A. Vain, *Doctor of Science (Engineering), Professor, University of Tartu (Tartu, Estonia)*

Janis Viba, *Doctor of Science (Engineering), Professor, Director of Institute of Mechanics, Riga Technical University (Riga, Latvia)*

Miroslav Gutten, *Doctor of Science (Engineering), Head of Department of Metrology and Applied Electrical Engineering, University of Žilina (Žilina, Slovakia)*

Sergei M. Dmitriev, *Doctor of Science (Engineering), Professor, Rector of R.E. Alekseev Nizhny Novgorod State Technical University (Nizhny Novgorod, Russia)*

Steven Danyluk, *PhD, Professor, Production and Research Center, Georgia Institute of Technology (Atlanta, USA)*

Anatoly L. Zharin, *Doctor of Science (Engineering), Professor, Information and Measuring Technologies Department, Belarusian National Technical University (Minsk, Belarus)*

Paweł Żukowski, *Doctor of Science (Engineering), Professor, Head of Department of Electrical Devices and High Voltages Technology, Lublin University of Technology (Lublin, Poland)*

Tomasz N. Koltunowicz, *Doctor of Science (Engineering), Professor, Lublin University of Technology (Lublin, Poland)*

Fadey F. Komarov, *Corresponding Member of the National Academy of Sciences of Belarus, Doctor of Science (Physics and Mathematics), Professor, Head of the Elionics Laboratory, A.N. Sevchenko Institute of Applied Physical Problems, Belarusian State University (Minsk, Belarus)*

Nikolay V. Kuleshov, Doctor of Science (Physics and Mathematics), Professor, Head of Laser Equipment and Technology Department, Belarusian National Technical University (Minsk, Belarus)

Petr V. Kuchynski, Doctor of Science (Physics and Mathematics), Director of A.N. Sevchenko Institute of Applied Physical Problems, Belarusian State University (Minsk, Belarus)

Alan Kemp, PhD, Professor, Institute of Photonics, University of Strathclyde (Glasgow, United Kingdom)

Xavier Mateos, PhD, Associate Professor, Rovira i Virgili University (Tarragona, Spain)

Vladimir A. Pilipenko, Corresponding Member of the National Academy of Sciences of Belarus, Doctor of Science (Engineering), Professor, Deputy Director of the State Center «Belmicroanalysis», Branch of the Scientific-Technical Center «Belmicrosystems» of JSC «INTEGRAL» – «INTEGRAL» Holding Managing Company (Minsk, Belarus)

Yuriy M. Pleskachevsky, Corresponding Member of the National Academy of Sciences of Belarus, Doctor of Science (Engineering), Professor, Head of Micro- and Nanotechnics Department, Belarusian National Technical University (Minsk, Belarus)

Alexander D. Pogrebnjak, Doctor of Science (Physics and Mathematics), Professor, Head of Department of Nanoelectronic, Sumy State University (Sumy, Ukraine)

Vladimir Ya. Raspopov, Doctor of Science (Engineering), Professor, Head of Control Devices Department, Tula State University (Tula, Russia)

Gryhoriy S. Tymchyk, Doctor of Science (Engineering), Professor, Dean of the Faculty of Instrumentation Engineering, National Technical University of Ukraine «Igor Sikorsky Kyiv Polytechnic Institute» (Kyiv, Ukraine)

Tse Li, Deputy Director of Northeast Scientific Research Institute of Sensor Technology (Harbin, China)

Sergei A. Chizhik, Academician of National Academy of Sciences of Belarus, Professor, Doctor of Science (Engineering), the First Vice Chairman of the Presidium of the National Academy of Sciences of Belarus (Minsk, Belarus)

Alexey P. Shkadarevich, Academician of the National Academy of Sciences of Belarus, Doctor of Science (Physics and Mathematics), Professor, Director of the Scientific and Technical Center «LEMT» of the BelOMO (Minsk, Belarus)

Konstantin V. Yumashev, Doctor of Science (Physics and Mathematics), Professor, Head of Experimental and Theoretical Physics Department, Belarusian National Technical University (Minsk, Belarus)

ADDRESS:

Belarusian National Technical University
Nezavisimosty Ave., 65, Minsk 220013, Belarus
Tel.: +375 (17) 293 96 67, fax: +375 (17) 292 67 94
e-mail: pimi@bntu.by
<http://pimi.bntu.by>

СОДЕРЖАНИЕ

Средства измерений

<i>V.Ya. Halchenko, R.V. Trembovetskaya, V.V. Tychkov</i> Surface Eddy Current Probes: Excitation Systems of the Optimal Electromagnetic Field (Review).....	91
<i>M. Terekhova, S. Rudikov, A. Shumski, A. Shkadarevich</i> System for Assessing the Effectiveness of Temporary Blinding Devices	105
<i>V.A. Alekseev, S.I. Yuran, V.P. Usoltsev, D.N. Shulmin</i> System of Laser Monitoring of Water Pollution with Application of Relative Description of Signal Shape.....	114
<i>M.A. Starasotnikau</i> Assessment of Temperature Effects in Interior Orientation Parameters Calibration of Optoelectronic Devices.....	122

Методы измерений, контроля, диагностики

<i>M. Turek</i> Ionization Efficiency in a Hot Flat Disc-Shaped Cavity.....	132
<i>C. Kozak</i> Tests of Impregnation Speed of Electrotechnical Pressboard with Insulating Oil.....	140
<i>E.G. Zaitseva, M.V. Chernetsky, N.A. Shevel</i> About Possibility of Remote Diagnostics of the Respiratory System by Auscultation.....	148
<i>А.Ф. Сабитов, И.А. Сафина</i> Реализация спектрального метода определения динамических характеристик средств измерений.....	155

CONTENTS

Measuring Instruments

<i>V.Ya. Halchenko, R.V. Trembovetskaya, V.V. Tychkov</i>	
Surface Eddy Current Probes: Excitation Systems of the Optimal Electromagnetic Field (Review).....	91
<i>M. Terekhova, S. Rudikov, A. Shumski, A. Shkadarevich</i>	
System for Assessing the Effectiveness of Temporary Blinding Devices.....	105
<i>V.A. Alekseev, S.I. Yuran, V.P. Usoltsev, D.N. Shulmin</i>	
System of Laser Monitoring of Water Pollution with Application of Relative Description of Signal Shape.....	114
<i>M.A. Starasotnikau</i>	
Assessment of Temperature Effects in Interior Orientation Parameters Calibration of Optoelectronic Devices.....	122

Methods of Measurements, Monitoring, Diagnostics

<i>M. Turek</i>	
Ionization Efficiency in a Hot Flat Disc-Shaped Cavity.....	132
<i>C. Kozak</i>	
Tests of Impregnation Speed of Electrotechnical Pressboard with Insulating Oil.....	140
<i>E.G. Zaitseva, M.V. Chernetsky, N.A. Shevel</i>	
About Possibility of Remote Diagnostics of the Respiratory System by Auscultation.....	148
<i>A.F. Sabitov, I.A. Safina</i>	
Implementation of the Spectral Method for Determining of Measuring Instruments' Dynamic Characteristics	155

Surface Eddy Current Probes: Excitation Systems of the Optimal Electromagnetic Field (Review)

V.Ya. Halchenko, R.V. Trembovetskaya, V.V. Tychkov

*Cherkasy State Technological University,
Shevchenko blvd., 460, Cherkasy 18006, Ukraine*

Received 27.01.2020

Accepted for publication 05.05.2020

Abstract

Development of technical tools with improved metrological and operational characteristics is the actual problem of the eddy current testing. Ensuring the optimal distribution of the electromagnetic excitation field in the testing zone carries out confident detection of the defects and determination of their geometrical parameters by means of eddy current testing. The purpose of the work was to conduct an analysis of scientific and technical information in the field of eddy current testing to study of the use of electromagnetic excitation fields with a priori specified properties, as well as to generalize and systematize the accumulated experience and approaches to conduct theoretical research in this direction.

A review of publications in the field of non-destructive electromagnetic testing devoted to the improvement of the excitation systems of eddy current flaw probes was carried out. The authors considered approaches in which a uniform distribution of the electromagnetic field on the control object surface was achieved by linear and non-linear optimal synthesis of excitation systems, provided the immobility of the probe relative to the testing object. Analysis of eddy current probe designs with a homogeneous excitation field created by circular, rectangular tangential and normal coils, as well as by creating a rotational excitation field was carried out. The authors studied designs of the excitation coils of probes with fields of complex configuration characterized by the original fractal geometry which can increase the probability of identifying defects that were not amenable to detection by classical probes.

Studies that suggested the formation of optimal configuration fields in a given area using magnetic cores, field concentrators made of conductive materials and specially shaped screens were analyzed. The authors studied approaches to the implementation of the optimal synthesis of excitation systems of probes with uniform sensitivity in the testing zone using surrogate optimization for cases of moving testing objects taking into account the speed effect.

The experience, as well as the results of theoretical studies devoted to the problem of designing eddy current probes with uniform sensitivity in the testing zone due to the uniform density distribution of the induced currents flowing in the object were generalized and systematized. As a result, the classification of probes on a number of features that characterize the excitation systems was proposed.

Keywords: eddy current probe, optimal electromagnetic excitation field, uniform eddy current density distribution, uniform sensitivity.

DOI: 10.21122/2220-9506-2020-11-2-91-104

Адрес для переписки:

В.В. Тычков
Черкасский государственный технологический университет,
б-р Шевченко, 460, г. Черкассы 18006, Украина
e-mail: v.tychkov@chdtu.edu.ua

Address for correspondence:

V.V. Tychkov
Cherkasy State Technological University,
Shevchenko blvd., 460, Cherkasy 18006, Ukraine
e-mail: v.tychkov@chdtu.edu.ua

Для цитирования:

V.Ya. Halchenko, R.V. Trembovetskaya, V.V. Tychkov.
Surface Eddy Current Probes: Excitation Systems
of the Optimal Electromagnetic Field (Review)
Приборы и методы измерений.
2020. – Т. 11, № 2. – С. 91–104.
DOI: 10.21122/2220-9506-2020-11-2-91-104

For citation:

V.Ya. Halchenko, R.V. Trembovetskaya, V.V. Tychkov.
Surface Eddy Current Probes: Excitation Systems
of the Optimal Electromagnetic Field (Review)
Devices and Methods of Measurements.
2020, vol. 11, no. 2, pp. 91–104.
DOI: 10.21122/2220-9506-2020-11-2-91-104

Накладные вихретоковые преобразователи: системы возбуждения оптимального электромагнитного поля (обзор)

В.Я. Гальченко, Р.В. Трёмбовецкая, В.В. Тычков

Черкасский государственный технологический университет,
б-р Шевченко, 460, г. Черкассы 18006, Украина

Поступила 27.01.2020

Принята к печати 05.05.2020

Актуальной задачей вихретокового контроля является разработка технических средств с улучшенными метрологическими и эксплуатационными характеристиками. Уверенное обнаружение дефектов и определение их геометрических параметров средствами вихретокового контроля осуществляется при обеспечении оптимального распределения электромагнитного поля возбуждения в зоне контроля. Цель работы заключалась в проведении анализа научно-технической информации в области вихретокового контроля для изучения сведений об использовании электромагнитных полей возбуждения с априори заданными свойствами, а также обобщения, систематизации накопленного опыта и подходов к проведению теоретических исследований в данном направлении.

Проведён обзор публикаций в области неразрушающего электромагнитного контроля, посвящённых совершенствованию систем возбуждения преобразователей вихретоковых дефектоскопов. Рассмотрены подходы, в которых однородное распределение электромагнитного поля на поверхности объекта контроля достигается линейным и нелинейным оптимальным синтезом систем возбуждения при условии неподвижности преобразователя относительно объекта контроля. Проведён анализ конструкций вихретоковых преобразователей с однородным полем возбуждения, созданным круговыми, прямоугольными тангенциальными и нормальными катушками, а также за счёт создания вращательного поля возбуждения. Изучались конструкции катушек возбуждения преобразователей с полями сложной конфигурации, характеризующиеся оригинальной фрактальной геометрией, которые позволяют увеличить вероятность выявления дефектов, не поддающихся обнаружению классическими преобразователями.

Также проанализированы исследования, в которых предлагается формирование полей оптимальной конфигурации в заданной зоне с применением магнитопроводов, концентраторов поля из проводящих материалов и экранов специальной формы. Изучались подходы к реализации оптимального синтеза систем возбуждения преобразователей с равномерной чувствительностью в зоне контроля с использованием суррогатной оптимизации для случаев движущихся объектов контроля с учётом эффекта скорости.

Обобщён и систематизирован опыт, а также результаты теоретических исследований, посвящённых проблеме проектирования вихретоковых преобразователей с равномерной чувствительностью в зоне контроля, обусловленной однородным распределением плотности индуцированных токов, протекающих в объекте. Предложена классификация преобразователей по ряду признаков, характеризующих их системы возбуждения.

Ключевые слова: вихретоковый преобразователь, оптимальное электромагнитное поле возбуждения, однородное распределение плотности вихревых токов, равномерная чувствительность.

DOI: 10.21122/2220-9506-2020-11-2-91-104

Адрес для переписки:

В.В. Тычков

Черкасский государственный технологический университет,
б-р Шевченко, 460, г. Черкассы 18006, Украина
e-mail: v.tychkov@chdtu.edu.ua

Address for correspondence:

V.V. Tychkov

Cherkasy State Technological University,
Shevchenko blvd., 460, Cherkasy 18006, Ukraine
e-mail: v.tychkov@chdtu.edu.ua

Для цитирования:

V.Ya. Halchenko, R.V. Trembovetskaya, V.V. Tychkov.

Surface Eddy Current Probes: Excitation Systems
of the Optimal Electromagnetic Field (Review)

Приборы и методы измерений.

2020. – Т. 11, № 2. – С. 91–104.

DOI: 10.21122/2220-9506-2020-11-2-91-104

For citation:

V.Ya. Halchenko, R.V. Trembovetskaya, V.V. Tychkov.

Surface Eddy Current Probes: Excitation Systems
of the Optimal Electromagnetic Field (Review)

Devices and Methods of Measurements.

2020, vol. 11, no. 2, pp. 91–104.

DOI: 10.21122/2220-9506-2020-11-2-91-104

Introduction

The problem of detecting defects by the eddy current method is quite complex. A comprehensive solution of the problem involves not only the detection, but also the determination of the defects shape, allowable geometric dimensions, and possible local structural deviations of the material. Using of the eddy current probes (ECP) with improved metrological and operational characteristics can solve this problem. The classical design of ECP [1] has typically an uneven sensitivity (Figure 1a) due to the inhomogeneous distribution of the eddy current density (ECD) which impedes the ability to effectively solve the problem of flaw detection and defectometry. The ECD distribution in the testing object (TO) volume depends on a combination of parameters, for example, the shape, geometrical and electrophysical characteristics of the TO, the mutual position of the excitation system (ES) relative to the TO, etc. It is the inhomogeneous ECD distribution limits the sensitivity of the

surface eddy current probe (SECP) to the testing defects, and accordingly, a priori determines the mutual position of the ES relative to the controlled surface. Moreover, this disadvantage manifests itself even more in the case when TO and the ECP move relative to each other, since in this case the transfer current additionally affects the distribution of the ECD, which manifests itself in the so-called speed effect. In order to reliably detect the defects and determine their geometrical parameters by eddy current testing, it is important to ensure the optimal electromagnetic field (EMF) of excitation in the testing zone (Figure 1a).

As optimal field, we understand such a field that has a priori given configuration, providing uniform or close to it sensitivity. For example, the U-shaped form of the EMF tension distribution, which is localized and maximally concentrated in the testing zone and has a zero value outside it. Possible options for generating a field are its given distribution both on the surface of the TO and at a certain depth of the TO (Figure 1b).

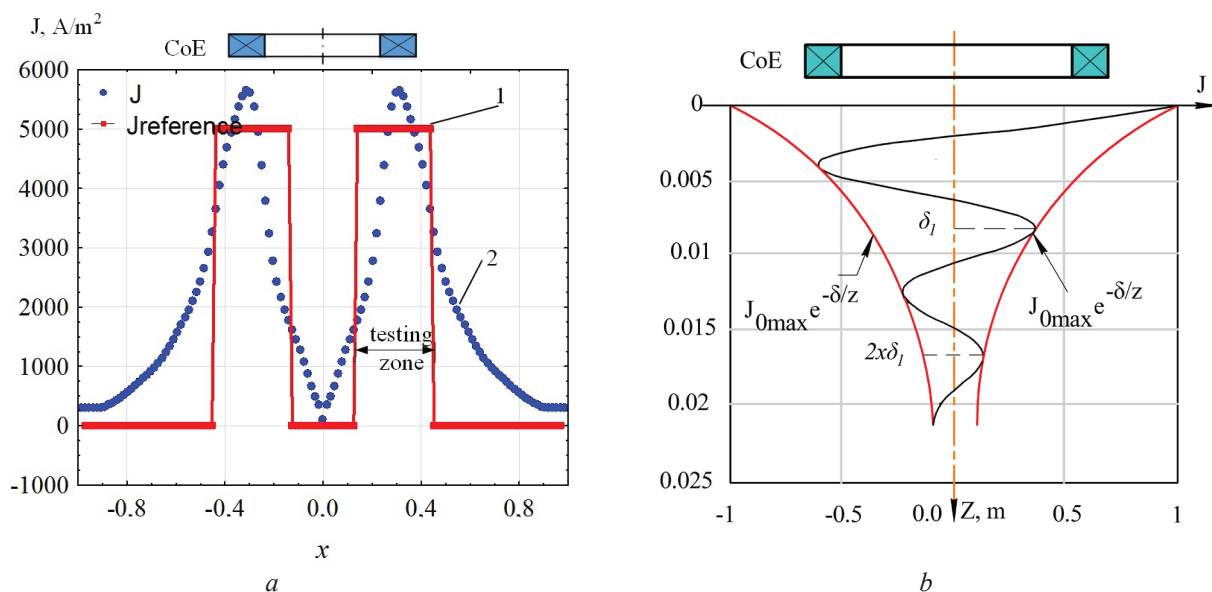


Figure 1 – The eddy current density distribution of a circular non-coaxial eddy current probe on the surface (a) and in depth (b) of the testing object: 1 – desired uniform distribution; 2 – characteristic distribution of the classic design

The purpose of the work was to analyze scientific and technical information in the field of eddy current testing to study the use of excitation EMF with a priori specified properties, as well as to generalize, systematize the experience and approaches to conducting theoretical research in this direction.

The solution of the problem

The developed fundamentals of the synthesis theory [2–9] allow implementing new technical solutions in constructions that positively affect the field of excitation of ECP. Different works with various objectives realized the idea of purposefully changing the probing properties of the generated EMF.

So, the solution of the problem of reducing the interaction zone of the ECP field with the product and reducing the magnetic fluxes of scattering [10] increased the noise immunity and selectivity. The creation of an EMF with a predetermined distribution topology improved the selectivity and sensitivity of ECP [1–9, 11–30]. Moreover, the improvement of both parts of the ECP, namely, the ES and the field detector, allowed achieving the desired results.

Summarizing the study of the problem of the formation of the optimal excitation EMF, the authors proposed the variant of the ECP classification

by this attribute (Figure 2). Firstly, authors dwelled on the problem of creating the EMF with specified properties for the case of the static TO. The case of generating a uniform EMF distribution is of particular note. The specified properties of EMF that changed in accordance with predetermined dependences are most often obtained in two ways. The first one is the creation of an uneven distribution of the excitation current in the ECP generator coil [2–4]. The second one is the using the specific geometry of the excitation winding of the ECP [8, 12–13].

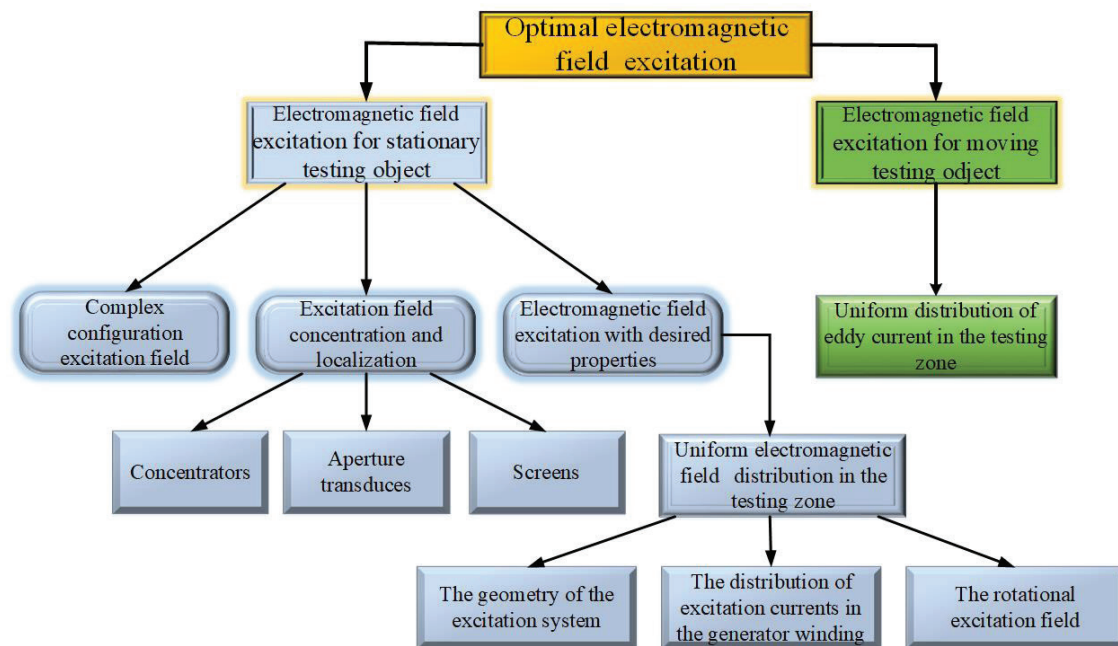


Figure 2 – A generalized classification scheme for eddy current probe with an optimal electromagnetic excitation field

The works [2–4, 8–28] studied this problem. The development of modern computer technology, new opportunities for using more advanced mathematical apparatus and software contribute to the intensification of the efforts of researchers in this direction.

Therefore, in [2–4] the main idea was the obtaining the desired field structure in the control zone by means of linear ECP synthesis. The works considered the problem of synthesizing the ECP excitation fields with given output characteristics from the spatial coordinates of the local inhomogeneities of the controlled products. The resulting structure of the plane-parallel EMF implemented the invariance of the probe output signal to the spatial position of the local defect. After determining the structure of the EMF, the problem of synthesizing the sectional windings of ECP was carried out, realizing the

necessary distribution of the field in the control zone. The resulting multisectional ES had $N = 8$ excitation windings with a normalized distance between the windings. The winding connection scheme, namely counter-coordinated inclusion of sections along the field and the number of turns W of each winding was determined. Experimental and theoretical data showed the possibility of practical implementation of a complex configuration of the excitation field, when its intensity increases with distance from the source. However, such a distribution can only be created in a limited area, beyond which the field decreases, approaching zero. The disadvantage of linear synthesis [3, 4] is the receiving the real values of the current density in the coil sections, which greatly complicates the practical implementation of the ECP, as well as the need to preset the number of sections, the distance between them and their geometrical

dimensions. The synthesis issue remains unresolved when the required field structure is achieved by the ECP parameters nonlinearly included in the formula for calculating the excitation field.

In [5], the authors proposed a solution to the problem of nonlinear optimal synthesis, namely, determining the location of the windings of the sections of the excitation coils (CoE) in space and their geometrical dimensions at a fixed density of the excitation current in the generator coil. Several options were considered. The first option – in accordance with the well-known EMF intensity distribution function, the radii of the sections of the generator coil were determined, providing such a distribution with fixed z -coordinates of the sections and magnetomotive forces (MMF) (Figure 3a). The second option involved determining the z -coordinates of the sections at fixed radii and MMF (Figure 3b). To search for the extremum of a nonlinear optimization problem, an algorithm that is suitable for multidimensional “ravine” objective functions was applied.

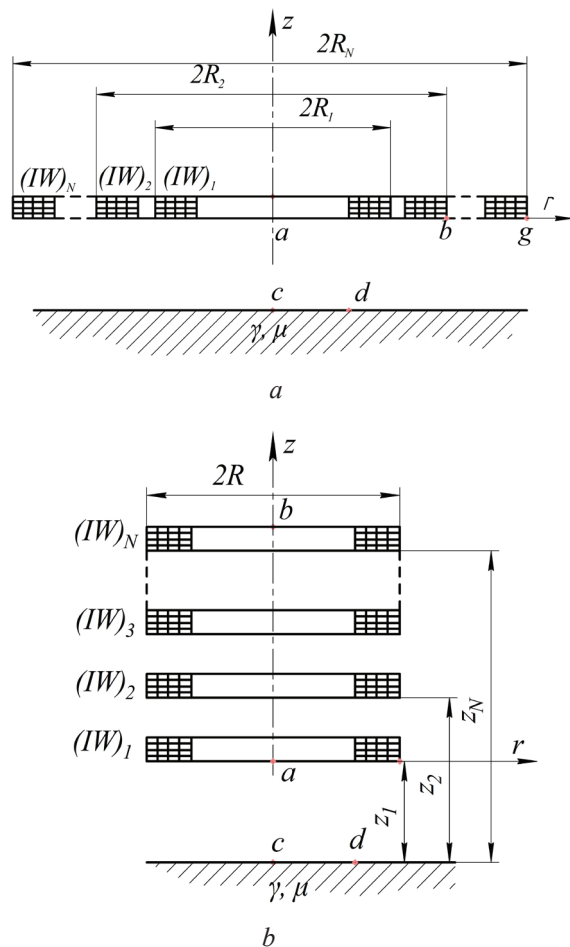


Figure 3 – Nonlinear synthesis of eddy current probe coil: $a - z_i, (IW)_i = \text{const}, R_i - \text{var}, i = 1, \dots, N$; $b - R_i, (IW)_i = \text{const}, z_i - \text{var}, i = 1, \dots, N$

The considered approaches [2–5] are parametric optimization methods and the problem of choosing the structure of the ES ECP, i. e. number of sections in the generator coil is still unresolved. The reason for this is the subjective difficulties in choosing a structure, which can lead to an unsuccessful version in the sense of reproducing a given distribution or to an excessively complex structure. It is impossible to correct the error of the choice of structure by means of parametric optimization.

One of the ways to overcome these difficulties was proposed in [6], namely, the method of structurally parametric synthesis of the source of excitation EMF. The purpose of the synthesis of such magnetic ECP system, along with the search for the optimal values of the section parameters, is to obtain the simplest ES design, which ensures a given distribution of the excitation field in space. The paper considers the probing field of the ECP without taking into account the TO reaction. Structural synthesis is performed by the stochastic optimization method, namely, using the genetic algorithm. The obtained values of the average relative deviations indicate a significant improvement in the quality of the generated field of the synthesized magnetic system compared to the results of [4]. A significant simplification of the ES structure in terms of the number of sections and a decrease in its length was achieved, and the number of turns in the sections was reduced by two orders of magnitude at the same current values. That is, a higher accuracy of reproducing a given field distribution was achieved, and at the same time, technical indicators of the system design was significantly improved.

A large number of scientific reports are devoted to various designs of ECP with a uniform field of excitation created by rectangular, tangential or other types of coils and, as a result, to the problems of increasing sensitivity to detection of defects [13–23, 30]. It is assumed that a uniform configuration of the EMF intensity in the control zone is generated and the corresponding excitation of the uniform distribution of the ECD in a static TO is caused by it.

In particular, in [14], several such configurational structures of unidirectional exciting and measuring coils were analyzed, as well as varieties of ECP designs that create rotational eddy currents (REC). A tangential rectangular

CoE with an alternating current source generates a magnetic field inducing eddy current (EC) on the surface of the test sample (Figure 4a). EC flows in straight lines perpendicular to the magnetic field (Figure 4b). The following structures of similar ES are considered: a tangential rectangular CoE and a circular measuring one (Figure 5a);

both coils are tangential and rectangular (Figure 5b); a system of tangential coils, one of which is exciting and two are measuring (Figure 5c); a tangential rectangular CoE and a detector, which is a magnetoresistive GMR sensor (Figure 5d); a rectangular CoE and two semicircular flat detector coils (Figure 5e).

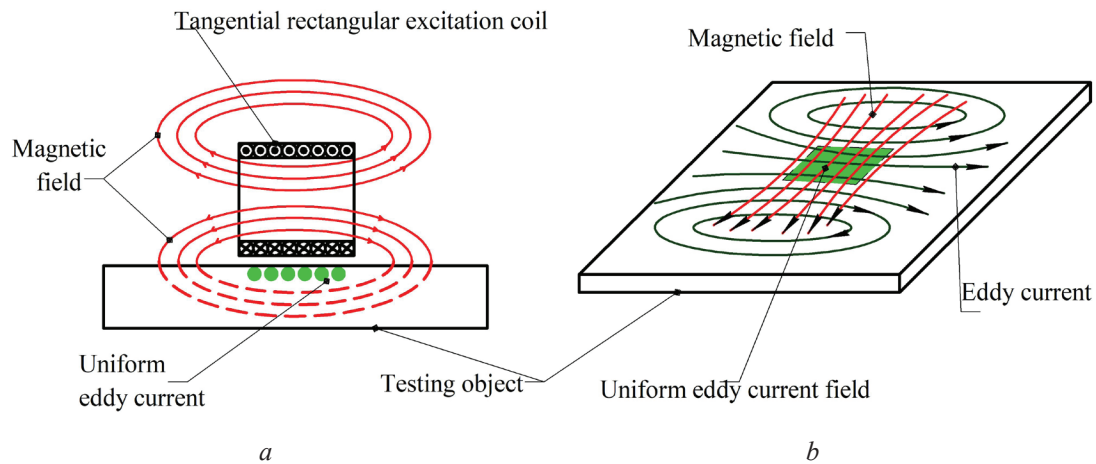


Figure 4 – The principle of generating a uniform eddy current density [14]: *a* – circulation of the magnetic field of the coil and the eddy current created by it; *b* – excitation zone of a uniform eddy current on the surface

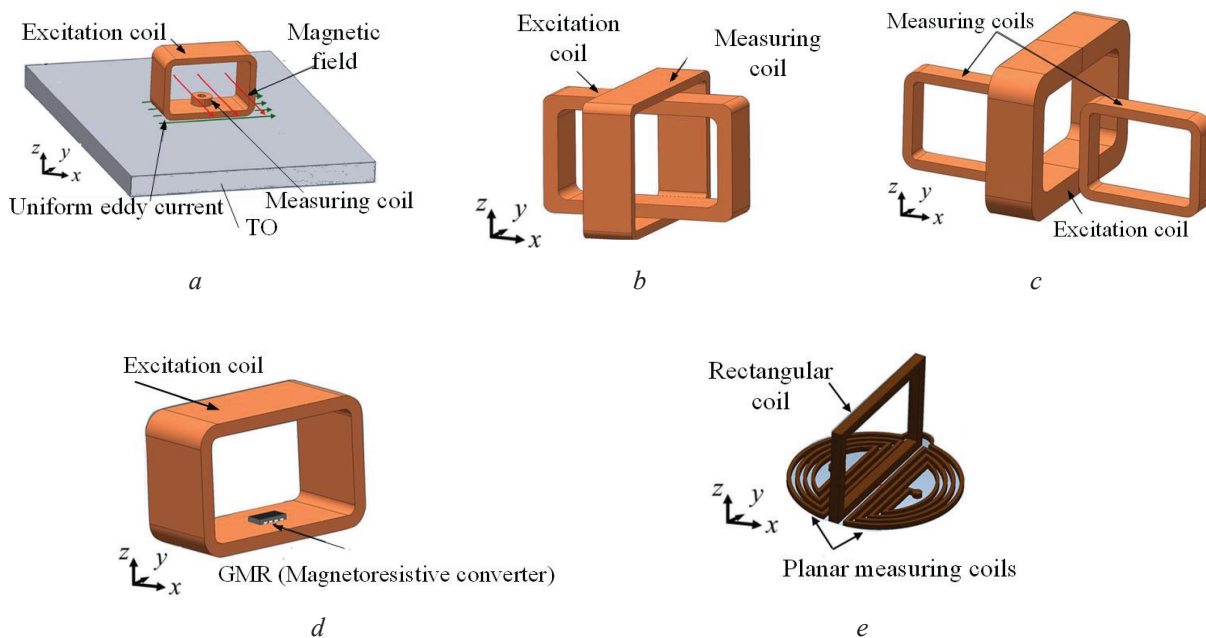


Figure 5 – Structures of the unidirectional exciting and measuring coils [14]

All presented designs create EC in only one direction. In addition, the paper did not address the choice of the ratio of the geometrical dimensions of CoE, which allow adjusting the width of the

testing zone. The implementation of a uniform EMF distribution with the help of a rectangular CoE was considered in [23], namely, its location when the winding faces the TO surface (Figure 6).

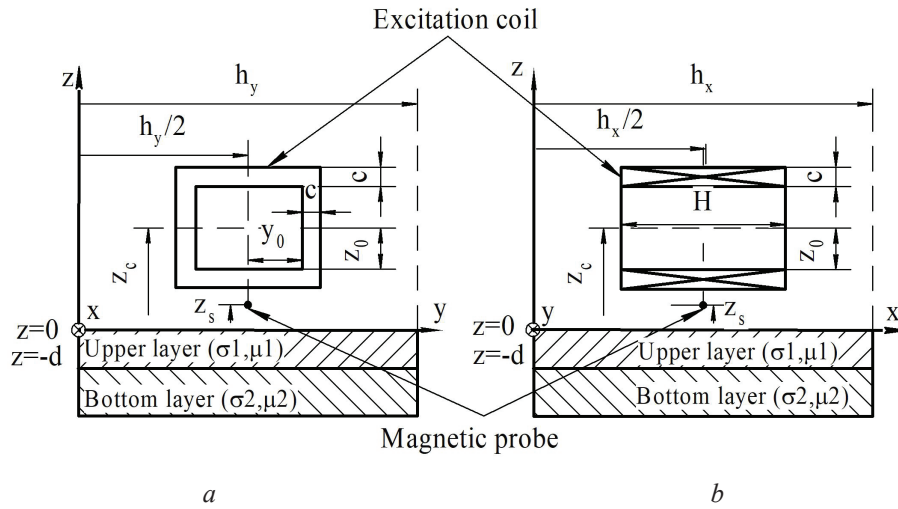


Figure 6 – The configuration of the eddy current probe located above the conductive testing object [23]: *a* – view in the *x*-direction; *b* – view in the *y*-direction

The uniformity of the EC and EMF configurations was investigated by modelling using the ETREE (Extended Truncated Region Eigenfunction Expansion)

method. The calculated distribution of ECD on the plate surface and the EMF components above the plate surface are shown in Figures 7, 8 respectively.

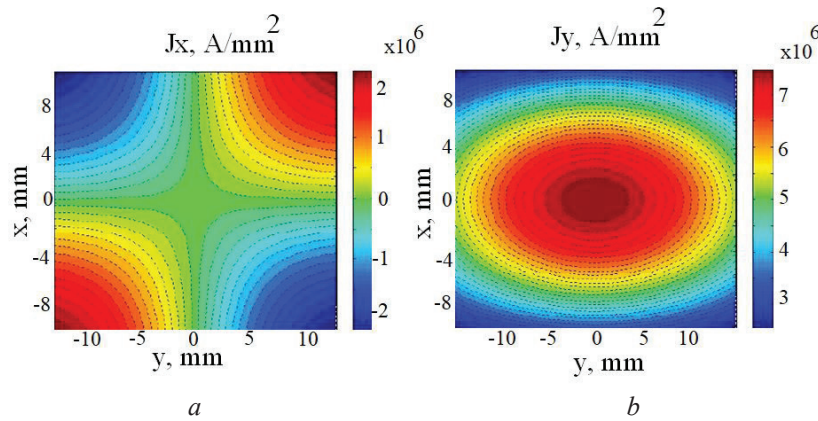


Figure 7 – The calculated eddy current density on the plate surface [23]: *a* – *x*-component; *b* – *y*-component

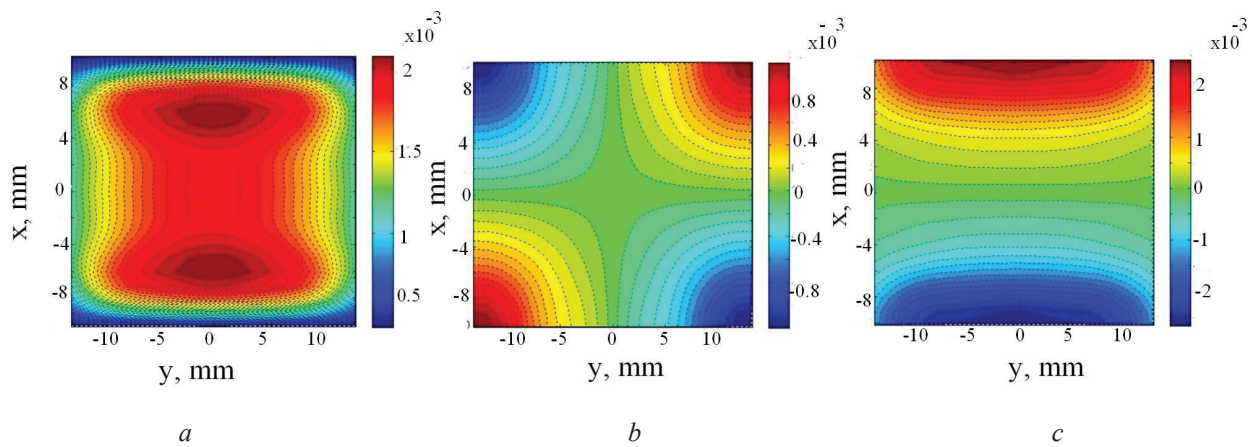


Figure 8 – The calculated values of the components of the electromagnetic field above the investigated surface [23]: *a* – B_x ; *b* – B_y ; *c* – B_z

The resulting degree of homogeneity is 20 ppm for EC and 5.9 ppm for induction of EMF. This indicates that in the control zone the EC on the plate surface and the total EMF above the upper surface of the plate are homogeneous, and this contributes to a highly sensitive detection of defects. But such a high degree of uniformity of both the field and the EC is provided only in the zone of small geometrical dimensions (2×2) mm.

In [13] the formation of a uniform distribution of the EC within the sensor testing zone was studied by determining the profile of the external radius of the CoE to obtain a uniform sensitivity in the scanning area. The resulting design of the sensor allows inducing a given distribution of the ECD inside the conductive cylinder (Figure 9).

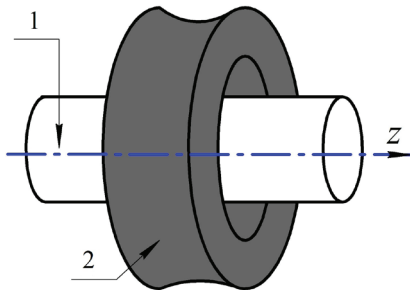


Figure 9 – Sensor design [13]: 1 – cylindrical sample under investigation; 2 – excitation coil

The design problem was solved by minimizing the deviation quadratic function between the desired and calculated values of the vector potential at the control points inside the study area:

$$F(p) = \frac{1}{2} \cdot \sum_{k=1}^K \left| A^e(r_k, z_k) - A^d(r_k, z_k) \right|^2.$$

The Newton optimization algorithm was used to minimize the objective functional. The problem of increasing the sensitivity to defects regardless of their orientation due to the creation of a rotational field of excitation is discussed in [12, 14, 24, 25]. One of these types of ECP with a uniform field is the creation of a variant with REC, for the generation of which two currents are used in the ES with a phase difference of 90°. For example, a Hoshi rotary sensor has two tangential rectangular CoE1 and CoE2 and one flat circular measuring coil (Figure 10) [14].

The proposed sensor can detect defects regardless of their direction on the surface of the investigated TO.

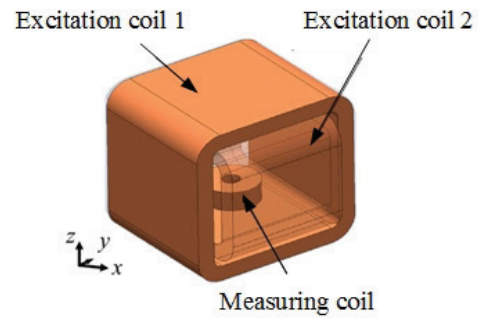


Figure 10 – Hoshi Rotary Sensor [14]

To develop the idea a double rotational sensor was proposed in [14], which has four tangential rectangular CoEs and four-pole quarter-circular detector coils (Figure 11), operating on the same principle. Using current and phase control, it is possible to identify defects as reliably as possible without changing the position of the ECP.

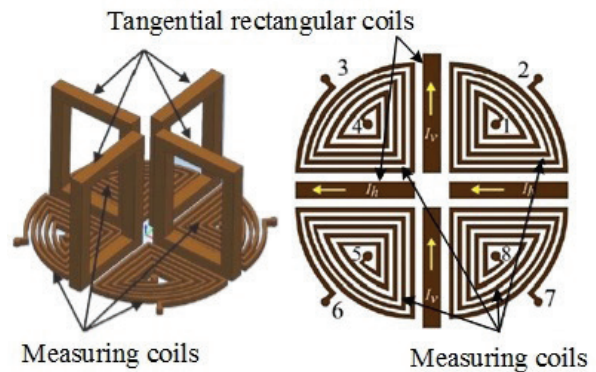


Figure 11 – Double rotary sensor [14]

The work [12] considered a variant of generating a rotational field of excitation, implemented by a system of orthogonal coils. First, an optimized ECD distribution was calculated, which provides uniform sensitivity to defects regardless of their spatial orientation, and then a coil design with an uneven winding density was created (Figure 12).

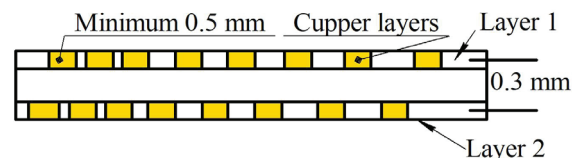
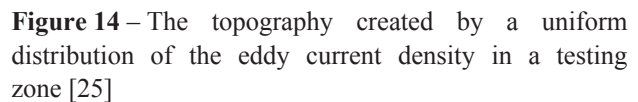
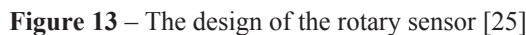


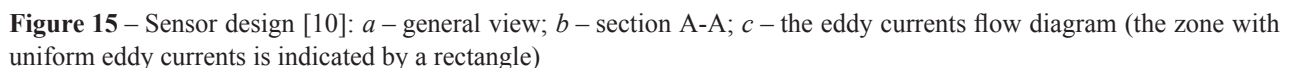
Figure 12 – The design of the rotary sensor multilayer coil [12]

Each coil consists of at least two layers. To obtain a higher degree of distribution continuity than in the case of a single-layer coil, in the 2-layer case, the copper layer of one of the coils was displaced, closing the air gaps. A feature of the optimized

The obtained zone of uniform distribution of ECD is quite large (Figure 14), therefore, the detection of defects by such an ECP is more efficient.



In the area under the coil (Figure 15c), the ECs merge and form homogeneous ECs with an intensity of almost two times greater than from a single coil.



Moreover, the maximum amplitude of the ECD is approximately 1.9 times greater than other peaks.

The disadvantage of such ETP, as well as for previous designs (Figure 5), is the formation of unidirectional EC, which requires a change in its orientation in space to identify defects with an unknown a priori orientation.

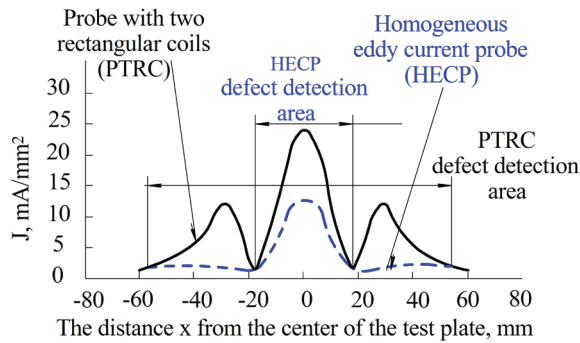


Figure 16 – The eddy current density distribution on the surface of the testing object [10]

The use of ETP with a predetermined EMF topography when detecting defects of complex shape and limited sizes, the control of which reveals the influence of the edge of the object on the ECP signals is relevant. In [8, 9] it is precisely such cases that were considered. In [8] the CoE optimization problem, which creates an almost uniform and tangential field on the surface of TO was solved by solving a multi-parameter multi-purpose optimization problem. The Monte Carlo method optimized a flat coil with several parameters varying: the number of turns, the core gap of the coil, the width of the copper strip of the printed conductor, the size of the air gaps, the length and width of the coil (Figure 17).

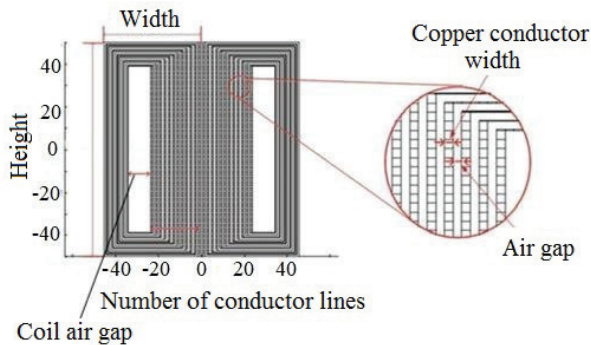


Figure 17 – The configuration of the excitation coil [8]

The work [9] considered the similar problem as in [8], which the genetic algorithm with non-dominant sorting (NSGAI) can solve. A modified NSGAI algorithm optimizes a flat coil, where the gaps between the turns are variables. For optimization objective functions f_1 and f_2 are set, which are respectively minimized and maximized. The first objective function is the standard deviation of the obtained ECD from a given uniform distribution, and, accordingly, the lower this value, the better the uniformity of the currents. The rate of induced EC

is a measure of its intensity. Therefore, the larger this value, the better the ability to detect defects. There is no single solution that satisfies both conditions. Therefore, a number of non-dominant solutions are found. Solution A has large values of f_1 and f_2 , which corresponds to unsatisfactory uniformity and a high value of the ECD (Figure 18). Solution B, on the contrary, has high uniformity and a low ECD value. Solution C is a compromise between the degree of homogeneity of the ECD and its values in the control area.

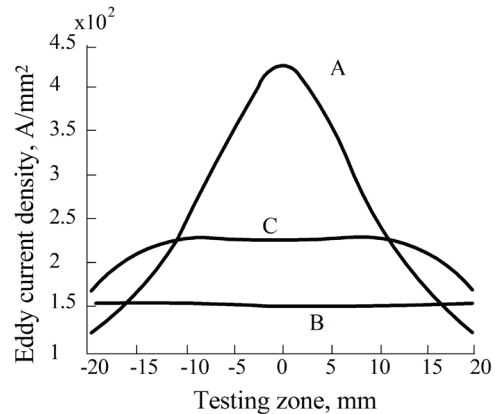


Figure 18 – Distribution of induced eddy currents [9]

For comparison, Figure 19 shows the images of coils with uniform gaps between the conductors with the same currents flowing in them and the optimized one with uneven gaps. The position of the lines of conductors for a conventional coil (Figure 19a) is uniform, whereas for an optimized coil, the lines of conductors are few in the center and more densely located at the edges. ECs induced by an optimized coil are more homogeneous than a conventional coil with uniform gaps between the conductors (Figure 19b).

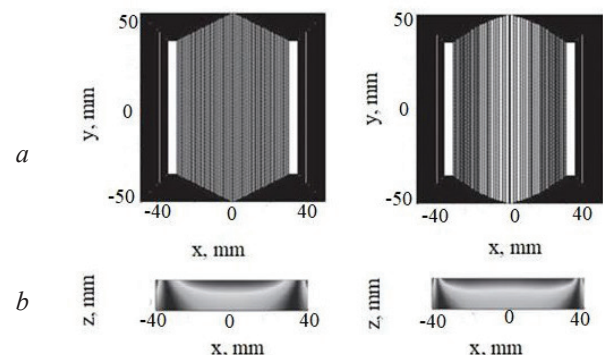


Figure 19 – Unidirectional eddy current probe with uniform eddy current density [9]: *a* – coil designs with uniform and uneven spacing between conductors; *b* – eddy current distribution

The works [26–28] are devoted to study of such drawback of ECP as the exponential attenuation of EC in depth in the sample under study and, accordingly, the application of various measures to eliminate this drawback. The main idea of these works is to suppress EC at the surface of the TO and implement deeper penetration of EC into the thickness of the material. This idea is realized by a combination of several coils, which are powered by an excitation current with different amplitudes and phases, which allows obtaining the desired effect [26]. The obtained results show that the radius of the coil and its height have a strong influence on the attenuation of the EC along the TO depth, when its thickness is several times greater than the standard depth of penetration of the EMF. As a disadvantage of this work, it is possible to note that the synthesis problem was not solved, but was only investigated by sorting a diverse combination of design parameters of the CoE and its height above the TO, and, accordingly, their effect on the attenuation of the EC along the depth of the investigated TO.

The authors analyzed the ECP excitation systems that generate fields of complex configuration at the next stage. A rather interesting study was published in [29]. In order to increase the sensitivity, it was proposed to use a fractal CoE, in particular, in the form of a Koch curve (Figure 20). Such system generates EC in the investigated TO, the topography of which is due to the multiradii

of the winding. This design of the CoE increases the probability of detecting defects that cannot be detected using an ECP with a circular CoE, namely those whose length is much less than the radius of the CoE.

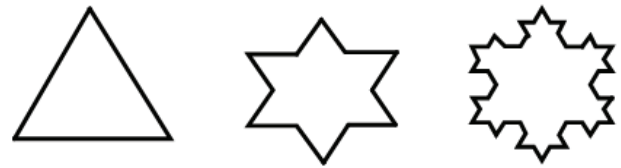


Figure 20 – The geometry of the excitation coil in the form of the first three shapes of the Koch curve [29]

The proposed sensor has a CoE with fractal geometry and measuring coils made by printing on a fourlayer printed circuit board (Figure 21a). The ECD diagrams on the surface of the test sample depending on the size of the defect were studied. The diagrams in Figure 21b show that the obtained ECD is approximately the same both for small and large sizes of defects, since multi-radii of ECs increase the probability of interaction between ECs and a defect.

We also investigated the obtained maximum values of the magnetic flux density depending on the location of defects on the TO with orientation at different angles (Figure 22). Despite the advantages of such planar ECP, the problem of creating a uniform distribution of ECD remains unresolved.

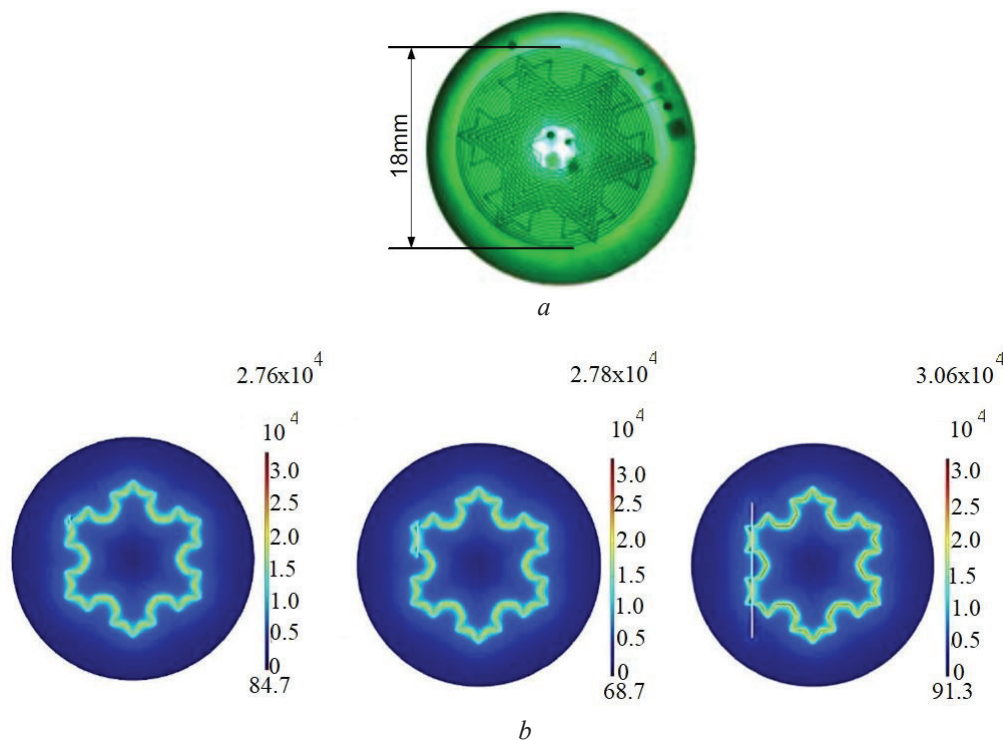


Figure 21 – Design and eddy current density distribution with fractal geometry of the excitation coil [29]: *a* – sensor design; *b* – eddy current density distribution

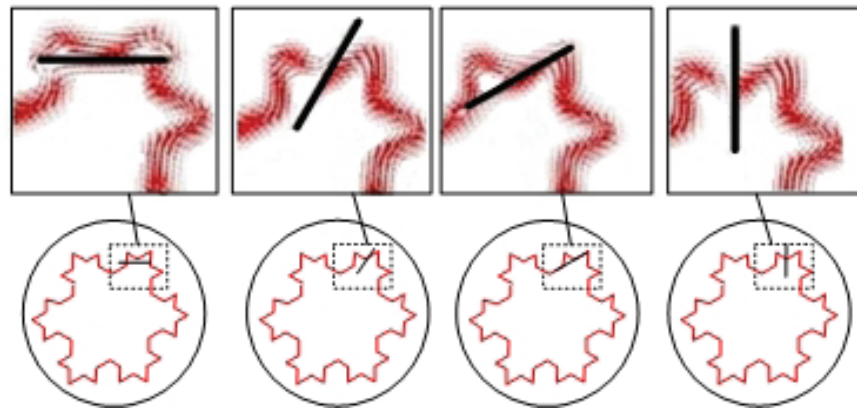


Figure 22 – Eddy current configuration according to defects location [29]

A different approach to the formation of the EMF of the optimal configuration in a given zone was used in [11, 14], where magnetic cores, field concentrators made of conductive materials, and screens of a special shape with and without "masks" are used. For example, a sensor with magnetization device was proposed in [14]. The sensor has an electromagnet with U-shaped core and a combination of a tangential rectangular detector coil for measuring the magnetic flux density B_x and a flat rectangular coil for measuring the magnetic flux density B_z (Figure 23).

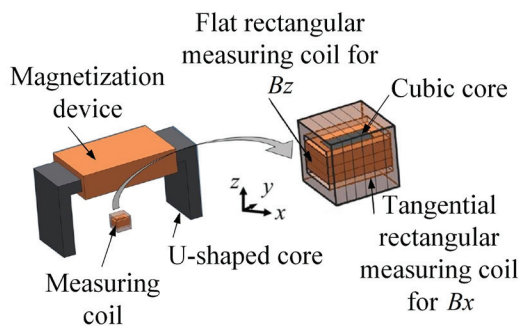


Figure 23 – The structure of the sensor with unidirectional eddy current [14]: *a* – general view; *b* – field detector

Sensors of this type [11, 14] are effective in detecting defects in TO of complex shape and limited sizes, in monitoring which, the effect of the edge of the object on the signals of the ECP is especially felt. For screened ECPs, when shielding elements are placed on the ends of the feedthrough probes, in addition to the positive effect, a negative one also arises, such as an increase in field inhomogeneity in the control zone. The use of "masked" ECP leads, along with an increase in locality, to a decrease in the sensitivity of ECP. Within these designs, it is much more difficult

to realize the uniformity of the EMF distribution in the control zone. In addition, the presence of metal structural elements of the ECP is undesirable in conditions of elevated temperature.

The above studies are devoted to the synthesis of ECPs with a given configuration of the probing field in the control zone, but they considered stationary TOs. As a result of the analysis, it was found that there is almost complete lack of information about solving the problem of creating a SECP with uniform sensitivity for moving TOs, which requires taking into account transfer currents during synthesis. In this direction a number of studies concerning circular SECP was carried out. So, in article [31] an optimal synthesis of ES probes with uniform sensitivity in the control zone using the so-called surrogate optimization was performed. Its use is due to the need to reduce the required computing resources in the synthesis and allows getting a solution search in real time [32]. At the same time, this approach requires the preliminary creation of probes metamodells using the theory of experimental design and the theory of artificial neural networks. The computerized design of the experiment is used to generate nodal points evenly spaced in the search hyperspace [33], while the neural network committee-cascade approximator is used for constructing a multidimensional response surface [31, 34].

The authors of [34] developed the theoretical foundations of the optimal surrogate parametric synthesis of moving circular non-coaxial SECPs with uniform sensitivity, having a planar ES structure. For the synthesis of ECP a metaheuristic hybrid algorithm of global optimization by a swarm of particles with the evolutionary formation of a swarm composition is used, which is effective for finding an extremum of multidimensional "ravine" target functions [35–37].

Conclusion

The paper analyzes the scientific and technical information in the field of eddy current testing for the use of eddy current probes with excitation electromagnetic field with a priori specified properties. The experience of theoretical research in this direction was generalized and systematized.

The works in which linear or nonlinear synthesis is used to achieve a uniform distribution of the electromagnetic field on the surface of the test sample for a stationary eddy current probe were considered. The eddy-current probe designs with a uniform field of excitation created by circular, rectangular tangential and normal coils, as well as through the use of a rotational field of excitation, were analyzed. The designs of excitation coils of probes with fractal geometry were considered. These designs make it possible to increase the probability of detecting defects that cannot be detected using classical eddy current probes. It is shown that similar studies for moving eddy-current probes are only in the initial stage. They are aimed at the realization of circular anaxial eddy current probes with excitation systems of a planar structure.

Thus, an analysis of scientific research on the design of eddy current probes with an a priori specified configuration of the excitation electro-magnetic field established that the issue of the synthesis of circular non-coaxial eddy-current probes with volumetric and mixed structures of excitation systems taking into account the speed effect remains unresolved. In addition, eddy-current probes of frame types, both normal and tangential, which are used to control moving testing object, require detailed studies.

References

1. Ida N., Meyendorf N. Handbook of advanced non-destructive evaluation. *Springer*, 2019, 1626 p.
2. Steblev Yu. [Synthesis of exciting fields of eddy current transducers for monitoring locally heterogeneous products and media]. *Defektoskopija* [Defectoscopy], 1988, no. 5, pp. 47–56 (in Russian).
3. Steblev Yu. [Synthesis of specified characteristics of eddy current probes]. *Defektoskopija* [Defectoscopy], 1984, no. 11, pp. 12–20 (in Russian).
4. Steblev Yu. [Synthesis of eddy-current transducers with specified structure of the exciting field in the zone of inspection]. *Defektoskopija* [Defectoscopy], 1986, no. 4, pp. 58–64 (in Russian).
5. Galchenko V.Ya., Vorobyov M.A. [Structural synthesis of surface eddy current probes with a given distribution of the probe field in the testing zone]. *Defektoskopija* [Defectoscopy], 2005, no. 1, pp. 40–46 (in Russian).
6. Halchenko V.Ya., Pavlov O.K., Vorobyov M.O. [Nonlinear synthesis of magnetic fields of excitation of eddy-current converters of flaw detectors]. *Metody i prylady kontrolju yakosti* [Methods and instruments of control quality], 2002, no. 8, pp. 3–5 (in Ukrainian).
7. Rosado L.S., Gonzalez J.C., Santos T.G., Ramos P.M., Piedade M. Geometric optimization of a differential planar eddy currents probe for non-destructive testing. *Sensors and Actuators A: Physical*, 2013, vol. 197, pp. 96–105. DOI: 10.1016/j.sna.2013.04.010
8. Su Z., Efremov A., Safdarnejad M., Tamburrino A., Udpa L., Udpa S. Optimization of coil design for near uniform interrogating field generation. *AIP Conference Proceedings*, 2015, vol. 1650, pp. 405–413. DOI: 10.1063/1.4914636
9. Su Z., Ye C., Tamburrino A., Udpa L., Udpa S. Optimization of coil design for eddy current testing of multilayer structures. *International Journal of Applied Electromagnetics and Mechanics*, 2016, vol. 52, no. 1–2, pp. 315–322. DOI: 10.3233/JAE-162030
10. Repelianto A.S., Kasai N., Sekino K., Matsunaga M. A uniform eddy current probe with a double-excitation coil for flaw detection on aluminium plates. *Metals*, 2019, no. 9, article № 1116. DOI: 10.3390/met9101116
11. Liu Z., Yao J., He C., Li Z., Liu X., Wu B. Development of a bidirectional-excitation eddy-current sensor with magnetic shielding: Detection of subsurface defects in stainless steel. *IEEE Sensors J.*, 2018, vol. 18, no. 15, pp. 6203–6216. DOI: 10.1109/JSEN.2018.2844957
12. Ye C., Udpa L., Udpa S. Optimization and Validation of Rotating Current Excitation with GMR Array Sensors for Riveted Structures Inspection. *Sensors*, 2016, vol. 16, no. 9, article № 1512. DOI: 10.3390/s16091512
13. Rekanos I.T., Antonopoulos C.S., Tsiaboukis T.D. Shape design of cylindrical probe coils for the induction of specified eddy current distributions. *IEEE Trans. Magnetics*, 1999, vol. 35, no. 3, pp. 1797–1800. DOI: 10.1109/20.767380
14. Repelianto A.S., Kasai N. The improvement of flaw detection by the configuration of uniform eddy current probes. *Sensors*, 2019, vol. 19, no. 2, article № 397. DOI: 10.3390/s19020397
15. Ribeiro A.L., Ramos H.G., Postolache O. A simple forward direct problem solver for eddy current non-destructive inspection of aluminum plates using uniform field probes. *Measurement*, 2012, vol. 45, no. 2, pp. 213–217. DOI: 10.1016/j.measurement.2011.03.029
16. Ribeiro A.L., Pasadas D., Ramos H.G., Rocha T. Using excitation invariance in the characterization of defects by eddy current image constructions. *Procedia*

Engineering, 2014, vol. 86, pp. 440–451.

DOI: 10.1016/j.proeng.2014.11.057

17. Postolache O., Ribeiro A.L., Ramos H. Induction defectoscope based on uniform eddy current probe with GMR. *Proc. IEEE Instrumentation and Measurement Technology Conf.*, 2010, vol. 1, pp. 1278–1283.

DOI: 10.1109/IMTC.2010.5488189

18. Postolache O., Ribeiro A.L., Ramos H.G. Uniform eddy current probe based on GMR sensor array and image processing for NDT. *Instrumentation and Measurement Technology Conference (12MTC). IEEE International*, 2012, pp. 458–463.

DOI: 10.1109/I2MTC.2012.6229366

19. Postolache O., Ribeiro A.L., Ramos H. A novel uniform eddy current probe with GMR for non destructive testing applications. *Proc Conf. on Telecommunications - ConfTele*, 2011, vol. 1, pp. 5–9.

DOI: 10.1109/EUROCON.2011.5929410

20. Postolache O., Lopes A., Ramos H.G. GMR array uniform eddy current probe for defect detection in conductive specimens. *Measurement*, 2013, vol. 46, pp. 4369–4378.

DOI: 10.1016/j.measurement.2013.06.050

21. Hoshikawa H., Koyama K. Uniform eddy current probe with little disrupting noise. *Review of Progress in Quantitative Nondestructive Testing*, 1998, vol. 17, pp. 1059–1066. **DOI:** 10.1007/978-1-4615-5339-7_137

22. Hoshikawa H., Koyama K., Mitsuhashi S. Eddy current and magnetic testing of magnetic material by uniform eddy current probe. *Review of Quantitative Nondestructive Evaluation*, 2005, vol. 24, pp. 494–501.

DOI: 10.1063/1.1916716

23. Li Y., Ren S., Yan B., Zainal Abidin I.M., Wang Y. Imaging of subsurface corrosion using gradient-field pulsed eddy current probes with uniform field excitation. *Sensors*, 2017, vol. 17, article № 1747.

DOI: 10.3390/s17081747

24. Su Z., Rosell A., Udpa L. Model-based study for evaluating the sensitivity of eddy current GMR probe inspection of multilayer structures. *AIP Conf. Proc.*, 2017, vol. 1806, no. 1, article № 110016-1-8.

DOI: 10.1063/1.4974694

25. Hashimoto M., Kosaka D., Ooshima K., Nagata Y. Numerical analysis of eddy current testing for tubes using uniform eddy current distribution. *Int. J. Appl. Electromagn. Mech.*, 2001/2002, vol. 14, pp. 95–99.

DOI: 10.3233/JAE-2002-511

26. Janousek J. Effect of exciting system configuration on eddy currents distribution in non-destructive evaluation of materials. *Przegląd Elektrotechniczny*, 2013, vol. 89 (3A), pp. 256–258.

27. Janousek L., Chen Z., Yusa N., Miya K. Excitation with phase shifted fields enhancing evaluation of deep cracks in eddy-current testing. *NDT & E Int.*, 2005,

vol. 38, pp. 508–515.

DOI: 10.1016/j.ndteint.2005.01.012

28. Ramos H.G., Rocha T., Pasadas D., Ribeiro A.L. Determination of linear defect depths from eddy currents disturbances. *Proc. 40th Annu. Rev. Progr. Quant. Nondestruct. Eval. AIP Conf.*, 2014, pp. 1448–1455.

DOI: 10.1063/1.4864992

29. Chen G., Zhang W., Pang W. Koch curve fractal geometry excitation probe for eddy current non-destructive testing. *Measurement*, 2018, vol. 124, pp. 470–478.

DOI: 10.1016/j.measurement.2018.04.031

30. Koyama K., Hoshikawa H., Mito Y. Surface flaw testing of weld zone by uniform eddy current probe. *J. Jpn. Soc. Non-Destruct. Insp.*, 2006, vol. 60, pp. 275–282. **DOI:** 10.1063/1.2184550

31. Halchenko V.Ya., Trembovetska R.V., Tychkov V.V., Storchak A.V. Nonlinear surrogate synthesis of the surface circular eddy current probes. *Przegląd elektrotechniczny*, 2019, no. 9, pp. 76–82.

DOI: 10.15199/48.2019.09.15

32. Trembovetska R.V., Halchenko V.Ya., Tychkov V.V. Studying the computational resource demands of mathematical models for moving surface eddy current probes for synthesis problems. *Eastern-European Journal of Enterprise Technologies*, 2018, vol. 95, no. 5/5, pp. 39–46. **DOI:** 10.15587/1729-4061.2018.143309

33. Halchenko V.Ya., Trembovetska R.V., Tychkov V.V. The neurocomputing using of the development meta-models stage in the optimal surrogate antennas synthesis process. *Visnyk NTUU KPI. Seriya - Radiotekhnika Radioaparaturbuduvannya*, 2018, vol. 74, pp. 60–72. **DOI:** 10.20535/RADAP.2018.74.60-72

34. Halchenko V.Ya., Trembovetska R.V., Tychkov V.V. Development of excitation structure RBF-metamodels of moving concentric eddy current probe. *Electrical Engineering & Electromechanics*, 2019, no. 1, pp. 28–38. **DOI:** 10.20998/2074-272X.2019.2.05

35. Gal'chenko V.Y., Yakimov A.N., Ostapushchenko D.L. Pareto-optimal parametric synthesis of axisymmetric magnetic systems with allowance for nonlinear properties of the ferromagnet. *Technical Physics*, 2012, vol. 57, no. 7, pp. 893–899.

DOI: 10.1134/s1063784212070110

36. Kuznetsov B.I., Nikitina T.B., Voloshko A.V., Bovdyj I.V., Vinichenko E.V., Kobilyanskiy B.B. Synthesis of an active shielding system of the magnetic field of power lines based on multiobjective optimization. *Electrical engineering & electromechanics*, 2016, no. 6, pp. 26–30. **DOI:** 10.20998/2074-272X.2016.6.05

37. Koshevoy N.D., Beliaeva A.A. Application particle swarm algorithm to minimize the cost of conducting multivariate experiment. *Radio Electronics, Computer Science, Control*, 2018, no. 1, pp. 41–49.

DOI: 10.15588/1607-3274-2018-1-5

System for Assessing the Effectiveness of Temporary Blinding Devices

M. Terekhova, S. Rudikov, A. Shumski, A. Shkadarevich

Scientific and Technical Center LEMT of the BelOMO,
Makayonok str., 23/1, Minsk 220114, Belarus

Received 02.02.2020

Accepted for publication 12.05.2020

Abstract

The development of non-lethal weapons and, in particular, temporary blinding devices is associated with problem of choosing boundaries of effectiveness. The aim of present work is determination of criteria for estimation of the effects of visual jamming devices action on the naked eye.

The present-day scoring system used for effectiveness estimation of laser temporary blinding devices is based on maximum permissible exposure and/or accessible emission level defined for each hazard class in accordance with operating standard.

In the present work we carried out analysis and modeling of the cases of application of temporary blinding laser devices. The proposed scoring system was founded on international standard IEC 60825-1-2014 as well as Manual on Laser Emitters and Flight Safety. The modeling of bright light action on observer eye was rested on CIE General Disability Glare Equation and provided quantitative description of jamming effectiveness. The main parameters used in this model and dictated by ambient light level and human eye characteristics, were veiling luminance and angle of distinguishing objects under it.

In terms of exposition level and perception effects we determined six zones – unallowed, hazard, temporary blinding, discomfort, alerting, completely safe. Proposed system combined with modeling provides with visual demonstration of perceived light source and allows to describe human physiological sensation and to establish the fact of jamming at different distances. This system was the basis of the development of temporary blinding device for revelation of safe but effective spatial boundaries of action.

Keywords: dazzle, temporary blindning, hazard class, veiling luminance.

DOI: 10.21122/2220-9506-2020-11-2-105-113

Адрес для переписки:

М.С. Терехова
Научно-технический центр «ЛЭМТ» БелОМО,
ул. Макаёнка, 23/1, г. Минск 220114, Беларусь
e-mail: terekhova.m.s@yandex.by

Для цитирования:

M. Terekhova, S. Rudikov, A. Shumski, A. Shkadarevich.
System for Assessing the Effectiveness of Temporary Blinding Devices.
Приборы и методы измерений.
2020. – Т. 11, № 2. – С. 105–113.
DOI: 10.21122/2220-9506-2020-11-2-105-113

Address for correspondence:

M. Terekhova
Scientific and Technical Center LEMT of the BelOMO,
Makayonok str., 23/1, Minsk 220114, Belarus
e-mail: terekhova.m.s@yandex.by

For citation:

M. Terekhova, S. Rudikov, A. Shumski, A. Shkadarevich.
System for Assessing the Effectiveness of Temporary Blinding Devices.
Devices and Methods of Measurements.
2020, vol. 11, no. 2, pp. 105–113.
DOI: 10.21122/2220-9506-2020-11-2-105-113

Система оценки эффективности устройств временного ослепления

М.С. Терехова, С.И. Рудиков, А.П. Шумский, А.П. Шкадаревич

Научно-технический центр «ЛЭМТ» БелОМО,
ул. Макаёнка, 23/1, г. Минск 220114, Беларусь

Поступила 02.02.2020

Принята к печати 12.05.2020

Разработка оружия нелетального действия, в частности устройств временного ослепления, сопряжена с проблемой выбора эффективных границ действия. Целью данной работы являлось установление критериев оценки действия устройств постановки зрительных помех невооружённому глазу.

Для определения эффективности действия представленных на рынке лазерных устройств временного ослепления обычно используется система оценки, основанная на предельно допустимом уровне излучения и/или предельной интенсивности излучения для выбранного класса опасности в соответствии с действующим стандартом.

В данной работе проведён анализ и моделирование ситуаций применения устройств временного ослепления на основе лазеров. Предложена система оценки, основанная как на международном стандарте IEC 60825-1-2014, так и на руководстве по лазерным излучателям в аспекте безопасности полётов. Моделирование воздействия яркого излучения на глаз наблюдателя базировалось на основном уравнении слепящей блескости (*CIE General Disability Glare Equation*) и обеспечивало количественную оценку эффективности постановки помех. В качестве основных параметров в модели использовались величины яркости засветки и угол различения объектов под ней, которые определялись параметрами человеческого глаза и внешней среды.

По уровню экспозиции и проявляемому эффекту было выделено шесть зон – запрещённая, опасная, временного ослепления, дискомфортная, оповещения, полностью безопасная. В совокупности с моделированием данная система позволяет описать физиологические ощущения человека, дать наглядное изображение воспринимаемого источника света и установить факт постановки помех на различных расстояниях. Эта система была положена в основу разработки устройства временного ослепления для выявления безопасных и эффективных пространственных границ действия.

Ключевые слова: даззлер, временное ослепление, класс опасности, яркость засветки.

DOI: 10.21122/2220-9506-2020-11-2-105-113

Адрес для переписки:

М.С. Терехова
Научно-технический центр «ЛЭМТ» БелОМО,
ул. Макаёнка, 23/1, г. Минск 220114, Беларусь
e-mail: terekhova.m.s@yandex.by

Для цитирования:

M. Terekhova, S. Rudikov, A. Shumski, A. Shkadarevich.
System for Assessing the Effectiveness of Temporary Blinding Devices.
Приборы и методы измерений.
2020. – Т. 11, № 2. – С. 105–113.
DOI: 10.21122/2220-9506-2020-11-2-105-113

Address for correspondence:

M. Terekhova
Scientific and Technical Center LEMT of the BelOMO,
Makayonok str., 23/1, Minsk 220114, Belarus
e-mail: terekhova.m.s@yandex.by

For citation:

M. Terekhova, S. Rudikov, A. Shumski, A. Shkadarevich.
System for Assessing the Effectiveness of Temporary Blinding Devices.
Devices and Methods of Measurements.
2020, vol. 11, no. 2, pp. 105–113.
DOI: 10.21122/2220-9506-2020-11-2-105-113

Introduction

Nowadays there is a growing interest in non-lethal weapons as a method of conducting humane combat. Non-lethal weapons (NLW) are a type of weapon designed for personnel temporarily disable, in the offensive or in the defensive, as well as to disrupt the operation of the enemy's weapons, military equipment and infrastructure while minimizing lethality, significant materiel destruction and environmental pollution [1]. One of the NLW development trends is creation of weapons based on temporary blinding of the enemy troops. Both coherent (laser) and incoherent radiation can be used as a light source. The advantage of using laser radiation (LR) is a longer range, high accuracy and lower required radiation power.

Vision is an irreplaceable sensory receptor and there are no prostheses or rehabilitation measures that can replace the lost sensory organ. Therefore, the magnitude of fear of losing sight for a sighted person (be it conscious or unconscious fear) [2, 3] and the concealed nature of the threat lead to a serious destabilization of the enemy's actions.

The NLW under discussion are in operational service with many countries. Examples of systems that cause temporary blindness are the products of E. Meyers Advanced Photonics (GLARE MOUNT and its modifications), Laser Energetics (Dazer Laser in various versions), Thales Group (GLOW), etc. Their

method of application usually involves preliminary detection, alerting the enemy, and then inducing interference by directing a beam of light into the eyes.

In the Republic of Belarus a device causing temporary blindness has also been created. The project design developed by STC LEMT of the BelOMO is a mobile complex for monitoring the terrain, buildings and structures ("ISKRA"). It can be operated in three channels with wavelengths $\lambda = 525$ nm, 640 nm, 808 nm. The specified output power for each channel is approximately 3 W. The radiation divergence for the green radiation channel constitutes 6×3 mrad, for the red radiation channel – 6×2 mrad, for the IR – 5.8×5.2 mrad.

This system is intended for use during military operations and has a universal action. The operation of channels with wavelengths of $\lambda = 525$ nm and $\lambda = 640$ nm provides for temporary blinding of the enemy, i.e. disabling of the personnel through disorientation, and issuance of warnings over a wide range of distances. The channel operating at a wavelength of $\lambda = 808$ nm is designed to jam the enemy night vision devices and TV cameras.

The device itself is mounted on a pan and tilt platform and allows for regulating the impact effectiveness by pre-aiming at the target, determining the distance to it with the help of the rangefinder and for automatically adjusting the radiation power.

The technical characteristics of the temporary blinding devices/dazzlers are specified in Table 1.

Table 1

Dazzler characteristics

Name	Manufacturer	Power, W	Declared distance of temporary blinding	Divergence, mrad
Medusa	Passive Force LLC	5.00	Not specified. Probably ≈ 2 km	5.0
Sealase II	Passive Force LLC	5.00	Not specified. Probably ≈ 2 km	2.0
Hydra	Passive Force LLC	1.00	Not specified. Probably ≈ 0.5 km	Adjustable
Photonic Disruptor	Wicked Lasers	0.10	Not specified. Probably ≈ 0.5 km	Adjustable, 1.5–7.5
Laser Dazer Guardian	Laser Energetics	0.20	25–300 m (depends on divergence)	for 300 m – 3.3
GLARE LA-9/P	B.E. Meyers Advanced Photonics	0.25	500 m	Not specified. Probably ≈ 5.0
ISKRA	STC "LEMT" BelOMO	3.00	50–2500 m	6.0×3.0

Prior to using temporarily blinding weapons, it is necessary to determine and register the emitter characteristics within the safety limits. The aim of this work is to establish the criteria for estimation of the effects of visual jamming devices action on the naked eye.

Temporary blinding devices / dazzlers efficiency criteria

Estimation of the effectiveness of temporary blinding devices is based on comparing the laser radiation characteristics with the limit values given in the standards. The main parameters used for comparison are the laser power density, or the power per pupil. At the same time, the standards assign the values of the maximum permissible exposure (MPE) levels of laser radiation, to which an object can be exposed without adverse consequences, and the accessible emission level (AEL) for each laser class¹. Comparing the parameters of the selected LR with the specified values allows to determine the effect of the LR on the eye.

Considering that the human perception is governed by the Weber-Fechner law, the described method is inaccurate, since it does not allow describing the physiological effect and the human response in case of significant decrease in the laser power density.

There are two types distinguished in the phenomenon of glare: discomfort glare and disability glare [4]. Discomfort glare is annoying and painful sensation caused by the light from a bright glare source. Nowadays, there are scales that allow to assess the discomfort glare, i.e. the subjective sensations of a human when exposed to bright light: the British Glare Index, the Discomfort Glare Index, the Unified Glare Rating, etc. [5]. However, they are applicable for sources whose solid angle for the observer is not less than 10^{-5} Sr (small sources) [6]. If the laser beam at the output aperture has dimensions of the order of 1×1 mm, then the solid angle at which the source is visible from the observer's position is much less than 10^{-5} Sr and tends to zero. At the same time the power density in the beam is large and can result in injuries. In view of this, there arises a need to discriminate additional power density boundary values that define certain conditional zones of LR impact and allow us to characterize the LR action at different distances and power outputs.

From henceforth, we will assume a continuous exposure mode, i.e. the one in which the pulse duration is equal to or greater than the duration of the wink reflex of 0.25 s [7].

We suggest to discriminate six zones with hazard scores assigned to them. The upper limit of the maximum allowable laser power density is determined based on the parameters which are characteristic of hazard class 3B, since observation of the radiation of this class is dangerous to vision. According to IEC 60825-1-2014, the AEL for class 3B laser falling on an aperture of 7 mm and corresponding to the diameter of the pupil adapted to night vision, of wavelengths $\lambda = 400\text{--}700$ nm, with a radiation pulse duration of 0.25 s constitutes 0.5 W (13 kW/m^2). Hence, when the power density increases above the specified value, irreversible effects occur. A zone where the power density exceeds 13 kW/m^2 is "forbidden" ("Unallowed") and has hazard score 6.

Since the laser class parameters are based on the MPE, which determines the LR level to which people can be exposed without negative effects, the next boundary is the laser power density of 25 W/m^2 . Irradiation of the eyes within the five-point hazard score zone (power density from 25 to $13 \cdot 10^3 \text{ W/m}^2$) will lead to temporary blinding, while the probability of causing physical damage is quite high.

Two subzones should be discriminated within the "danger" zone: from 25 to 130 W/m^2 and from 130 to $13 \cdot 10^3 \text{ W/m}^2$. An additional boundary is related to the characteristics of hazard class 3R (with the above-specified parameters, the AEL is $5 \cdot 10^{-3} \text{ W--}130 \text{ W/m}^2$). The division into sub-zones is necessary in order to focus on the growing risk of damage with an increase in power density (i.e., 130 to $13 \cdot 10^3 \text{ W/m}^2$), which should be kept in mind when setting the operating modes of equipment aimed at temporary eye-blinding.

The next boundaries are set in accordance with the Manual on Laser Emitters and Flight Safety (ICAO (Doc 9815-AN/447, 2003)). In accordance with this document [8], in the immediate vicinity of the airfield three flight zones are distinguished in accordance to AEL (sensitive (1 W/m^2), critical ($5 \cdot 10^{-2} \text{ W/m}^2$), free (from laser radiation) ($5 \cdot 10^{-4} \text{ W/m}^2$)). Therefore, a zone where the power density varies from 1 to 25 W/m^2 is a four-point zone of "temporary blinding". At this power density, the effects of short-term blindness or afterimages may begin to occur, but without permanent damage to the eye caused.

¹ IEC 60825-1:2014

The LR power density range from $5 \cdot 10^{-2}$ to 1 W/m^2 is a three-point "discomfort" zone, where glaring effects may occur, but the phenomenon of flashblinding will not be achieved. At the same time, any negative effects on the eyes are also completely excluded.

In the two-point "alert" zone, the LR power density (from $5 \cdot 10^{-4}$ to $5 \cdot 10^{-2} \text{ W/m}^2$) is not sufficient to cause glare, but it is large enough to warn/illuminate the target.

If the power density is less than $5 \cdot 10^{-4} \text{ W/m}^2$, the zone is "completely safe" and has hazard score one.

Analysis of the known characteristics of some of the above-mentioned devices allows us to make a theoretical calculation (Formula 1) of the radiation power density at different distances from the emitter (Figure 1):

$$E = \frac{P}{\pi \cdot \operatorname{tg} \frac{\varphi_1}{2} \cdot \operatorname{tg} \frac{\varphi_2}{2} \cdot L^2}, \quad (1)$$

where E is the radiation power density, W/m^2 ; L is the distance from the emitter, m; P is the LR power, W; φ_1 , φ_2 are the LR divergence angles along both axes.

With $L = 0$, all outputted radiation falls on the object, while the power density is maximal and depends on the beam diameter (r) at the output of the emitter. Accordingly, formula (1) is applicable for distances $L > \frac{r}{\operatorname{tg} \frac{\varphi}{2}}$, where $\varphi = \max[\varphi_1, \varphi_2]$.

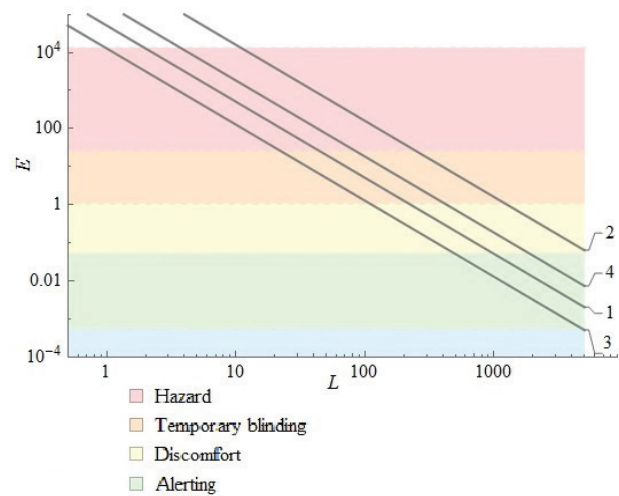


Figure 1 – Dependence of the radiation power density (E , W/m^2) on the distance to the source (L , m) for different devices: 1 – Hydra; 2 – Sealase II; 3 – GLARE LA-9/P; 4 – ISKRA system

Knowing the initial parameters of the systems, a theoretical calculation has been made (Table 2) of the distances (Formula 2) at which certain effects from each device are manifested:

$$L = \left(\frac{P}{E \cdot \pi \cdot \operatorname{tg} \frac{\varphi_1}{2} \cdot \operatorname{tg} \frac{\varphi_2}{2}} \right)^{1/2}. \quad (2)$$

Table 2

Effective zones of temporary blinding devices/dazzlers depending on the distance to the source

E , W/m^2		More than $13 \cdot 10^3$	$13 \cdot 10^3$ –25	25–1	1 – $5 \cdot 10^{-2}$	$5 \cdot 10^{-2}$ – $5 \cdot 10^{-4}$	Less than $5 \cdot 10^{-4}$
Score points		●●●●●	●●●●●	●●●●	●●●	●●	●
Zone name		Unallowed	Hazard	Temporary blinding	Discomfort	Alerting	Completely safe
		Effective range, m					
Name	Medusa	Less than 4	Up to 101	Up to 505	Up to 2300	Up to 23000	Over 23000
	Sealase II	Less than 11	Up to 252	Up to 1000	Up to 5600	Up to 56000	Over 56000
	Hydra	Less than 2	Up to 45	Up to 226	Up to 1000	Up to 10000	Over 10000
	Photonic Disruptor	Less than 2	Up to 48	Up to 238	Up to 1000	Up to 10600	Over 17000
	Laser Dazer Guardian	Less than 1	Up to 31	Up to 153	Up to 684	Up to 7000	Over 7000
	GLARE LA-9/P	Less than 1	Up to 23	Up to 113	Up to 505	Up to 5000	Over 5000
	ISKRA	Less than 4	Up to 86	Up to 430	Up to 2000	Up to 20000	Over 20000

Comparison of the data (Table 2) with the established zone boundaries allows to assess the effect of temporary blinding systems. If operation of the devices is analyzed based only on the laser classification, their effectiveness is extremely low. However, the use of the proposed system of six zones allows us to fully characterize the action of the systems at different distances. Thus, all the devices discussed provide the necessary effect at the stated distance.

Modeling of laser radiation effects on eyes

One of the manifestations of blinding is disability glare, which is understood to mean a decrease in visibility caused by irradiation by a bright light source. In this case, subjective sensations are not taken into account [4]. As a result, the apparent brightness of the object that a person is looking at decreases on the retina exposed to the bright counter-flash, and it becomes impossible to distinguish the object. The use of the blinding glare parameters together with the zones of permissible power densities correlated with physiological effects allows us to fully assess and substantiate the effect of temporary blinding devices on the human eye.

The characteristic of the disability glare is the brightness of the veiling luminance, which is described by the *CIE General Disability Glare Equation* [9]:

$$g(\theta) = \frac{L_{veil}}{E_{glare}} = \frac{10}{\theta^3} + \left(\frac{5}{\theta^2} + \frac{0.1 \cdot p}{\theta} \right) \cdot \left(1 + \left(\frac{A}{62.5} \right)^4 \right) + 0.0025 \cdot p, \quad (3)$$

where E_{glare} is irradiance from the source of flash, lx; L_{veil} is brightness of the veiling luminance, Cd/m²; θ is the angle between the visual direction and the direction of the source beam ($0,1^\circ < \theta < 100^\circ$) (Figure 2), degrees; p is the iris pigmentation coefficient (equal to 1.2 for very light-colored eyes, θ – for very dark eyes); A is the age of the observer.

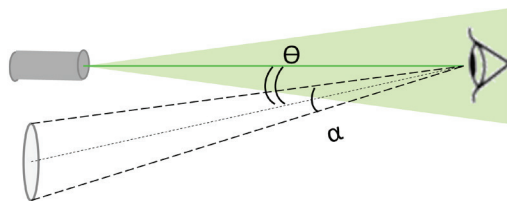


Figure 2 – Schematic representation of the laser radiation effect on the viewer's eye: α is the visible angular size of the target; θ is the angle between the visual direction and the direction of the laser beam

The luminous efficiency (visibility curve) allows to assess the effect of a certain radiation wavelength. Taking into account the calibration coefficients, the final formula showing the variation of the veiling luminance brightness depending on the radiation power density on the eye, has the following form [10]:

$$L_{veil} = g(\theta) \cdot 0.9239 \cdot L_b^{0.6795} \cdot C \cdot V_\lambda \cdot E, \quad (4)$$

where L_b – background ‘ambient’ luminance (bright day, twilight, night), cd/m²; V_λ – eye’s photopic efficiency at the wavelength, λ ; E – radiation power density, W/m²; $C = 683$ Lm/W is the multiplicative constant.

In practice, disability glare can be estimated using the concept of maximum dazzle exposure (MDE) [11], which shows the value of the laser field illuminance, above which the object located behind the field cannot be detected. The calculation takes into account the angular size of the target that a person is looking at, the age and the degree of pigmentation of the person's eyes, the brightness of the background and the target contrast:

$$MDE = \frac{\left(\frac{L_b \cdot C_{orig}}{\Omega \cdot AF} - L_b \right)}{g(\theta) \cdot 0.9239 \cdot L_b^{0.6795} \cdot C \cdot V_\lambda}, \quad (5)$$

where MDE is the maximum dazzle exposure, W/m²; C_{orig} is the target contrast in the absence of a laser field (nondimensional value, the ratio of the object brightness to the field brightness); Ω is the calibration factor including the target angular size α and total luminance; AF is the age factor.

Since at the set distance the viewer's eye is exposed (Figure 2) to a well-defined power density (Formula 1) it is possible to determine the maximum angle θ at which an object with angular size α will not be distinguished by equating this value to the MDE (Formula 5). Therefore, the simulated zone model can be supplemented with the values of the object distinguishing angle.

The results of the MDE calculation (Formula 5) for the ISKRA system for the established zones are presented in Table 3. The following initial input parameters of the system were used: radiation wavelength – 525 nm, human age – 30 years, eye pigmentation – 0.5 (brown), target contrast – 0.8, external luminance – 10000 cd/m² (bright day), target size – 5 m. The calculation does not consider the dark adaptation of the eyes, because at close distances (unallowed and hazard zones), the entire

field of view is filled with the light from the source, which makes it impossible to distinguish the object. At long distances (temporary blinding zone, discomfort zone, alerting zone, completely safe zone), the angular size of the target is small, and with its low contrast can not be distinguished in low external lighting conditions, even at low radiation power density.

It should be emphasized that the calculation of the maximum object distinguishing angles does not take into account the sensations of the subject. Literature data [12] suggest that, despite the possibility of detecting an object under the field of veiling luminance, observation of radiation is discomforting and affects the subject's activity (in particular, the shooting accuracy and rate decreases).

Table 3

Operating range of ISKRA, angle of object detection (θ) under veiling luminance and effects in dependence on distance from light source (L) and angular size of a target (α) in case of light adaptation of eyes

$E, \text{W/m}^2$	Zone name	Score points	L, m	α , degrees	θ , degrees	Effect
More than $13 \cdot 10^3$	Unallowed	●●●●●	Less than 4	Over 51.33	All field dazzled	Blinding
From – to $13 \cdot 10^3$ –25	Hazard	●●●●●	Up to 86	Up to 3.32	At least 5.83	Temporary flash blinding, potential injuries
From–to 25–1	Temporary blinding	●●●●	Up to 430	Up to 0.72	At least 1.73	Temporary blinding, afterimages, without injury
From – to 1 – $5 \cdot 10^{-2}$	Discomfort	●●●	Up to 2000	Up to 0.15	At least 0.84	Temporary blinding effects, afterimages of short duration
From – to $5 \cdot 10^{-2}$ – $5 \cdot 10^{-4}$	Alerting	●●	Up to 20000	Up to 0.02	At least 1.22	Illumination, blinking
Less than $5 \cdot 10^{-4}$	Completely safe	●	Over 20000	Less than 0.02	Less than 1.22	Illumination

Based on the recalculation mechanism proposed in [11], the disability glare was visualized for the three channels of the ISKRA system under conditions of the daytime adaptation of the eye. The resulting distribution was superimposed on the photograph of the selected horizontal field of view for better visual clarity (Table 4). The image is a model of a light spot on the retina of the eye and serves as an additional way to visualize the boundaries of the zones presented above.

From Table 4 it is evident that the green channel has a greater effect on the human visual organ, which is explained by the structure of the eye's receptor cells and is numerically fixed in the spectral sensitivity curve of the eye.

Figure 3 schematically shows the value of the object distinguishing angle when exposed to radiation

with a power density of 1 W/m^2 . Diverting the eye by this angle is necessary, but not sufficient to distinguish the target, because the person will experience discomfort, causing impairment of responses.

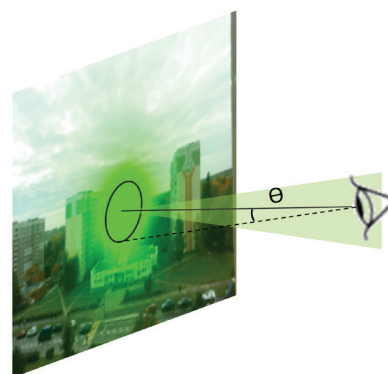












Figure 3 – Schematic representation of the object distinguishing angle (θ) under exposure to veiling luminance

Table 4

Simulated image of dazzle spot on eye retina exposed to irradiation with power density E

Zone name	$E, \text{W/m}^2$	Irradiation wavelength, nm	
		525	640
Unallowed	$13 \cdot 10^3$		
Hazard	25		
Temporary blinding	1		
Discomfort	$5 \cdot 10^{-2}$		
Alerting	$5 \cdot 10^{-4}$		

Based on the proposed pattern, one can assess the efficacy of the devices under various conditions. For example, the ISKRA system provides for induction of sensible visual interference at a distance of up to ≈ 2 km ("discomfort" zone), while temporary blinding is achieved at distances of up to ≈ 0.5 km. This provides for the effect of evasion of the bright light source (disorientation), due to a physiological reaction, as well as the effect of disruption of the human work activity due to the veiling luminance of part of the field of view and the inability to properly perform actions aimed at excluding the source of radiation. The efficiency of the $\lambda = 525$ nm channel is higher compared to the other channels, since the radiation wavelength is close to the maximum spectral sensitivity of the eye. The highest effectiveness of the device is achieved during the dark adaptation of the eye under low ambient luminance conditions.

Conclusion

As a result of the study, a system of power density zones has been established that allows us to characterize and to provide visual demonstration of the perception of the irradiated human during operation of temporary blinding devices at different distances (unallowed, hazard, temporary blinding, discomforting, alerting, completely safe zones).

In the case of development of the new device it has been proposed to use the angle of object detection, which depends on the parameters of the emitter, external space and the human, along with the zone system for numerical demonstration of device operation. Based on the described system, the parameters of the new device designed for suppressing the enemy's actions by means of laser radiation were estimated.

References

1. Hoffberger E. Non-lethal weapons: The Principle of proportionality in armed conflict and the right to health in law enforcement. *Zb Pravnog Fak Sveučilišta U Rijeci*, 2017, vol. 38, no. 2, pp. 831–853. DOI: 10.30925/zpfsr.38.2.6
2. Peters A. Blinding Laser Weapons: New Limits on the Technology of Warfare. *Loy LA Int'l & Comp LJ*, 1996, vol. 18, pp. 733–766.
3. Giridhar P., Dandona R., Prasad M.N., Kovai V., Dandona L. Fear of Blindness and Perceptions about Blind People. *The Andhra Pradesh Eye Disease Study. INDIAN J Ophthalmol*, 2002, vol. 50, no. 3, pp. 8.
4. Bullough J.D., Sweater-Hickcox K., Narendran N. A method for estimating discomfort glare from exterior lighting system. *Alliance Solid-State Illum Syst Technol*, 2011, vol. 9, pp. 1–7.
5. Clear R. Discomfort glare: What do we actually know? *Light Res Technol*, 2013, vol. 45, no. 2, pp. 141–158. DOI: 10.1177/1477153512444527
6. Tyukhova Y.I. Discomfort glare from small, high luminance light sources in outdoor nighttime environments. *Architectural Engineering – Dissertations and Student Research. Lincoln*, 2015, 295 p.
7. Denniston A., Murray P. Oxford Handbook of Ophthalmology. *OUP Oxford*, 2014, 1108 p.
8. IKAO [ICAO]. Available at: <https://www.favt.ru/dejatelnost-mezhdunarodnaja-dejatelnostikao/?id=796> (accessed 17 September 2019).
9. Vos J.J. On the cause of disability glare and its dependence on glare angle, age and ocular pigmentation. *Clin Exp. Optom.*, 2003, vol. 86, no. 6, pp. 363–370. DOI: 10.1111/j.1444-0938.2003.tb03080.x
10. Williamson C.A. Simple computer visualization of laser eye dazzle. *J Laser Appl.*, 2016, vol. 28, no. 1, pp. 012003. DOI: 10.2351/1.4932620
11. Williamson C.A., McLin L.N. Nominal ocular dazzle distance (NODD). *Appl. Opt.*, 2015, vol. 54, no. 7, pp. 1564. DOI: 10.1364/AO.54.001564
12. Vandewal M., Eeckhout M., Budin D. Estimation of Laser Dazzle Effects on Shooting Performance. *Hum Factors Mech. Eng. Def. Saf.*, 2019, vol. 3, no. 1, p. 12. DOI: 10.1007/s41314-019-0028-2

System of Laser Monitoring of Water Pollution with Application of Relative Description of Signal Shape

V.A. Alekseev¹, S.I. Yuran², V.P. Usoltsev¹, D.N. Shulmin¹

¹Kalashnikov Izhevsk State Technical University,
Studencheskaya str., 7, Izhevsk 426069, Russia

²Izhevsk State Agricultural Academy,
Studencheskaya str., 11, 426069, Izhevsk, Russia

Received 16.03.2020

Accepted for publication 18.05.2020

Abstract

As a rule, the wastewater treatment system is not designed to filter substances formed, as a result of beyond design basis accident. The nature of the beyond design basis accident is associated with the shortterm appearance of a clot of these substances in wastewater, determined by the volume of the substance storage tank. Therefore, a rational approach is to divert this portion of the formed substances into a separate branch of the sewage system or sedimentation tanks. The aim of the work is to implement this approach by creating a laser monitoring system for water pollution.

The article proposes a system for automatic detection of a clot of emergency discharge of pollutants into the wastewater of an industrial enterprise. The structural diagram of the system and the purpose of its main elements are given. The system should provide clot detection in real time. To ensure this function, a preliminary study is made of the spectral characteristics of all substances that may appear in wastewater in the event of an emergency.

Based on these data, the wavelengths of laser radiation in the system are selected. The obtained measurement data from several probes are presented in the form of a lattice function, which is translated into a relative description representing the order relationship matrix on the set of lattice function components. The relative description is invariant to linear changes in the lattice function. The decision to detect any substance from emergency discharges is made based on a comparison of the relative description of the measurements with the standards prepared at the stage of system setup.

The article provides an example of the formation of standards for emergency clots from glycerin and allyl alcohol. The graphs of the lattice functions obtained from the IR spectra of emergency discharges of these substances are given; algorithms for constructing a lattice function and comparison of lattice functions.

Thus, using the developed mathematical description of the shape of digital signals based on the relative description, the signal of the monitoring curve can be described in the form of a curve of the optical density change of an aqueous medium.

Keywords: emergency discharges, clot, spectroscopy, laser probe, relative description.

DOI: 10.21122/2220-9506-2020-11-2-114-121

Адрес для переписки:

С.И. Юран
Ижевская государственная сельскохозяйственная академия,
ул. Студенческая, 11, Ижевск 426069, Россия
e-mail: yuran-49@yandex.ru

Address for correspondence:

S.I. Yuran
Izhevsk State Agricultural Academy,
Studencheskaya str., 11, 426069, Izhevsk, Russia
e-mail: yuran-49@yandex.ru

Для цитирования:

V.A. Alekseev, S.I. Yuran, V.P. Usoltsev, D.N. Shulmin.
System of Laser Monitoring of Water Pollution with Application
of Relative Description of Signal Shape.
Приборы и методы измерений.
2020. – Т. 11, № 2. – С. 114–121.
DOI: 10.21122/2220-9506-2020-11-2-114-121

For citation:

V.A. Alekseev, S.I. Yuran, V.P. Usoltsev, D.N. Shulmin.
System of Laser Monitoring of Water Pollution with Application
of Relative Description of Signal Shape.
Devices and Methods of Measurements.
2020, vol. 11, no. 2, pp. 114–121.
DOI: 10.21122/2220-9506-2020-11-2-114-121

Система лазерного мониторинга загрязнений водной среды с применением относительного описания формы сигналов

В.А. Алексеев¹, С.И. Юран², В.П. Усольцев¹, Д.Н. Шульмин¹

¹Ижевский государственный технический университет имени М.Т. Калашникова,
ул. Студенческая, 7, Ижевск 426069, Россия

²Ижевская государственная сельскохозяйственная академия,
ул. Студенческая, 11, Ижевск 426069, Россия

Поступила 16.03.2020

Принята к печати 18.05.2020

Как правило, система очистки сточных вод не рассчитана на фильтрацию веществ, образованных в результате запроектной аварии. Характер запроектной аварии связан с кратковременным появлением сгустка этих веществ в сточных водах, определяемый объёмом ёмкости хранения веществ. Поэтому рациональным подходом является отведение этой порции образовавшихся веществ в отдельную ветвь сточной системы или отстойники. Целью работы являлась реализация указанного подхода путем создания системы лазерного мониторинга загрязнений водной среды.

В статье предлагается система автоматического обнаружения сгустка аварийного сброса загрязняющих веществ в сточные воды промышленного предприятия. Приведена структурная схема системы и назначение основных её элементов. Система должна обеспечить обнаружение сгустков в реальном масштабе времени. Для обеспечения этой функции предварительно проводится исследование спектральных характеристик всех веществ, возможных к появлению в сточных водах в случае аварийной ситуации.

На основании этих данных выбираются длины волн лазерного излучения в системе. Полученные данные измерений от нескольких зондов представляются в виде решётчатой функции, которая переводится в относительное описание, представляющее матрицу отношения порядка на множестве составляющих решётчатой функции. Относительное описание инвариантно к линейным изменениям решётчатой функции. Решение об обнаружении какого-либо вещества из аварийных сбросов принимается на основании сравнения относительного описания измерений с эталонами, подготовленными на стадии настройки системы.

Приведён пример формирования эталонов для аварийных сгустков из глицерина и аллилового спирта. Приведены графики решётчатых функций, полученных из ИК-спектров аварийных сбросов этих веществ; алгоритмы построения решётчатой функции и сравнения решётчатых функций.

Таким образом, с помощью разработанного математического описания формы цифровых сигналов на основе относительного описания может быть описан сигнал кривой мониторинга в виде кривой изменения оптической плотности водной среды.

Ключевые слова: аварийные сбросы, сгусток, спектроскопия, лазерный зонд, относительное описание.

DOI: 10.21122/2220-9506-2020-11-2-114-121

Адрес для переписки:

С.И. Юран
Ижевская государственная сельскохозяйственная академия,
ул. Студенческая, 11, Ижевск 426069, Россия
e-mail: yuran-49@yandex.ru

Address for correspondence:

S.I. Yuran
Izhevsk State Agricultural Academy,
Studencheskaya str., 11, 426069, Izhevsk, Russia
e-mail: yuran-49@yandex.ru

Для цитирования:

V.A. Alekseev, S.I. Yuran, V.P. Usoltsev, D.N. Shulmin.
System of Laser Monitoring of Water Pollution with Application
of Relative Description of Signal Shape.
Приборы и методы измерений.
2020. – Т. 11, № 2. – С. 114–121.
DOI: 10.21122/2220-9506-2020-11-2-114-121

For citation:

V.A. Alekseev, S.I. Yuran, V.P. Usoltsev, D.N. Shulmin.
System of Laser Monitoring of Water Pollution with Application
of Relative Description of Signal Shape.
Devices and Methods of Measurements.
2020, vol. 11, no. 2, pp. 114–121.
DOI: 10.21122/2220-9506-2020-11-2-114-121

Introduction

Wastewater monitoring of enterprises is carried out by periodic sampling, processing and analysis of samples in laboratories. To study the parameters of wastewater, electrochemical, pyro-UV-fluorescence, thermocatalytic, photometric methods and others are used [1]. A characteristic feature of known research is the inability to conduct research in real time.

In the case of spectral analysis methods, research is usually carried out by sequentially scanning the sample with optical radiation with different wavelengths, which does not allow for real-time

Various types of analytical equipment and complexes for physicochemical measurements are known, adapted to specific working conditions at chemical and petrochemical enterprises, pipeline systems, as well as in the metallurgical and processing industries. Among them are complexes for continuous monitoring of process safety and environmental monitoring. The main requirements for such complexes:

- automatic sampling;
- fast automatic analysis;
- automated or automatic control.

Known automated viscometers, densitometers, refractometers, photometers, laser analyzers of the parameters of the aquatic environment [2]. Examples of such analyzers are IR analyzers in the wavelength range up to 4000 nm, for example, a *PIONIR 1024* spectrophotometer from *AIT*, *M412* from *Guided Wave*, *MATRIX-F* from *BRUKER* [2] and others.

Laboratory instruments for sample analysis have several disadvantages:

- lack of measurement continuity;
- time delay associated with sample delivery, measurement and data processing;
- the possibility of losing the properties of the investigated material in the samples;
- the inability to automate the full monitoring cycle.

Although the known devices and complexes have high accuracy and the ability to measure many parameters of aqueous media, such as equipment of the German company Hach [3], they do not allow real-time detection of emergency discharge of pollutants and prevent its entry into the system sewage enterprise.

Optical spectroscopy eliminates the above disadvantages, which makes it possible to create complexes of continuous measurement in real time and to automate monitoring of environmental

studies. The aim of the work was to implement this approach by creating a laser monitoring system for water pollution.

The basic principles of the system

As a rule, the wastewater treatment system is not designed to filter substances formed as a result of beyond design basis accident [4–7]. The nature of the beyond design basis accident is associated with the shortterm appearance of a clot of these substances in wastewater, determined by the volume of the storage capacity of the substances. Therefore, a rational approach is to divert this portion of the formed substances into a separate branch of the sewage system or sedimentation tanks.

To implement this approach, at the first stage, it is necessary to determine the type of substance from the list of all substances stored at the enterprise in order to divert the clot to another selected branch of the sewage pipe in real time.

To ensure clot detection in real time, it is proposed to use a system for laser monitoring of water pollution based on parallel optoelectronic spectroscopy with many laser probes [8–13].

For this, a preliminary study of the spectral characteristics of all substances stored in the factory is carried out. Separate points on the spectral curves (for example, extrema) are selected from the obtained absorption or transmission spectra. Of these, several points (at least two or three points) for each of the substances are distinguished. The obtained values of the absorption wavelengths for all substances are taken as Wastewater sensing scale to determine the type of substance. Moreover, each substance has its own portrait of the emission spectrum at all sensing wavelengths. The obtained portraits of the spectra are the standards for determining the substance.

The portrait of a substance can be represented in the form of the lattice function $LF_i \{L_1, L_2, \dots, L_n\}$, where L_n is the value of the spectrum at a wavelength n from a set of probe laser radiation. We get k lattice functions, where $i = 1, k$ is the number of standards.

The wavelengths of individual laser probes will be finally determined on the basis of the available wavelengths of laser diodes or lasers existing for a given period. Therefore, it is necessary to refine the portrait of the substance and present it in the form of a lattice function of the LF .

One of the problems of real-time diagnostics of a substance is a significant spread of the spectrometry values due to an unknown concentration

of the substance in the clot and deviations in the radiation wavelength associated with the choice of a specific laser probe.

However, the relation between the main components of the portraits of the spectrum of a substance is invariant to linear changes.

Figure 1 shows a diagram of a diagnostic system for the emergency discharge of substances in the enterprise's wastewater treatment system.

The device registers a change in the optical density of wastewater in a selected range of radiation wavelengths. The spectrometry data processing system forms a lattice function, which is continuously compared with the standards.

When an emergency discharge of a certain type is detected, a control signal is received for the valves, which change the direction of movement of the wastewater in the wastewater system, directing the emergency discharge to a special filter or sump.

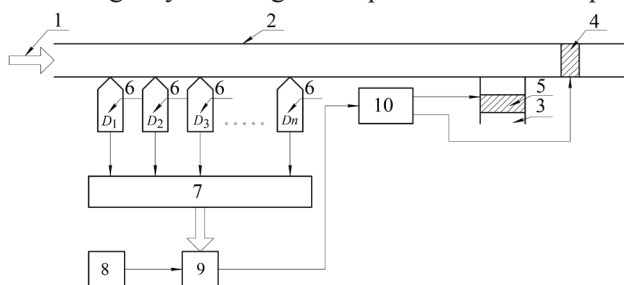


Figure 1 – Diagram of the system for diagnostics of emergency discharge of substances in the wastewater treatment system of an enterprise: 1 – wastewater; 2 – channel for the movement of wastewater; 3 – branch; 4 – general filter; 5 – an additional filter installed in the branch; 6 – laser probes $D_1, D_2, D_3, \dots, D_n$ with emission wavelength $\{1, 2, 3, \dots, n\}$; 7 – a diagram of recording and processing spectrum components; 8 – block standards; 9 – flaps control diagram

In order to provide real-time diagnostics of the emergency discharge portrait, the lattice function is transformed using a relative description into a homomorphic etalon of the relationship matrix in the form of two diagonals (main and adjacent diagonals) [14, 15].

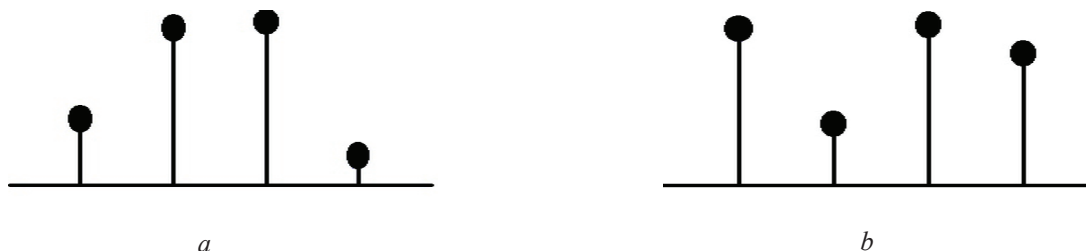


Figure 4 – Graphs of lattice functions of glycerin (a) and allyl alcohol (b) and their main diagonals of matrixes of the relations

$$R^I = \{S_1 R_{12} S_2, S_2 R_{23} S_3, S_3 R_{34} S_4, \dots, S_{n-1} R_{(n-1)n} S_n\};$$

$$R^{II} = \{S_1 R_{13} S_3, S_2 R_{24} S_4, S_3 R_{35} S_5, \dots, S_{n-2} R_{(n-2)n} S_n\},$$

where R_t^I, R_t^{II} are the current values of the relative description, which are equal in the number of components to the standards and which change their components over time. If the current descriptions of R_t^I, R_t^{II} coincide with the standards R^I and R^{II} , a decision is made about the presence of a clump of emergency discharge in the sewer.

An example of setting the basic system parameters

Consider an example. Let there be two clots: one clot of glycerol, the other – allyl alcohol. Considering the IR spectra of these substances (Figures 2, 3), the following characteristic points can be distinguished. For glycerin, this is 800 nm, 1000 nm, 1500 nm, 3500 nm. For allyl alcohol, we select the same points – 800 nm, 1000 nm, 1500 nm, 3500 nm. In this case, the lattice functions for these substances will differ (Figure 4). The main diagonals of the relationship matrix in the form of depicting numbers will also differ.

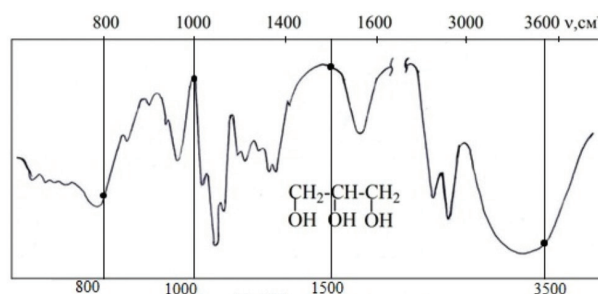


Figure 2 – IR spectrum of glycerin

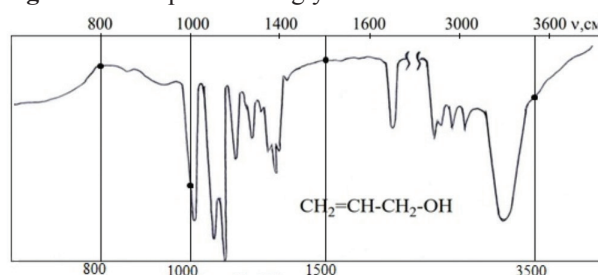


Figure 3 – IR spectrum of allyl alcohol

In this example, four probes are used at selected wavelengths. The wavelengths for each substance may vary. In this case, we get the maximum number of probes at four identification points, namely, 4 probes. When choosing laser diodes with a power of 100–300 mW, we select the wave-lengths: 792 nm, 905 nm, 1550 nm and 3500 nm.

Algorithm for constructing the lattice function of the measured spectrum

An algorithm for constructing a lattice function is developed. The scheme of the algorithm is shown in Figure 5 [16].

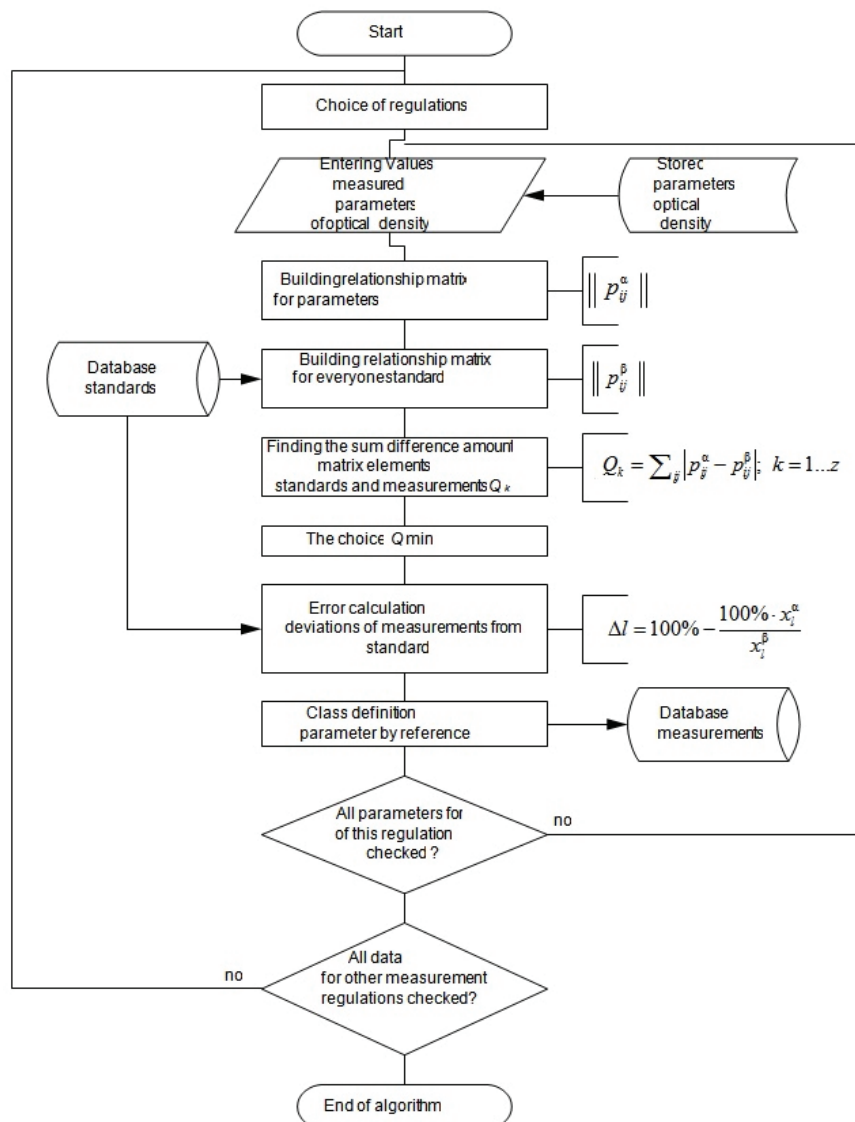


Figure 5 – Scheme of work of an algorithm

Input data: a database for storing information about measurements of the optical density of the water environment containing emergency discharges (clots), their parameters and standards.

Output data: It is necessary to determine the class of the curve for each measured trend of optical density.

Calculation algorithm: measurement regulations is selected from a variety of Reg. Values are entered for all parameters of the optical density of this

regulation (values for the selected wave-lengths of the probes).

There will be 2 ways to enter data in the system:

- a) data input manually;
- b) loading measurements automatically from the generated file.

1. A relationship matrix is constructed by measured values $\|p_{ij}^{\alpha}\|$ for one measurement $n \times n$, where n is the number of optical density parameters, according to the rule:

$$P_{ij} = \begin{cases} 0, & X_i R X_j \\ 1, & \neg(X_i R X_j) \end{cases}, i=1...n-1, i < j < n,$$

where P_{ij} is the element of the relationship matrix; X_i, X_j – elements of the set M (the set of values of the parameters of optical density); $R, \neg R$ – the ratio between the elements of the set (R = "more", $\neg R$ = "not more").

Relationship matrix $\|P_{ij}\|$ presented as follows:

$$\|P_{ij}\| = [R] = \begin{bmatrix} X_1 R_{11} X_1 & X_1 R_{12} X_2 & \dots & X_1 R_{1n} X_n \\ X_2 R_{21} X_1 & X_2 R_{22} X_2 & \dots & X_2 R_{2n} X_n \\ \dots & \dots & \dots & \dots \\ X_n R_{n1} X_1 & X_n R_{n2} X_2 & \dots & X_n R_{nn} X_n \end{bmatrix} = \begin{bmatrix} P_{11} & P_{12} & \dots & P_{1n} \\ P_{21} & P_{22} & \dots & P_{2n} \\ \dots & \dots & \dots & \dots \\ P_{n1} & P_{n2} & \dots & P_{nn} \end{bmatrix}.$$

2. A relationship matrix is constructed for each standard $\|P_{ij}^\beta\|$ for a given parameter according to the selected regulation.

3. The sum of the differences of the elements of the diagonals of the two matrices – the measured and the standard:

$$Q_k = \sum_{ij} |p_{ij}^\alpha - p_{ij}^\beta|, k=1...z,$$

where $\|p_{ij}^\alpha\|$ is the element of the relationship matrix of measured values; $\|P_{ij}^\beta\|$ – an element of the relationship matrix of the standard; z is the number of standards for the k -th parameter.

Choose $Q = \min(Q_k)$ for the most accurate definition of the standard.

4. The error of measurement deviation from the standard is calculated. The deviation error for each parameter is found:

$$\Delta l = 100\% - \frac{100\% \cdot x_l^\alpha}{x_l^\beta},$$

where Δl is the error of deviation of the measured value from the standard in l -parameter; x_l^α – value of the measured l -parameter; x_l^β – the value of the standard l -parameter.

The average deviation error is determined for all parameters:

$$\Delta_a = \frac{\sum_{i=1}^n \Delta l_i}{n}.$$

Selected $\Delta = \min(\Delta_a)$ for the most accurate definition of the standard.

So, the standard is selected by comparing the relationship matrices and determining the deviation error.

5. The actions of p. 3 – p. 6 are performed for each parameter according to the selected regulation. The calculated values are written to the database.

6. At the output of the algorithm, we obtain the class of standards of the optical density parameter with a known value that most closely matches the measurement parameters. The calculated values are written to the database in the following form: <Date, Regulation, Parameter, Type of emergency>.

As a result of the classification, each measured parameter, with the selected procedure, is brought into correspondence with the standard value of the optical density parameter for this type of accident.

If the relationship matrices of different orders or the function in question is periodic, or the origin of its values is shifted, then in this case it is necessary to provide for the possibility of transforming the relationship matrices corresponding to the rearrangement of the first elements of the lattice function at the end. The description of the comparison function of two matrices during the implementation of the algorithm (Figure 6) can be constructed as follows. Pointers to the relationship matrices are fed to the input, the matrix with the highest dimension is selected from them. At the output of the function, the ratio of the maximum number of matches to the number of elements of the smaller relationship matrix is obtained. The considered algorithm is implemented program-matically [17].

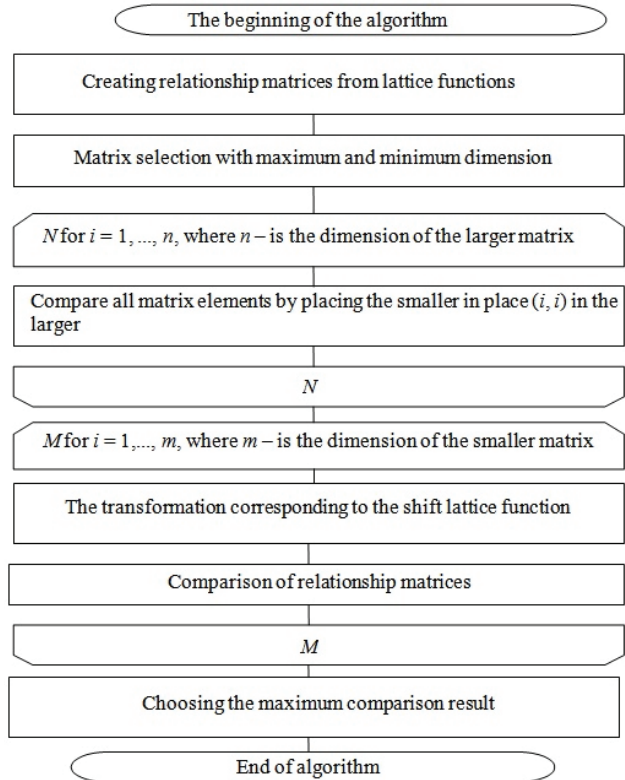


Figure 6 – General algorithm for comparing lattice functions

Thus, using the developed mathematical description of the shape of digital signals based on the relative description, the signal of the monitoring curve can be described in the form of a curve of the optical density of an aqueous medium.

Conclusion

The considered approach to constructing a system for detecting emergency discharges into the wastewater of an industrial enterprise is applicable in various branches of the engineering, processing and chemical industries. Application of the considered system allows reducing the likelihood of pollution of water bodies in the event of an emergency at the production.

To ensure the detection of emergency discharges in real time, it is proposed to use parallel spectroscopy of substances by several laser probes. In each particular case, the wavelengths of the laser probes will be different. For this, a preliminary study of the spectra of substances for choosing wavelengths for the detection of emergency discharges is proposed.

To ensure the invariance of the description of the spectra of substances, it is proposed to use a relative description representing the elements of the relationship matrices of the components of the measured points of the spectrum of substances that are invariant to linear changes in the amplitudes of the components of the spectrum, depending on the concentration of the detected substances in the clots of emergency discharges.

A relative description in the form of relationship matrices, in contrast to an analytical description, is a qualitative description and allows you to describe the shape of the measuring signal with an error determined by the completeness of the elements of the relationship matrix. The use of depicting numbers to describe the relationship matrix allows binary logic to be used for presentation in computer systems.

References

1. Drugov Yu.S., Rodin A.A. *Ekologicheskie analizy pri razlivah nefi i nefteproduktov* [Environmental analyses in oil and oil product spills]. Moscow, BINOM. Knowledge lab Publ., 2014, 270 p.
2. Kopyltsova A.B., Tarasov B.P., Klim O.V. Modern practice and problems when using industrial and laboratory spectrophotometer analyzers of the physicochemical properties of petroleum and petroleum products. *Measurement techniques*, 2013, vol. 56, no. 3, pp. 322–327. DOI: 4 <https://doi.org/10.1007/s11018-013-0203-4>
3. Website of Hach Company. TU5300sc / TU5400sc Online Laser Turbidity Analyzers. Available at: <https://www.hach.com/turbidity-analyzers/tu5300sc-tu5400sc>. (accessed 03.04.2020).
4. Akimov V.A. *Prirodnye i tekhnogennye chrezvychajnye situacii: opasnosti, ugrozy, riski* [Natural and technogenic emergencies: dangers, threats, risks]. Moscow, Delovoy Express Publ., 2001, 341 p.
5. Bonitenko Y.Y., Nikiforov A.M. *CHrezvychajnye situacii himicheskoy prirody* [Emergency chemical nature]. Saint Petersburg, Hippocrates Publ., 2004, 464 p.
6. Gabrichidze T.G. *Osnovy kompleksnoj sistemy bezopasnosti kriticheski vaznykh (potencial'no opasnykh) ob"ektov municipal'nogo i regional'nogo urovnej* [Fundamentals of the integrated security system of critically important (potentially dangerous) objects of municipal and regional levels]. Samara, SamNC RAS Publ. House, 2012, 390 p.
7. Shahmaryan M.A., Akimov V.A., Kozlov K.A. [Ural region of Russia – natural, man-made and environmental hazards]. *Ekologiya i promyshlennost' Rossii* [Ecology and industry of Russia], 2002, no. 3, pp. 4–8 (in Russian).
8. Obukhov A.E. Optical spectroscopy and the structure of polyfunctional hydrocarbon compounds and oil products. *Optics and Spectroscopy*, 2018, vol. 124, no. 5, pp. 696–702. DOI: <https://doi.org/10.1134/S0030400X18050168>
9. Penkovsky A.I., Nikolaev V.F., Borovkova N.S. New optical methods and devices for analyzing the quality of motor fuels. *Journal of Optical Technology*, 2016, vol. 83, no. 4, pp. 244–248. DOI: <https://doi.org/10.1364/JOT.83.000244>
10. Venzel' V.I., Gorelov A.V., Egorova E.S., Kuznetsova N.Ya., Lavrent'ev, E.S. Obraztsov V.S., Sinel'nikov M.I. Monitoring the optical homogeneity of materials for the IR region. *Journal of Optical Technology*, 2014, vol. 81, no. 9, pp. 551–555. DOI: <https://doi.org/10.1364/JOT.81.000551>
11. Deck L. Multiple surface phase-shifting interferometry. *Proc. SPIE 4451, Optical Manufacturing and Testing IV*, 2001, pp. 424–431. DOI: <https://doi.org/10.1117/12.453640>
12. Divyanin N.N., Rukosueva E.A., Garmash A.V., Beklemishev M.K. Recognition of model analyte mixtures in the presence of blood plasma using a mixture of fluorophores ("Fluorescent tongue"). *Journal of Analytical Chemistry*, 2018, vol. 73, pp. 1195–1201. DOI: <https://doi.org/10.1134/S1061934818120043>
13. Bhargava R. Infrared Spectroscopic Imaging: The Next Generation. *Applied Spectroscopy*, 2012, vol. 66, no. 10, pp. 1091–1120. DOI: 10.1366/12-06801

14. SHrejder YU.A. *Logika znakovyh sistem: elementy semiotiki* [Logic of sign systems: elements of semiotics]. Moscow, Librocom Publ., 2012, 64 p.

15. Alekseev V.A., Dizendorf K.I., YUran S.I. [Classifier of pulse curves using ratio matrices]. *Intellektual'nye sistemy v proizvodstve* [Intelligent systems in manufacturing], 2010, no. 1(15), pp. 231–235 (in Russian).

16. Yannikov I.M., Alekseev V.A. [Construction of a classifier of lattice functions for a relative description of the results of biomonitoring of potentially dangerous

objects]. *Intellektual'nye sistemy v proizvodstve* [Intelligent systems in manufacturing], 2009, no. 2(14), pp. 10–13 (in Russian).

17. Alekseev V.A., Usoltsev V.P., Yuran S.I., Shulmin D.N. [An automated system of volley water pollution control by optical methods]. *Vestnik Permskogo nacional'nogo issledovatel'skogo politekhnicheskogo universiteta. Prikladnaya ekologiya. Urbanistika* [PNRPU. Applied ecology. Urban development], 2018, no. 3, pp. 119–132 (in Russian).

DOI: 10.15593/2409-5125/2018.03.10

Assessment of Temperature Effects in Interior Orientation Parameters Calibration of Optoelectronic Devices

M.A. Starasotnikau

JSC “Peleng”,
Makayonka str., 2, Minsk 220114, Belarus

Received 30.03.2020

Accepted for publication 22.05.2020

Abstract

A digital micromirror device (DMD) micromirrors periodic spatial structure is a measuring scale in interior orientation parameters calibration of optoelectronic devices problems, when using a DMD as a test-object. It is important that DMD micromirrors periodic spatial structure remains constant. Change in a DMD micromirrors spatial structure may occur due to heating. In addition to heating a DMD, an optoelectronic device photodetector is also subject to heating and, accordingly, change in its spatial structure. It is necessary to estimate change in a spatial structure of DMD micromirrors and an optoelectronic device photodetector.

A DMD micromirrors spatial drift and a DMD micromirrors spatial drift together with a digital camera photodetector pixels spatial drift for operation 4 h are analyzed. The drift analysis consisted in the points array position assessing formed by a DMD and projected onto a digital camera. When analyzing only a DMD micromirrors drift, a digital camera was turned on only for shooting time for exclude digital camera influence. A digital camera did not have time to significantly heat up, during this time. After a digital camera it cooled to a room temperature.

Average drift of all DMD micromirrors determines the accuracy of interior orientation parameters calibration of optoelectronic devices using a DMD in time. Maximum drift of all micromirrors after switching on is observed. Minimum DMD warm-up time is 60 min for average drift of all micromirrors less than 1 μm is necessary. Minimum DMD warm-up time is 120 min when using a DMD together with a digital camera is necessary.

A DMD expansion uniformity determines the accuracy of interior orientation parameters calibration of optoelectronic devices using a DMD, because irregular expansion disturbs micromirrors periodicity. The average change in distance of neighboring points is less than 0.1 μm for every 20 min.

Thus, a DMD can be used as a test-object in interior orientation parameters calibration of optoelectronic devices. The results can be used as compensation coefficients of change in DMD micromirrors spatial structure due to temperature effects during operation, if more accurate are necessary.

Keywords: DMD, optoelectronic device, interior orientation parameters, photodetector, temperature drift.

DOI: 10.21122/2220-9506-2020-11-2-122-131

Адрес для переписки:

Н.О. Старосотников
ОАО «Пеленг»,
ул. Макаенка, 25, г. Минск 220114, Беларусь
e-mail: starasotnikau@gmail.com

Address for correspondence:

M.A. Starasotnikau
JSC “Peleng”,
Makayonka str., 2, Minsk 220114, Belarus
e-mail: starasotnikau@gmail.com

Для цитирования:

M.A. Starasotnikau.
Assessment of Temperature Effects in Interior Orientation
Parameters Calibration of Optoelectronic Devices.
Приборы и методы измерений.
2020. – Т. 11, № 2. – С. 122–131.
DOI: 10.21122/2220-9506-2020-11-2-122-131

For citation:

M.A. Starasotnikau.
Assessment of Temperature Effects in Interior Orientation
Parameters Calibration of Optoelectronic Devices.
Devices and Methods of Measurements.
2020, vol. 11, no. 2, pp. 122–131.
DOI: 10.21122/2220-9506-2020-11-2-122-131

УДК 681.2.083, 681.786

Оценка влияния температурных эффектов в схемах геометрической калибровки оптико-электронных аппаратов

Н.О. Старосотников

ОАО «Пеленг»,
ул. Макаенка, 25, г. Минск 220114, Беларусь

Поступила 30.03.2020

Принята к печати 22.05.2020

При использовании цифрового микрозеркального устройства (*Digital Micromirror Device* – DMD) в качестве тест-объекта, периодическая структура микрозеркал которого является измерительной шкалой, в частности, в задачах геометрической калибровки оптико-электронных аппаратов (ОЭА), важно, чтобы пространственная структура микрозеркал оставалась постоянной. Изменение пространственной структуры может произойти из-за нагрева. Помимо нагрева DMD, фотоприёмник ОЭА также подвержен нагреву, и соответственно изменению его пространственной структуры. Цель работы заключалась в оценке величины изменения пространственной структуры DMD и фотоприёмника ОЭА.

Проведён анализ пространственного дрейфа микрозеркал DMD и пространственного дрейфа микрозеркал DMD совместно с пространственным дрейфом пикселей фотоприёмника цифровой камеры за 4 ч работы. Анализ дрейфа заключался в оценке положения массива точек сформированного DMD и спроецированного на цифровую камеру. Для исключения влияния цифровой камеры при анализе дрейфа обусловленного микрозеркалами DMD цифровая камера включалась только в течении съёмки. За это время цифровая камера не успевала существенно нагреться. После чего она остывала до температуры помещения.

Средняя величина дрейфа всех микрозеркал влияет на точность при необходимости геометрической калибровки ОЭА при помощи DMD длительное время. После включения наблюдается максимальный дрейф всех микрозеркал. Чтобы средняя величина дрейфа всех микрозеркал была не более 1 мкм необходимо минимальное время прогрева DMD – 60 мин. При использовании DMD совместно с цифровой камерой требуемое минимальное время прогрева DMD – 120 мин.

Равномерность расширения DMD будет определять точность геометрической калибровки ОЭА с помощью DMD, поскольку при неравномерном расширении будет нарушаться периодичность микрозеркал, т. е. не будет известно взаимное расположение микрозеркал друг относительно друга. Среднее изменение расстояний между соседними точками – не более 0,1 мкм за каждые 20 мин работы.

Таким образом, DMD можно использовать в качестве тест-объекта в задачах геометрической калибровки ОЭА. При необходимости более точных геометрических калибровок ОЭА полученные результаты можно использовать в качестве коэффициентов компенсации изменения пространственной структуры DMD из-за температурных эффектов в процессе работы.

Ключевые слова: геометрическая калибровка, оптико-электронный аппарат, температурный дрейф, фотоприёмник, цифровое микрозеркальное устройство.

DOI: 10.21122/2220-9506-2020-11-2-122-131

Адрес для переписки:

Н.О. Старосотников
ОАО «Пеленг»,
ул. Макаенка, 25, г. Минск 220114, Беларусь
e-mail: starasotnikau@gmail.com

Address for correspondence:

M.A. Starasotnikau
JSC “Peleng”,
Makayonka str., 2, Minsk 220114, Belarus
e-mail: starasotnikau@gmail.com

Для цитирования:

М.А. Старосотников.
Assessment of Temperature Effects in Interior Orientation
Parameters Calibration of Optoelectronic Devices.
Приборы и методы измерений.
2020. – Т. 11, № 2. – С. 122–131.
DOI: 10.21122/2220-9506-2020-11-2-122-131

For citation:

M.A. Starasotnikau.
Assessment of Temperature Effects in Interior Orientation
Parameters Calibration of Optoelectronic Devices.
Devices and Methods of Measurements.
2020, vol. 11, no. 2, pp. 122–131.
DOI: 10.21122/2220-9506-2020-11-2-122-131

Introduction

When using a digital micromirror device (*Digital Micromirror Device* – DMD) as a test-object, the micromirror sizes of which are a measuring scale, in particular in the problems of interior orientation parameters calibration of optoelectronic devices [1–2] it is important that the spatial structure of micromirrors remains constant. The spatial structure of micromirrors may be disturbed due to heating during operation and, accordingly, expansion of the CMOS matrix, in the cells of which micromirrors are installed [3]. The change in the spatial structure of micromirrors can be compensated. With uniform expansion, this can be done with a single scale factor or a scale factor horizontally and vertically. It is more difficult to compensate for uneven expansion; this requires a polynomial for each DMD section, depending on the duration of the DMD operation. Shifting all DMD micromirrors in one direction affects interior orientation parameters over time. Thus, to assess the possibility of using DMD as a device, which is a test-object for interior orientation parameters calibration of optoelectronic devices, it is necessary to evaluate the change in the spatial structure of DMD depending on the duration of operation, as well as the possibility of compensation. A change in the spatial structure of less than 1 μm is acceptable for most tasks of interior orientation parameters calibration of optoelectronic devices and is comparable in accuracy with high-precision two-coordinate stages [4] in which you can install a test-object in the form of a glass plate with a pattern deposited on it with a photolithographic method and use it for interior orientation parameters calibration of optoelectronic devices.

In problems of interior orientation parameters calibration of optoelectronic devices, the matrix structure of the photodetector is also a measuring scale [5]. In addition to heating the DMD, the optoelectronic device photodetector is also subject to heating, and, accordingly, to a change in its spatial structure. The purpose of the investigations was the need to estimate the value of the change in spatial structure of the photodetector calibrated by the optoelectronic device so as not to set excessive requirements on the accuracy of measuring the distortion of the lens, since its value may exceed the change in the spatial structure of the photodetector during the calibration time and the operation of the optoelectronic device as intended. This assessment will make it possible to decide on the duration

of operation during which a change in the spatial structure of the optoelectronic device photodetector is acceptable, as well as on the need for an additional cooling system for the optoelectronic device photodetector.

Description of scheme

Calibration consists in projecting a test array consisting of a matrix of points with a constant distance between points on the camera photodetector and assessing the change in the distance between points over a long time of DMD operation, which will change due to heating of the DMD. The DMD calibration pattern is similar to interior orientation parameters calibration of optoelectronic devices [6, 7]. In this case, the DMD lens–camera lens system magnify the DMD image 3–5 times to increase all DMD manufacturing errors, whereas in to interior orientation parameters calibration of optoelectronic devices schemes it is customary to use the collimator–optoelectronic device lens system that reduces the image 3–1 times to reduce the effect of manufacturing errors: alignment, calibration of the collimator.

The realized calibration scheme, block diagram of which is shown in Figure 1, and calibration test set-up in Figure 2, includes the *DLP LightCrafter 4500*, $f' = 500$ mm lens, which projects the *DLP LightCrafter 4500* image into the collimator. *DLP LightCrafter 4500* includes a DMD that is illuminated by an illumination system. In the *DLP LightCrafter 4500*, whose appearance during operation is shown in Figure 3, the full-time lens is removed. Instead of a full-time test-object, a *Basler ace acA2040-90 um* (CMOS photodetector CMOSIS CMV4000) [8] camera is installed in the collimator. The collimator housing is made of invar and has a low coefficient of linear expansion, and the $f' = 1500$ mm collimator lens is designed and constructed in such a way as to ensure minimum thermal stability, i. e. the mounting materials of the optical components compensate for the effect of temperature changes on the optical components, which ensures the stability of optical characteristics. This ensures stability in the first place, the position of the focal plane of the collimator lens $f' = 1500$ mm relative to the plane of the camera photodetector.

DMD is a bistable spatial light modulator, including an array of rotating micromirrors functionally installed in memory cells on a CMOS matrix. The CMOS matrix controls the position of

the micromirrors. It is possible to control the position of the micromirrors using software and thus form the desired pattern, which can be used as a test-

object. Since micromirrors are installed in the cells of the CMOS matrix, the DMD is characterized by thermal effects like cameras with CMOS photodetectors.

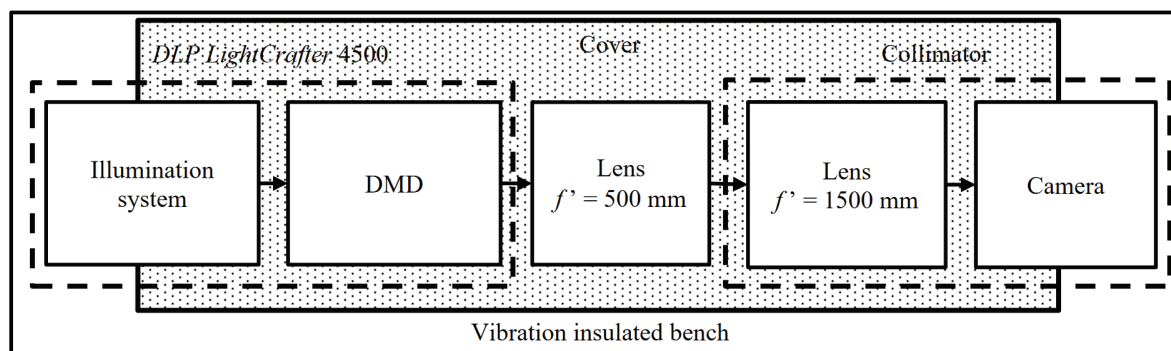


Figure 1 – Calibration block diagram

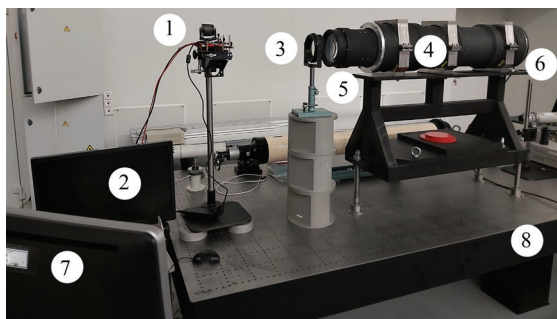


Figure 2 – Calibration test set-up (cover not shown): 1 – DLP LightCrafter 4500; 2 – DLP LightCrafter 4500 control PC; 3 – lens $f' = 500$ mm; 4 – collimator; 5 – lens $f' = 1500$ mm; 6 – camera; 7 – camera control PC; 8 – vibration isolation bench

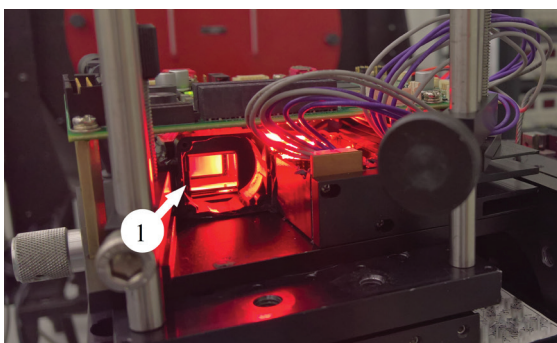


Figure 3 – DLP LightCrafter 4500 in operation (full-time lens is removed): 1 – exit window of DLP LightCrafter 4500, illumination from DMD

To eliminate distortions in the optical path of the calibration scheme due to air refraction, the optical path is closed by the cover. The use of the cover removes the influence of the movement of air masses in the room on the calibration process. The cover is installed so that the calibration schemes of the illuminator and camera parts that are not

included in the optical path remain open. This is necessary to freely remove the heat generated by them during calibration. In addition, the cover must be porous to ensure heat removal from the optical path, as well as to eliminate stagnation of air masses. The room temperature requirements [5] are the same as for interior orientation parameters calibration of optoelectronic devices¹. Changes in temperature in the room are minimized (during the measurement period they were no more than 0.1 °C). To reduce the effect of vibrations, the calibration scheme is mounted on a vibration isolation bench. The described methods for removes the influence of external factors make it possible to bring the calibration closer to ideal conditions and directly measure the temperature drift.

Description of methodology

Calibration of DMD

1. DMD, lens $f' = 500$ mm, collimator are visually aligned.

2. Camera and DLP LightCrafter 4500 turns on. Pattern of the test-object with a required period and the size of points is loaded into DMD.

3. Illuminator current value of DLP LightCrafter 4500 or camera exposure is determined, to provide illumination of the camera photodetector at the level of 80–90 % of the value of its saturation capacity. Several layers of astrolon are installed in the illumination system when the adjustment range of the illuminator

¹ GOST 8.050-73 State system for ensuring the uniformity of measurements. Normal conditions for linear and angular measurements (with Change No. 1)

current is insufficient, which works like frosted glass reduces luminous flux by about 50 % and makes it uniform. The frequency of micromirrors operation is selected together with the illuminator current value so that, due to an synchronization error of the operation of individual micromirrors or micromirrors blocks of the DMD and because of inconsistency in the frequency of operation of the DMD and the camera, flicker is not observed. It is checked that the test-object pattern is not formed by non-working micromirrors (micromirrors that do not change position from the nominal state to the working state, for *DLP LightCrafter* 4500 no more than 10 pieces on DMD), if necessary, a test-object pattern shifted by several micromirrors is loaded in the DMD.

4. The image from the camera's photodetector achieves the location of the DMD pattern in the center of the focal plane by turning the collimator around three axes. 25 points of the DMD pattern are projected onto the camera.

5. Camera and *DLP LightCrafter* 4500 turn off and cool to room temperature.

6. *DLP LightCrafter* 4500 turns on.

7. Camera turns on. 100 frames of the DMD pattern are shot at a frequency of 90 frames/s. After shooting, the camera immediately turns off, i. e. power is removed from it. This allows us to exclude the influence of the temperature drift of the camera when analyzing the temperature drift of DMD, since the camera does not manage to heat up significantly during this time – less than 1 min. The camera cools to room temperature.

8. Point 7 is repeated with an interval of 20 min in the first hour, 30 min – the second hour, 1 h – the remaining two hours, since at the beginning of shooting the greatest drift is observed. All time shooting 4 h.

9. Every 100 frames are averaged. The coordinates of the point centers are calculated. A drift chart of all 25 points is plotted.

Calibration of DMD with camera

1. Camera and *DLP LightCrafter* 4500 cool to room temperature.

2. Camera and *DLP LightCrafter* 4500 turns on. 100 frames of the DMD pattern are captured every minute within 4 h. After shooting, the *DLP LightCrafter* 4500 and camera turn off.

3. Every 100 frames are averaged. The coordinates of the point centers are calculated. A drift chart of all 25 points is plotted within 4 h with step

of shooting 1 min, drift analysis in intervals 20 min in the first hour, 30 min – the second hour, 1 h – the remaining two hours.

Results Processing

The resulting images are processed according to a similar algorithm [6].

1. The signal value $I_{n,m}$ in each pixel n, m is averaged for captured 100 frames.

To reduce the effect of noise on average frames, a Wiener filter of 5×5 pixels is applied and a threshold restriction is introduced [6, 9], signal values below which were taken equal to "0". The threshold value was 5 times the average value of the background signal.

2. The position of the image of one of the points of the DMD pattern on the photodetector is previously visually determined. Taking into account the known period between micromirrors [10] and magnification of system lens $f' = 500$ mm – lens $f = 1500$ mm, the preliminary coordinates of the points of the DMD pattern on the photodetector are determined, which are used to set the center of the area for calculating the exact coordinates.

3. The exact image coordinates of each point of the DMD pattern are determined by the energy center of gravity:

$$C = \begin{pmatrix} \frac{\sum_N \sum_M (I_{n,m} \cdot n)}{\sum_N \sum_M I_{n,m}} \\ \frac{\sum_N \sum_M (I_{n,m} \cdot m)}{\sum_N \sum_M I_{n,m}} \end{pmatrix},$$

where $I_{n,m}$ – the signal value in pixel n, m ; n, m – serial numbers of pixels in the columns and rows of the photodetector; N, M – the total number of columns and rows of the area of calculation of the coordinates of the center of gravity, an area of 70×70 pixels was used.

4. For each point in the DMD pattern, plots of the point position on the photodetector matrix structure are constructed at different moments of shooting within 4 h.

5. The drift value is calculated relative to the coordinates of the points on the photodetector of previous operating time intervals:

$$D_{t+1} = (C_c)_{t+1} - (C_c)_t,$$

where c – image coordinates of each point of the DMD drawing in columns and rows; $t = 0, 1, 2, \dots, 8$ – points correspond to the moments of shooting 0 min, 20 min, 40 min, 60 min, 90 min, 120 min, 180 min, 240 min operating of DMD.

6. To analyze the values and performance of the drift, the average drift value for all points, RMS and the maximum spread are calculated. The obtained values V are converted from the camera coordinate system in pixels to the DMD coordinate system:

$$V_{DMD} = V \cdot p / v,$$

where $p = 5.5 \mu\text{m}$ – pixel size of camera; $v = 3$ – magnification system of collimator lens-camera lens.

7. To analyze the relative drift, the value of the change in the distance along the rows and columns between neighboring points on the photodetector is calculated (characterizes how much the drift is the same throughout the array):

$$T_{Ns+1} = (C_c)_{Ns+1} - (C_c)_{Ns},$$

where $N_s = 0, 1, 2, \dots, 4$ row or column number. Similarly to p. 5, the value of the change in relative drift over time is calculated, Similarly to p. 6 to analyze the relative drift, the average value of the relative drift over all points, the RMS, and the maximum spread are calculated.

8. For a presentation of the drift in the plots, the drift value is increased by a selected coefficient k :

$$D_{t+1} = D_{t+1}k + (C_c)_{t+1}.$$

9. According to the obtained plots, values of average, RMS and maximum spread, one can judge the drift of DMD micromirrors and DMD micromirrors together with the pixels of a camera.

Analysis of the results

The drift of the points images formed by DMD micromirrors for 4 h in the form of a plot in the camera pixels is shown in Figure 4, its value

is shown in Table 1. The analysis was carried out for 4 h, since this time is sufficient for the DMD and the camera to reach a stable operating mode, this time is sufficient for interior orientation parameters calibration of optoelectronic devices, and this time also covers the operating time of most optoelectronic devices. It can be seen that the points drift mainly along the lines. In addition to the point drift, one can note its slight non-uniformity for different parts of the DMD micromirror array.

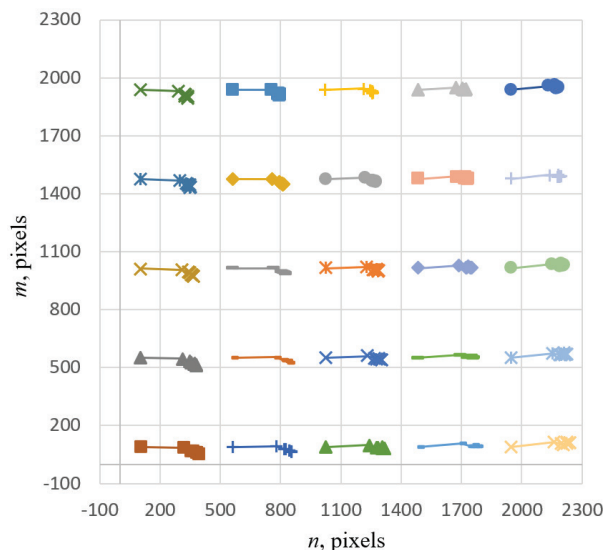


Figure 4 – Point drift due to micromirrors within 4 h (points correspond to drift after 20 min, 40 min, 60 min, 90 min, 120 min, 180 min, 240 min processing of DMD. For presentation, the drift value is increased 25 times

The average offset of all points characterizes the drift value of the entire micromirror structure of the DMD, which will affect the accuracy of the interior orientation parameters calibration of optoelectronic devices over time. If it is necessary to carry out a long time interior orientation parameters calibration

Table 1

The drift value of DMD micromirrors relative to the coordinates of the points on the photodetector of previous shooting intervals (in μm , recalculated to coordinate system of DMD)

Offset of all points		Shooting interval, min							
		0	20	40	60	90	120	180	240
By columns	Average	–	14.84	2.64	0.38	0.99	0.54	-0.19	-0.79
	RMS	–	0.65	0.13	0.08	0.31	0.26	0.09	0.03
	Max spread	–	1.99	0.37	0.26	0.92	0.80	0.33	0.11
By rows	Average	–	0.52	-0.88	-0.15	-0.14	-0.15	-0.19	0.70
	RMS	–	0.68	0.15	0.08	0.20	0.31	0.09	0.07
	Max spread	–	2.23	0.43	0.25	0.63	0.96	0.32	0.23

of optoelectronic devices, it is necessary to preheat the DMD until the drift of the micromirrors becomes such that it will not have a significant effect on the required accuracy of the interior orientation parameters calibration of optoelectronic devices. It is necessary to compensate for the value of the change in the period of micromirrors from the initial state of DMD. The analysis of Table 1 shows the predominance of column offset in the first 40 min of operation. The average drift after 20 min of operation on all points is 28 times greater than on the lines. The highest average column drift in the first 20 min of operation is up to 1.5 μm . The value of the drift of all points after 60 min of operation is less than 1 μm . The oscillation of the average drift after 60 min of operation is due mainly to random processes, primarily photodetector noise and vibrations. Thus DMD must warm up before calibrating optoelectronic device 60–120 min.

The displacement RMS of all points characterizes the uniformity of the DMD expansion, which will determine the accuracy of the interior orientation parameters calibration of optoelectronic

devices using DMD, since uneven expansion will be disrupted the periodicity of micromirrors, that is, the relative position of the micromirrors with respect to each other will not be known. The value of the RMS of all points of DMD micromirrors is less than 1 μm . The maximum spread in the first 20 min of DMD operation in rows and columns is 2 μm , the rest of the time does not exceed 1 μm . Changing the distance between neighboring points also characterizes the uniformity of DMD expansion. From Table 2 it can be seen that the average change in the distances between neighboring points is no more than 0.1 μm . Thus, we can assume that the value of the change in the distance between neighboring points is the same over the entire array of micromirrors, is negligible and is random. The distance between neighboring points does not change over time. The residual effect of the uneven expansion of DMD during interior orientation parameters calibration of optoelectronic devices using DMD can be compensated by determining the coefficients of uneven drift for each DMD micromirror.

Table 2

The change value in the distance between neighboring points on the photodetector relative to the coordinates of the points on the photodetector of previous shooting intervals (in μm , recalculated to coordinate system of DMD)

Offset of all points		Shooting interval, min							
		0	20	40	60	90	120	180	240
By columns	Average	–	-0.04	0.00	0.01	0.01	0.02	-0.05	-0.01
	RMS	–	0.02	0.01	0.00	0.01	0.02	0.02	0.02
	Max spread	–	0.09	0.04	0.02	0.03	0.05	0.07	0.05
By rows	Average	–	-0.08	0.00	0.01	-0.01	0.03	-0.06	0.05
	RMS	–	0.01	0.01	0.01	0.02	0.03	0.02	0.01
	Max spread	–	0.11	0.01	0.02	0.05	0.09	0.09	0.07

From Figure 5 the points drift within 3 h after 1 h of heating shows that the points drift 2 times more for the lower left part of the DMD than for the upper right part of the DMD. The points drift within 2 h after 2 h of heating becomes uniform. Residual non-uniform point drift can be caused by parallax, i. e. non-parallelism of the plane of the object formed by the DMD micromirrors and the plane of the camera photodetector.

The points drift due to the micromirrors of the DMD and camera pixels for 4 h in the form of a plots in the camera pixels is shown in Figure 6, its value is shown in Table 3.

Table 3 shows the prevalence of column offsets in the first 120 min of work. The average drift after 20 min of operation on all points is 8.6 times greater than on the rows. The highest average column drift in the first 20 min of operation is 17 μm . When comparing with drift only due to the DMD from Table 1, an additional influence of the camera on the points drift appeared. The value of the drift of all points after 120 min of operation is 1 μm . Thus, the DMD and the camera must be warmed up during interior orientation parameters calibration of optoelectronic devices, heated for at least 120 min. When interior orientation parameters calibration another camera or

any optoelectronic devices, it is necessary to study the drift of their photodetector matrix structure (or

several photodetectors). However, the time for preheating will be approximately the same – 120 min.

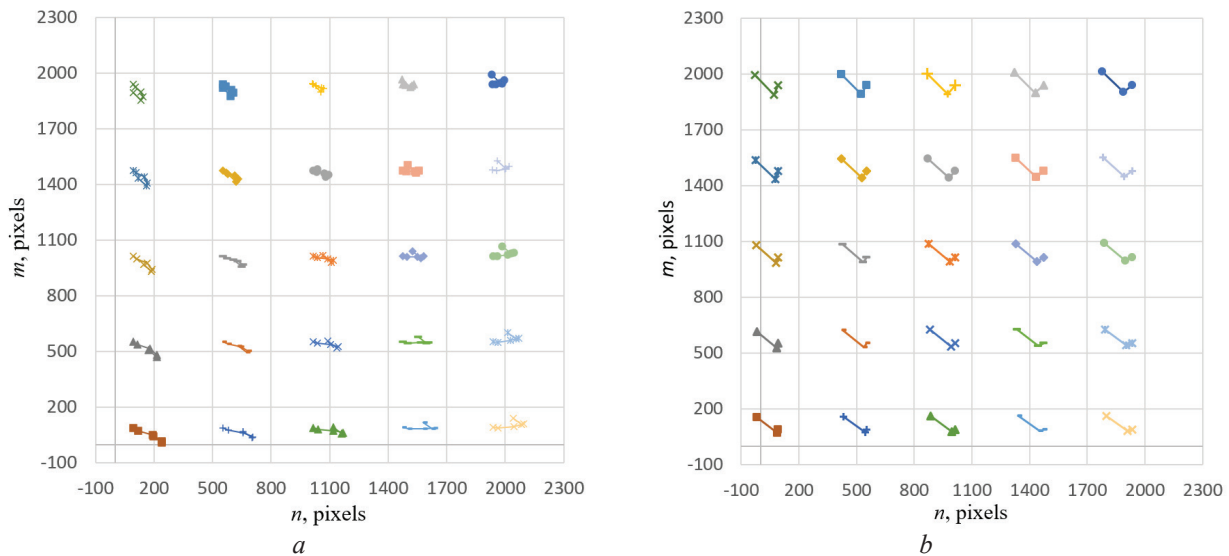


Figure 5 – Point drift due to micromirrors: *a* – within 3 h, after 1 h of operating, drift value increased 100 times; *b* – within 2 h, after 2 h of operating, drift value increased 250 times

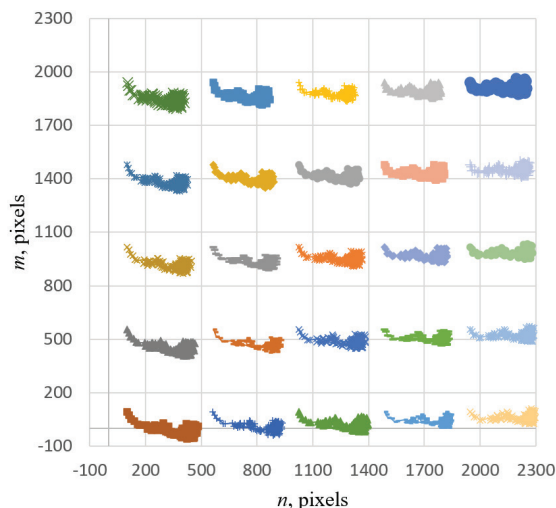


Figure 6 – Point drift due to micromirrors and pixels of camera within 4 h (step of shooting 1 min). For presentation, the drift value is increased 25 times

The RMS value of the displacement of all points is less than 1 μm , except for the first 20 min, which is acceptable for most cases of interior orientation parameters calibration of optoelectronic devices. In the first 20 min, the largest non-uniform expansion is observed; the RMS is 1.5 μm . The maximum spread in the first 20 min of operation on rows and columns is 4 μm , the rest of the time does not exceed 1 μm . From Table 4 the average change in the distances between neighboring points is not more than 0.1 μm . Thus, we can assume that the value of the change in the distance between neighboring points is the same, negligible, and random. The distance between neighboring points does not change over time.

Table 3

The drift value of DMD micromirrors and pixels of camera relative to the coordinates of the points on the photodetector of previous shooting intervals (in μm , recalculated to coordinate system of DMD)

Offset of all points		Shooting interval, min							
		0	20	40	60	90	120	180	240
By columns	Average	–	17.19	4.75	3.92	1.47	0.86	0.17	0.47
	RMS	–	1.21	0.41	0.21	0.36	0.19	0.07	0.08
	Max spread	–	3.71	1.39	0.75	1.19	0.62	0.29	0.28
By rows	Average	–	-2.00	-1.85	0.40	1.06	0.32	-0.08	-0.53
	RMS	–	1.32	0.31	0.05	0.04	0.09	0.14	0.13
	Max spread	–	3.98	0.99	0.19	0.14	0.37	0.54	0.51

Table 4

The change value in the distance between neighboring points on the photodetector relative to the coordinates of the points on the photodetector of previous shooting intervals (in μm , recalculated to coordinate system of DMD)

Offset of all points		Shooting interval, min							
		0	20	40	60	90	120	180	240
By columns	Average	–	0.05	-0.07	0.13	-0.24	0.09	-0.05	0.03
	RMS	–	0.06	0.04	0.08	0.08	0.07	0.03	0.04
	Max spread	–	0.18	0.15	0.32	0.48	0.25	0.14	0.14
By rows	Average	–	0.06	0.02	0.03	0.00	-0.01	0.07	-0.06
	RMS	–	0.03	0.03	0.02	0.06	0.07	0.05	0.03
	Max spread	–	0.13	0.11	0.08	0.17	0.26	0.17	0.11

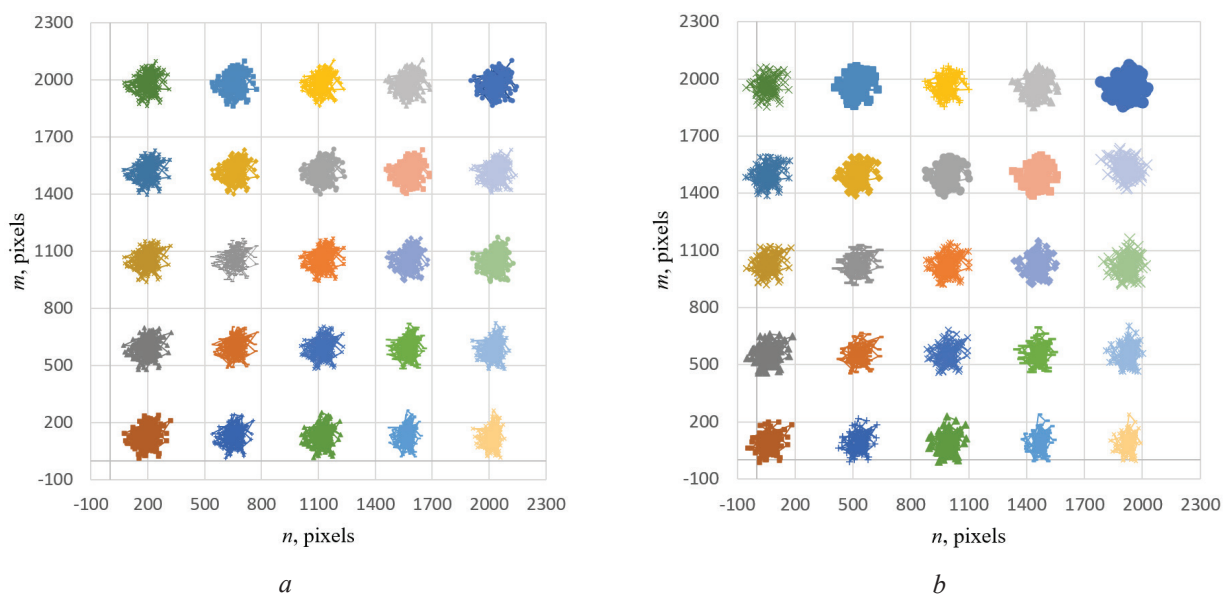


Figure 7 – Point drift due to micromirrors and pixels of camera (step of shooting 1 min): *a* – within 3 h, after 1 h of operating; *b* – within 2 h, after 2 h of operating. For presentation, the drift value is increased 100 times

From Figure 7 the points drift within 3 h after 1 h of heating shows that the points drift mainly along the rows and more for the left side than for the top. The points drift within 2 h after 2 h of heating becomes uniform. The spread in the position of the same point is due to noise and vibration, a more pronounced spread for the lower right corner is due to residual parallax, i. e. DMD and photodetector planes are not parallel.

Conclusion

When using DMD as a test-object in problems of interior orientation parameters calibration of optoelectronic devices, the average drift value of the entire array of DMD micromirrors will affect the accuracy of calibration. In the course of the research

it was found that the drift of DMD micromirrors occurs mainly along the rows in the first 60 min of operating. The value of the drift of all points after 60 min of operation is less than $1 \mu\text{m}$.

The uniformity of expansion of the DMD will determine the accuracy of interior orientation parameters calibration of optoelectronic devices using DMD, since uneven expansion will disrupt the periodicity of micromirrors, that is, the relative position of the micromirrors relative to each other will not be known. It is determined that the RMS of the offset is less than $1 \mu\text{m}$.

It has been established that the value of the change in the distance between neighboring points is the same throughout the micromirror array, is negligible, and is random in nature. If necessary, the residual effect of the uneven expansion

of DMD during interior orientation parameters calibration of optoelectronic devices using DMD can be compensated by determining the coefficients of uneven drift for each DMD micromirror.

Thus, DMD can be used as a test-object in the problems of interior orientation parameters calibration of optoelectronic devices. If more accurate interior orientation parameters calibration of optoelectronic devices are necessary, the results obtained can be used as compensation coefficients for changes in the spatial structure of DMD due to temperature effects during operation.

References

1. Zhengrong Huang, Jiangtao Xi., Yanguang Yu., Qinghua Guo. Accurate Projector Calibration Based on a New Point to Point Mapping Relationship Between the Camera and Projector Images. *Applied Optics*, 2015, vol. 54, iss. 3, pp. 347–356. **DOI:** 10.1364/ao.54.000347
2. Zhongwei Li, Yusheng Shi, Congjun Wang, Yuanyuan Wang. Accurate calibration method for a structured light system. *Optical Engineering*, 2008, vol. 47(5), p. 053604. **DOI:** 10.1117/1.2931517
3. Benjamin Lee. Introduction to ± 12 Degree Orthogonal Digital Micromirror Devices (DMDs). DLPA008B–July 2008 – Revised February 2018.
4. Aerotech PlanarDLA Hardware Manual. Revision: 1.03.00.
5. Arkhipov S.A., Zavarzin V.I., Malyhin V.A., Morozov S.A. Adjustments and certification of a long-focus three-mirror lens with an eccentrically located image. *Vestnik Moskovskogo Gosudarstvennogo Tekhnicheskogo Universiteta imeni N.E. Baumana* [Herald of the Bauman Moscow State Technical University], Series Instrument Engineering, 2009, no. 4, pp. 24–36 (in Russian).
6. Starasotnikau M.A., Feodortsau R.V. Accuracy Comparison of Algorithms for Determination of Image Center Coordinates in Optoelectronic Devices. *Science & Technique*, 2018, vol. 17(1), pp. 79–86 (in Russian). **DOI:** 10.21122/2227-1031-2018-17-1-79-86
7. Arkhipov S.A., Gasich G.V., Zavarzin V.I., Morozov S.A. Photogrammetric parameters of optoelectronic equipment. *Vestnik Moskovskogo Gosudarstvennogo Tekhnicheskogo Universiteta imeni N.E. Baumana* [Herald of the Bauman Moscow State Technical University], Series Instrument Engineering, 2008, no. 4, pp. 105–115 (in Russian).
8. Addendum to EMVA Data Report. Basler acA2040-90um EMVA Standard 1288.
9. Starasotnikau M.A., Feodortsau R.V. Method for Decreasing Influence of Background Signal Noise while Determining Energy Gravity Centre Coordinates for Images in Electrooptical Devices. *Priborostroenie-2016: Materialy 9-i Mezhdunarodnoi Nauch.-Tekhn. Konferentsii* [Instrumentation-2016: Materials of the 9th International Scientific and Technical Conference], Minsk, Belarusian National Technical University, 2016, pp. 133–135 (in Russian).
10. TI DLP® LightCrafter™ 4500. Evaluation Module. User's Guide. Literature Number: DLPU011F July 2013 – Revised July 2017.

Ionization Efficiency in a Hot Flat Disc-Shaped Cavity

M. Turek

*Institute of Physics, Maria Curie-Skłodowska University in Lublin,
pl. M. Curie-Skłodowskiej 1, 20-031 Lublin, Poland*

Received 14.02.2020

Accepted for publication 20.04.2020

Abstract

Hot cavity ion sources of different kinds are widely used in nuclear and mass spectroscopy, especially in on-line isotope separation devices attracting attention of scientists and engineers looking for high ionization efficiency, robustness and beam purity. In the paper a new type of hot ionizer cavity is proposed: namely cavity having the shape of a flat disc, which may be especially suitable for short-lived nuclides to be ionized.

A numerical model of the ion source is presented in the paper. The particle tracking code takes into account ionization at hot surfaces and enables modeling of both flat disc cavity and standard elongated cavity ionizers. The code enables calculation of total ionization efficiency and is suitable for stable and long-lived nuclides.

Influence of the flat disc cavity geometry (thickness and radius) and its temperature on total ionization efficiency was considered – it was shown that the efficiency increases with cavity radius due to the growing number of particle-wall collisions. This effect may be important in the case of the hard-to-ionize nuclides.

The optimal ionizer geometry is characterized by 90 % efficiency, even for substances with rather low ionization coefficient (of order 0.05). The role played by the size of the extraction opening is explained – it is demonstrated that the ionization efficiency increases due to the opening radius reduction. It is also proven that extraction voltage of 1–2 kV is sufficient to maintain optimal ionizer efficiency.

Keywords: ionizer, ionization efficiency, cavity, extraction opening.

DOI: 10.21122/2220-9506-2020-11-2-132-139

Адрес для переписки:

M. Turek
*Institute of Physics, Maria Curie-Skłodowska University in Lublin,
pl. M. Curie-Skłodowskiej 1, 20-031 Lublin, Poland
e-mail: mturek@kft.umcs.lublin.pl*

Для цитирования:

M. Turek.
Ionization Efficiency in a Hot Flat Disc-Shaped Cavity.
Приборы и методы измерений.
2020. – Т. 11, № 2. – С. 132–139.
DOI: 10.21122/2220-9506-2020-11-2-132-139

Address for correspondence:

M. Turek
*Institute of Physics, Maria Curie-Skłodowska University in Lublin,
pl. M. Curie-Skłodowskiej 1, 20-031 Lublin, Poland
e-mail: mturek@kft.umcs.lublin.pl*

For citation:

M. Turek.
Ionization Efficiency in a Hot Flat Disc-Shaped Cavity.
Devices and Methods of Measurements.
2020, vol. 11, no. 2, pp. 132–139.
DOI: 10.21122/2220-9506-2020-11-2-132-139

Эффективность ионизации в горячей плоской дискообразной полости

М. Турек

Институт физики, Университет имени Марии Кюри-Склодовской в Люблине,
пл. имени М. Кюри-Склодовской, 1, г. Люблин 20-031, Польша

Поступила 14.02.2020

Принята к печати 20.04.2020

Ионизаторы с горячей полостью различного типа находят широкое применение в атомной и масс-спектрологии, в частности, в устройствах для разделения изотопов в режиме онлайн, представляют большой интерес для учёных и инженеров вследствие высокой эффективности ионизации, надёжности и чистоты луча. В работе предложен новый тип горячей ионизационной полости, а именно полости в форме плоского диска, особенно эффективной для ионизации короткоживущих нуклидов.

Представлена численная модель ионного источника. Модель отслеживания частиц учитывает ионизацию на горячих поверхностях и позволяет моделировать как полость плоского диска, так и стандартные ионизаторы с удлинённой полостью. Модель позволяет выполнять расчёт общей эффективности ионизации и применима к стабильным и долгоживущим нуклидам.

Рассмотрено влияние геометрии полости плоского диска (толщина и радиус) и его температуры на общую эффективность ионизации – показано, что эффективность увеличивается с радиусом полости из-за растущего числа столкновений частиц со стенками. Данный эффект может оказаться важен для трудноионизируемых нуклидов.

Оптимальная геометрия ионизатора характеризуется эффективностью 90 % даже для трудноионизируемых веществ с коэффициентом ионизации порядка 0,05. Объясняется роль, которую играет размер экстракционного отверстия – показано, что эффективность ионизации увеличивается из-за уменьшения радиуса отверстия. Также доказано, что выходное напряжение 1–2 кВ достаточно для поддержания оптимальной эффективности.

Ключевые слова: ионизатор, эффективность ионизации, полость, экстракционное отверстие.

DOI: 10.21122/2220-9506-2020-11-2-132-139

Адрес для переписки:

M. Turek
Institute of Physics, Maria Curie-Skłodowska University in Lublin,
pl. M. Curie-Skłodowskiej 1, 20-031 Lublin, Poland
e-mail: mturek@kft.umcs.lublin.pl

Для цитирования:

M. Turek.
Ionization Efficiency in a Hot Flat Disc-Shaped Cavity.
Приборы и методы измерений.
2020. – Т. 11, № 2. – С. 132–139.
DOI: 10.21122/2220-9506-2020-11-2-132-139

Address for correspondence:

M. Turek
Institute of Physics, Maria Curie-Skłodowska University in Lublin,
pl. M. Curie-Skłodowskiej 1, 20-031 Lublin, Poland
e-mail: mturek@kft.umcs.lublin.pl

For citation:

M. Turek.
Ionization Efficiency in a Hot Flat Disc-Shaped Cavity.
Devices and Methods of Measurements.
2020, vol. 11, no. 2, pp. 132–139.
DOI: 10.21122/2220-9506-2020-11-2-132-139

Introduction

Surface ionization ion sources equipped with hot cavities proved to be useful tools e.g. in nuclear spectroscopy [1], mass spectroscopy [2, 3] and are widely used in on-line isotope separation (ISOL) projects [4–7]. Hot cavity ion sources in its pure form were invented almost five decades ago [8, 9] and evolved into the resonant ionization laser ion sources (RILIS) [10–12] based on an excitation of the valence electron to the continuum by tunable lasers. It is worth mentioning that the evolution has not stopped and next hybrid ion sources for ISOL purposes still appear [13]. Numerous advantages of hot cavity ion sources like: compact design, robustness and reliability, very low energy spread of the ion beam and its high purity and, probably most of all, high efficiency and very small amounts of ionized substance needed to obtain a good quality ion beam made these devices attractive to physicist and engineers.

There is a variety of hot cavity ion sources, but in their classical form the basic part is a semi-opened ionizer made of refractory metal or ceramics, heated to a high working temperature (≈ 2500 K or more) either by electron beams [14] or ohmically [15, 16] or even inductively [17]. Most often the ionizer is connected to a target irradiated in order to produce isotopes by a kind of transfer line [18], but in some solutions the ionizer itself could serve as the target and the produced isotopes are released immediately into the hot cavity [14]. As it has been already said, the cylindrical ionizer is the most common solution, but spherical ones are also used in some devices [19, 20].

In a series of previous papers a numerical models of a variety of hot cavity ion source were presented, including those concerning tubular [21–23], spherical or hemispherical [24] and also conical ionizers [25]. Results presented by other groups also showed that ionizer of complex shapes are characterized by very high efficiencies [26, 27]. At the early version of the model ionization of stable isotopes was considered, later on the model was upgraded in order to take into account effects of radioactive decay and delays of the particle emission due to diffusion and effusion in the ionizer [28]. The ionization model is based on the assumption that multiple collisions of particles with hot ionizer walls enhance total ionization efficiency. It should be mentioned here that e.g. electron impact ionization could also provide very important contribution, especially in the case of hard-to-ionize elements [22].

As it has been said before, geometry of the ionizer cavity may be crucial for obtaining high ionization efficiency. It was e. g. demonstrated that spherical ionizers with small extraction openings achieve higher efficiency than tubular semi-opened ionizers in the case stable nuclides, while in the case of short-lived isotopes either hemispherical or conical ionizers are superb. In the current paper another shape of the ionizer is postulated. It is a flat disc cavity ionizer, which could be understood as a limiting case of cylindrical ionizer, but characterized by shorter length compared to its radius. The flat shape of the cavity should result in a large number of collisions of the particle traveling to the extraction opening. Simultaneously, small length of the cavity makes the penetration of the extraction field easier, leading to fast and effective ion evacuation. It should be also mentioned that manufacturing of the flat disc cavity seems to be easier task than in the case of spherical or even conical cavities, especially in the case of hard-to-machine materials. The paper contains brief description of the numerical model suitable for stable and very long-lived isotopes. Dependency of the ionization efficiency on the cavity shape (its elongation an radius) is studied. The influence of the extraction opening size on the efficiency is under consideration. The current-voltage curves obtained for different values of ionization coefficient are also presented and discussed. The changes of the ion yield due the ionizer temperature are investigated.

Numerical model

The numerical code used for calculation of ionization efficiency in a disc cavity is a trajectory tracking code similar to that considered in previous papers [21–25, 28]. The code follows trajectories of both ions and neutral particles that are confined in a hot cavity until they reach the extraction opening. A schematic cross-section through the simulated cavity-extraction electrode system is presented in Figure 1.

It should be stressed once again that standard cylindrical ionizer is characterized by $r_i \ll L$ condition, whilst for a flat disc cavity L should be much smaller or at least comparable to r_i . The results presented in the paper were obtained for L of order of 1 mm. The simulation system is discretized using by $100 \times 400 \times 400$ rectangular numerical mesh with cell sizes $\Delta x = \Delta y = \Delta z = 0.05$ mm. The electrostatic potential is worked out by numerical solving of Laplace equation (with boundary condition imposed

by electrodes) employing the successive over-relaxation method, as in [29, 30]. The classical equations of motion are integrated using 4th order Runge–Kutta algorithm. The forces used by the push subroutine are found by linear interpolation of the electric field values at six nodes nearest to the particle position. Starting velocities of particles depend on the ionizer temperature, while their initial directions are chosen randomly. A neutral particle or ion that hits the ionizer's hot internal surface could undergo ionization/neutralization with a probability (also called ionization coefficient) β , which is related to ionization degree by formula:

$$\beta = \alpha / (1 + \alpha). \quad (1)$$

The latter magnitude (α) is usually defined as the ratio of the numbers of ions and neutral atoms detaching from the hot surface and could be estimated using the Saha–Langmuir formula:

$$\alpha = G \exp(-(V_i - \phi_e) / kT). \quad (2)$$

In the above formula V_i and ϕ_e are the ionization potential and the work function of the ionizer material, respectively, while the G prefactor depends e.g. on the atom-surface reflection coefficient. As it was already mentioned, the code follows the particles until they exit the cavity through the extraction hole and registers the total numbers of ions (N_+) and of neutrals (N_0). The total ion source ionization efficiency is calculated as:

$$\beta_s = \frac{N_+}{N_+ + N_0}. \quad (3)$$

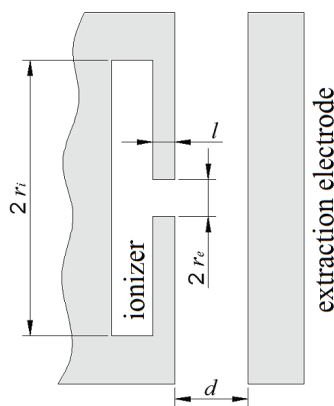


Figure 1 – Schematic view of the simulated system

One should have in mind that particles inside the cavity undergo many collisions with the ionizer hot walls. As the collision number reaches hundreds or even thousands, and charged particles are caught by the extraction field, the β_s could be by orders

of magnitude larger than ionization probability during a single collision, predicted by the Saha–Langmuir formula (2).

Simulation results

The influence of ionizer cavity shape on ionization efficiency was investigated as the first. Namely, r_i radius was changed starting from 0.8 mm up to 7 mm while the ionizer length L was kept constant ($L = 1$ mm). The flat extraction electrode on potential $V_{ext} = -2$ kV) was set at the distance $d = 1$ mm from the extraction hole of radius $r_e = 0.5$ mm. The extraction channel length was chosen as $l = 0.2$, unless otherwise stated. The simulation timestep was chosen as 10–2 μ s. Simulation runs were performed using 20000 test particles of 150 a.m.u. mass. The ionizer temperature was set to $kT = 0.3$ eV, unless otherwise stated. Calculation results are shown in Figure 2. As one can see, β coefficient changed over two and a half decades. Obtained total efficiency increases very fast with β . As one may expect ionization efficiency increases with the cavity radius and this effect is especially important in the case of hard-to-ionize substances (the case of β of order 0.01 or less). The total ionization efficiency could be several tens times larger than efficiency predicted by Saha–Langmuir law. For example, for $\beta = 0.01$ the total efficiency reaches 0.5 in the case of flat enough cavities ($r_i = 4$ mm or more). The 90 % efficiency, marked as a dotted horizontal line, could be achieved for β larger than 0.06, which is significantly better than efficiencies achieved in the case of cylindrical [21] and hemispherical ionizers and comparable to that reached in spherical ionizers [24]. As it was already mentioned, the efficiency gain is reached due to the increasing number of particle-wall collisions in the case of flat cavities. As one can see in Figure 2. the average number of collisions increase dramatically with r_i . For small values of β it reaches 700 in the case of very flat cavity while it is ≈ 30 for the compact shape. It could be seen that $\langle n_{hit} \rangle$ decreases with β – the easier is an atom to be ionized, the faster is caught by the extraction field.

On the other hand, in a flat disc shaped cavity the volume that is far away from the extraction field increases very fast with the ionizer radius. Decreasing probability of ion extraction leads to the saturation of ionization efficiency growth with r_i . As it could be seen in Figure 3 an excessive increase

of r_i —above 7 mm in the considered case—is pointless, as it will not result in efficiency improvement.

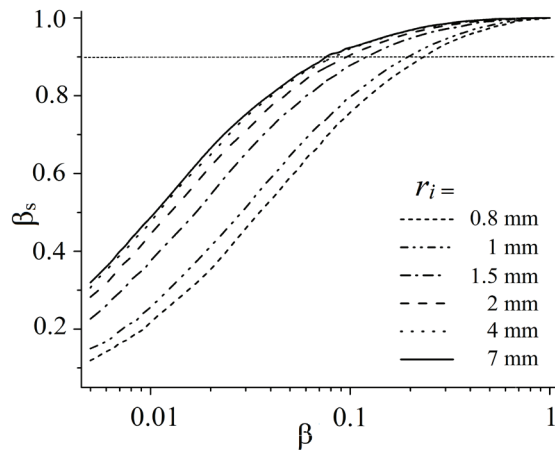


Figure 2 – Total ionization efficiency as a function of ionization coefficient β for different values of ionizer radius r_i

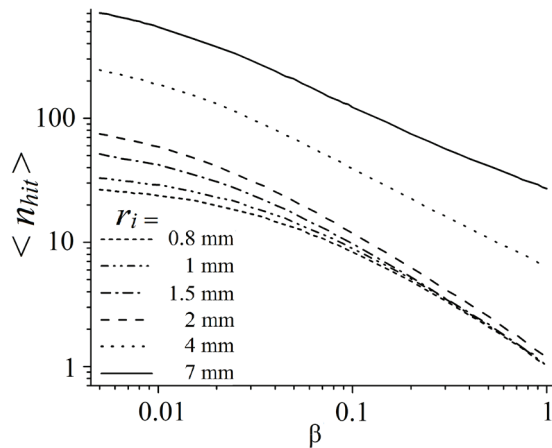


Figure 3 – Average number of particle-wall collisions calculated for different values of ionizer radius r_i

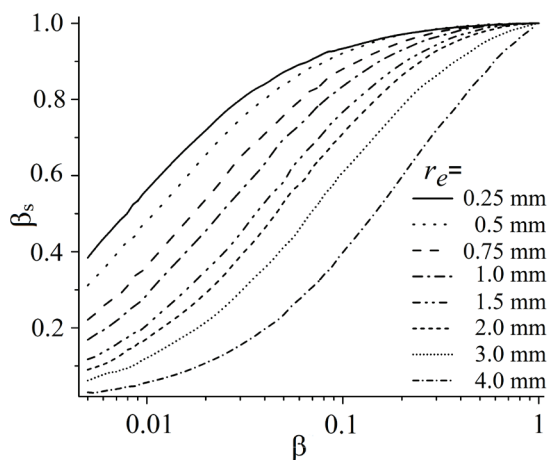


Figure 4 – Total ionization efficiency as a function of ionization coefficient β for different values of extraction opening radius r_e

The influence of extraction hole radius was also under investigation. Calculations were done for a disc cavity of diameter $r_i = 5$ mm and $L = 1$ mm. Results for r_e changing in the range from 0.25 mm up to 4 mm are presented in Figure 4. One can see that total ionization efficiency increases with r_e . Once again that effect is more important for smaller β . The explanation is very similar to that given in the previous case: the smaller is the extraction hole, the more collision with the hot wall each particle undergoes, which enlarges the total ionization probability. The average number of collisions as function of β is shown in Figure 5. The increase of the average number of collisions by three orders of magnitude when the extraction hole radius is reduced to 0.2 mm is meaningful. One should, however, have in mind that the presented results were obtained for stable isotopes. More particle-wall collisions result in longer total time a particle stays in the ionizer, which may play a crucial role in the case of short-lived isotopes.

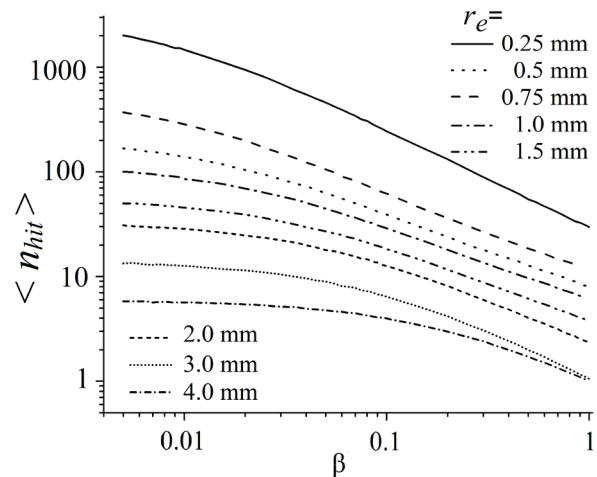


Figure 5 – Average number of particle-wall collisions calculated for different values of extraction opening radius r_e

The role played by the disc cavity thickness L was also checked out. Simulations were performed for $r_i = 2$ mm and $r_e = 0.05$ mm, all other parameters were as in the previous cases. The results are shown in Figure 6. One can see slight reduction of ionization efficiency for a very thin cavity ($L = 0.5$ mm). This could be probably due to the fact that the penetration of extraction field is limited in the case of such a flat cavity. For larger values of L the changes of efficiency are rather subtle, independently on the ionization coefficient.

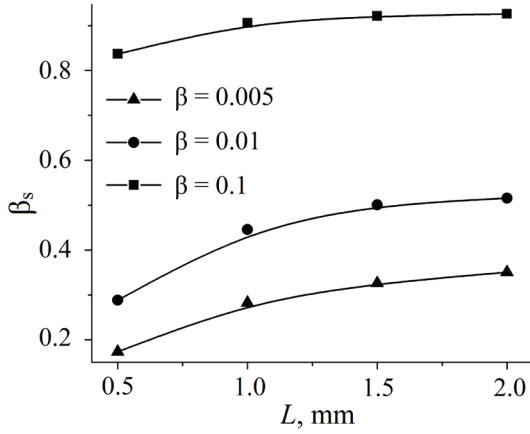


Figure 6 – Influence of disc-shaped cavity thickness L on the total ionization efficiency

Ionizer temperature may play an important role in achieving large ionization efficiencies. Figure 7 presents results of simulations of β_s evolution with kT for a flat disk cavity. Simulations were performed for $L = 1$ mm, $r_i = 5$ mm and $r_e = 0.5$ mm. Two cases were considered: ionization coefficient in the lowest considered temperature $kT = 0.2$ eV was set either to 0.01 or 0.001. Ionization coefficient for higher temperatures was calculated using Saha–Langmuir formula assuming $V_i - \phi_e = 0.9$ eV. Changes of ionization coefficient with kT are shown in Figure 7b. It could be seen that β increases several times in the considered temperature range. This is not the only magnitude that changes with ionizer temperature. Hollow symbols show the dependence of the desorbing particle initial temperature on kT – that change was also taken into account by the code. As it is shown in Figure 7a, total ionization efficiency increases with kT . The increase is nearly linear for $\beta(0.2 \text{ eV}) = 0.001$, while a kind of saturation could be expected in the cases of higher initial ionization coefficient β .

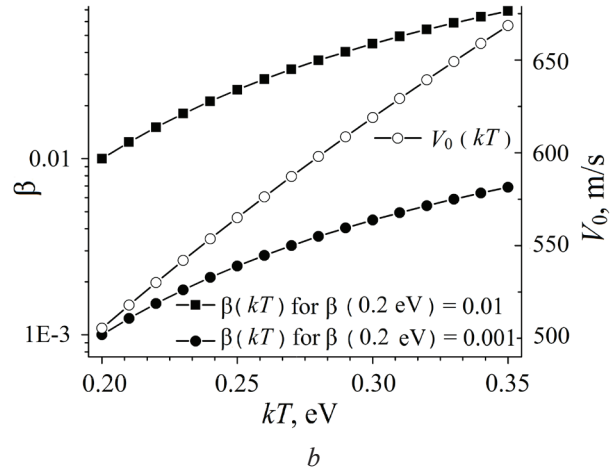
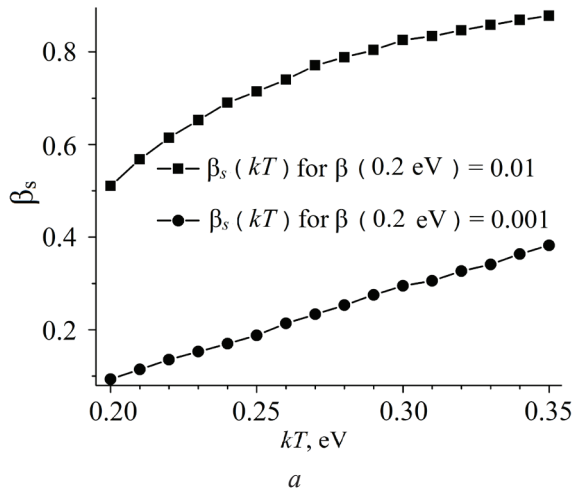


Figure 7 – Total ionization efficiency as a function of ionizer temperature kT (a) and dependence of ionization coefficient β and initial velocity of the desorbing particle on ionizer temperature kT (b)

As for other shapes of the ionizer, simulations of the current-voltage curves were done (see Figure 8).

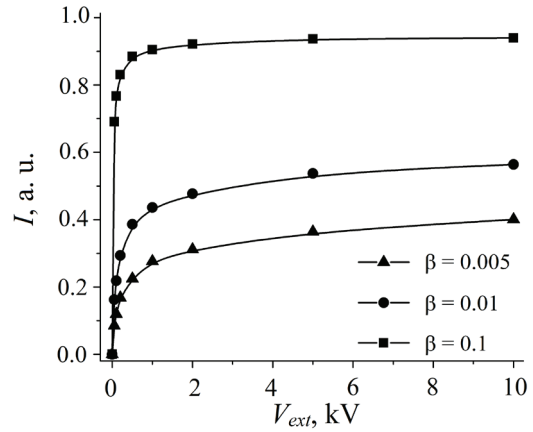


Figure 8 – Current-voltage curves calculated for different values of ionization coefficient β

The case of $L = 1$ mm, $r_i = 5$ mm and $r_e = 0.5$ mm was considered (the same set of parameters as previously). Extraction voltage was increased up to 20 kV. One can observe very rapid increase of ion current with V_{ext} rising up to ≈ 1 kV. Above 1–2 kV a saturation of current-voltage curve is observed. This happens when the extraction field is able to catch and extract ions almost immediately after they are created. It should be kept in mind that excessive (more than 1–2 keV in the considered case) increase of the V_{ext} is pointless – it does not lead to any significant increase of β_s and may result in electrical breakdown. It is worth noting that the shape of the calculated curves is close to that obtained for tubular [23, 28] ionizers and to experimental curves measured for the tubular ionizers [31].

Conclusion

Stable isotope ionization in a novel kind of hot cavity, namely flat disc-shaped one, was considered in the paper. The brief description of the numerical model was given for completeness. Influence of the ionizer geometry on ionization efficiency was considered. It was shown that the efficiency increases with the disc ionizer radius reaching values higher than these obtained for elongated cylindrical or hemispherical ionizer. Ionization efficiency of 90 % could be reached even in the cases of the ionization coefficient of order 0.05. This effect is mostly to the large number of particle-ionizer wall collisions (reaching several hundreds) in the case of flat cavities.

Numerical simulation performed using the model showed also that:

- ionization efficiency of stable isotopes could be significantly enhanced by the reduction of the extraction opening radius;
- excessive reduction of that thickness (below 0.5 mm) may lower the total ionization efficiency;
- extraction voltage of 1–2 kV is sufficient to achieve almost maximal efficiencies at given geometry.

Simulations of the influence of the ionizer temperature on the total ionization efficiency showed that the efficiency increases with kT , mostly due to the fact that ionization probability usually increases with the surface temperature. Thus, it is crucial to maintain possible high ionizer temperature (for typical ionization conditions) and reduce chances of forming "cold spots" that could reduce efficiency to a large extent.

Acknowledgments

The research was cofunded by the Plenipotentiary Representative of the Government of the Republic of Poland at JINR Dubna in the frame of the project № 75/07/2020.

References

1. Studer D., Maske L., Windpassinger P., Wendt K. Laser spectroscopy of the 1001-nm ground-state transition in dysprosium. *Phys. Rev. A*, 2018, vol. 98, pp. 042504. DOI: <https://doi.org/10.1103/PhysRevA.98.042504>
2. Duan Y., Danen R.E., Yan X., Steiner R., Cuadrado J., Wayne D., Majidi V., Olivares J.A. Characterization of an improved thermal ionization cavity source for mass spectrometry. *Journal of the American Society for*

Mass Spectrometry, 1999, vol. 10, pp. 917–1052.

DOI: 10.1016/S1044-0305(99)00065-3

3. Maden C., Trinquier A., Fauré A.-L., Hubert A., Pointurier F., Rickli J., Bourdon B. Design of a prototype thermal ionization cavity source intended for isotope ratio analysis. *International Journal of Mass Spectrometry*, 2018, vol. 434, pp. 70–80.

DOI: 10.1016/j.ijms.2018.09.006

4. Babcock C., Day Goodacre T., Gottberg A. Target and Ion Source Development for Better Beams in the ARIEL Era. IOP Conf. Series: *Journal of Physics: Conf. Series*, 2018, vol. 1067, pp. 052019.

DOI: 10.1088/1742-6596/1067/5/052019

5. Alton G.D., Liu Y., Stracener D.W. High-efficiency target ion sources for radioactive ion beam generation. *Rev. Sci. Instrum.*, 2006, vol. 77, pp. 03A711.

DOI: 10.1063/1.2173968

6. Köster U., Arndt O., Bouquerel E., Fedoseyev V.N., Franberg H., Joinet A., Jost C., Kerkinen I.S.K., Kirchner R. The TARGISOL Collaboration, Progress in ISOL target-ion-source-system. *Nucl. Instrum. Meth. B*, 2008, vol. 266, pp. 4229–4239.

DOI: 10.1016/j.nimb.2008.05.152

7. Woo H.J., Kang B.H., Tshoo K., Seo C.S., Hwang W., Park Y.H., Yoon J.W., Yoo S.H., Kim Y.K., Jang D.Y. Overview of the ISOL facility for the RISP. *Journal of the Korean Physical Society*, 2015, vol. 66, pp. 443–448. DOI: 10.3938/jkps.66.443

8. Beyer G.J., Herrmann E., Piotrowski A., Raitko V.I., Tyroff H. A new method for rare-earth isotope separation. *Nucl. Instrum. Meth.* 1971, vol. 96, pp. 437–439. DOI: 10.1016/0029-554X(71)90613-6

9. Johnson P.G., Bolson A., Henderson C.M. A high temperature ion source for isotope separators. *Nucl. Instrum. Meth.*, 1973, vol. 106, pp. 83–87.

DOI: 10.1016/0029-554X(73)90049-9

10. Liu Y., Jost C.U., Mendez II A.J., Stracener D.W., Williams C.L., Gross C.J., Grzywacz R.K., Madurga M., Miernik K., Miller D. On-line commissioning of the HRIBF resonant ionization laser ion source. *Nucl. Instrum. and Meth. B*, 2013, vol. 298, pp. 5–12.

DOI: 10.1016/j.nimb.2012.12.041

11. Lecesne N. Laser ion sources for radioactive beams. *Rev. Sci. Instrum.*, 2012, vol. 83, pp. 02A916. DOI: 10.1063/1.3681148

12. Henares J.L., Lecesne N., Hijazi L., Bastin B., Kron T., Lassen J., Le Blanc F., Leroy R., Osmond B., Raeder S., Schneider F., Wendt K. Hot-cavity studies for the Resonance Ionization Laser Ion Source. *Nucl. Instr. Meth. B*, 2016, vol. 830, pp. 520–525.

DOI: 10.1016/j.nima.2015.10.061

13. Day Goodacre T., Billowes J., Catherall R., Cocolios T.E., Crepieux B., Fedorov D.V., Fedosse-
ev V.N., Gaffney L.P., Giles T., Gottberg A., Lynch K.M.,

- Marsh B.A., Mendonça T.M., Ramos J.P., Rossel R.E., Rothe S., Sels S., Sotty C., Stora T., Van Beveren C., Veinhard M. Blurring the boundaries between ion sources: The application of the RILIS inside a FEBIAD type ion source at ISOLDE. *Nucl. Instr. Meth. B*, 2016, vol. 376, pp. 39–45. **DOI:** 10.1016/j.nimb.2016.03.005
14. Kalinnikov V.G., Gromov K.Ya., Janicki M., Yushkevich Yu.V., Potempa A.W., Egorov V.G., Bystrov V.A., Kotovsky N.Yu., Evtisov S.V. Experimental complex to study nuclei far from the beta-stability line – ISOL-facility YASNAPP-2. *Nucl. Instr. and Meth. B*, 1992, vol. 70, pp. 62–68.
DOI: 10.1016/0168-583X(92)95910-J
15. Zhai L., Deng H., Wei G., Li Z., Wang C., Li X., Zhou G., Su Y., Zhang Z. A new, ohmic-heating based thermal ionization cavity source for mass spectrometry. *International Journal of Mass Spectrometry*, 2011, vol. 305, pp. 45–49. **DOI:** 10.1016/j.ijms.2011.05.015
16. Eléon C., Jardin P., Gaubert G., Saintlaurent M., Alcantaranunez J., Alvesconde R. Development of a surface ionization source for the production of radioactive alkali ion beams in SPIRAL. *Nucl. Instr. and Meth. B*, 2008, vol. 266, pp. 4362–4367.
DOI: 10.1016/j.nimb.2008.05.067
17. Reponen M., Moore I.D., Pohjalainen I., Rothe S., Savonen M., Sonnenschein V., Voss A. An inductively heated hot cavity catcher laser ion source. *Rev Sci Instrum.* 2015, vol. 86, pp. 123501.
DOI: 10.1063/1.4936569
18. Alton G.D., Zhang Y. A fast effusive-flow vapor-transport system for ISOL-based radioactive ion beam facilities. *Nucl. Instrum. and Meth. A*, 2005, vol. 539, pp. 540–546. **DOI:** 10.1016/j.nima.2004.11.027
19. Alton G.D., Liu Y., Zaim H., Murray S.N. An efficient negative surface ionization source for RIB generation. *Nucl. Instrum. and Meth. B*, 2003, vol. 211, pp. 425–435. **DOI:** 10.1016/S0168-583X(03)01365-X
20. Hausladen P.A., Weisser D.C., Lobanov N.R., Fifield L.K., Wallace H.J. Simple concepts for ion source improvement. *Nucl. Instrum. and Meth. B*, 2002, vol. 190, pp. 402–404.
DOI: 10.1016/S0168-583X(01)01307-6
21. Turek M., Pysznik K., Drozdziel A., Sielanko J. Ionization efficiency calculations for cavity thermoionization ion source. *Vacuum*, 2008, vol. 82, pp. 1103–1106. **DOI:** 10.1016/j.vacuum.2008.01.025
22. Turek M., Pysznik K., Drozdziel A. Influence of electron impact ionization on the efficiency of thermoemission ion source. *Vacuum*, 2009, vol. 83, pp. S260–S263. **DOI:** 10.1016/j.vacuum.2009.01.077
23. Turek M., Drozdziel A., Pysznik K., Maczka D., Slowinski B. Simulations of ionization in a hot cavity surface ion source. *Rev. Sci. Instrum.*, 2012, vol. 83, pp. 023303. **DOI:** 10.1063/1.3685247
24. Turek M. Modeling of Ionization in a Spherical Surface Ionizer. *Acta Phys. Pol. A*, 2011, vol. 120, pp. 188–191. **DOI:** 10.12693/APhysPolA.120.188
25. Turek M. Ionisation Efficiency in Conical Hot Cavities. *Acta Phys. Pol. A*, 2017, vol. 132, pp. 259–263. **DOI:** 10.12693/APhysPolA.132.259
26. Maden C., Baur H., Fauré A.-L., Hubert A., Pointurier F., Bourdon B. Determination of ionization efficiencies of thermal ionization cavity sources by numerical simulation of charged particle trajectories including space charge. *Int. J. Mass Spectr.*, 2016, vol. 405, pp. 39–49. **DOI:** 10.1016/j.ijms.2016.05.013
27. Liu Y., Batchelder J.C., Galindo-Uribarri A., Chu R., Fan S., Romero-Romero E., Stracener D.W. Ion source development for ultratrace detection of uranium and thorium. *Nucl. Instrum. and Meth. B*, 2015, vol. 361, pp. 267–272. **DOI:** 10.1016/j.nimb.2015.04.081
28. Turek M. Ionization of short-lived isotopes in a hot cavity – Numerical simulations. *Vacuum*, 2014, vol. 104, pp. 1–12. **DOI:** 10.1016/j.vacuum.2013.12.016
29. Hadjidimos A. Successive overrelaxation (SOR) and related methods. *Journal of Computational and Applied Mathematics*, 2000, vol. 123, pp. 177–199.
DOI: 10.1016/S0377-0427(00)00403-9
30. Press W.H., Teukolsky S.A., Vetterling W.T., Flannery B.P. Numerical recipes in FORTRAN (2nd ed.): The art of scientific computing, 1992, Cambridge University Press New York.
31. Latuszyński A., Maczka D. High temperature cavity thermo-ionizer. *Vacuum*, 1998, vol. 51, pp. 109–112. **DOI:** 10.1016/S0042-207X(98)00142-0

Tests of Impregnation Speed of Electrotechnical Pressboard with Insulating Oil

C. Kozak

Lublin University of Technology,
Nadbystrzycka str., 38A, Lublin 20-618, Poland

Received 04.03.2020

Accepted for publication 21.04.2020

Abstract

The paper presents a new test stand for investigating the rate of penetration of transformer oil through electrotechnical pressboard. The stand consists of a pipe, to the lower end of which is glued a pressboard plate. The pipe is filled with insulating oil. A mirror is placed under the plate, which directs its image to the lens of the camera, which takes a series of photographs at a given time interval. After being saturated with the insulating oil, the pressboard changes colour from light to dark yellow. The absorbing time is defined as the time in which a dark yellow spot appears on the lower light surface of the pressboard after the pipe is filled with oil.

A new way of determining capillary diameters has been developed when the number of capillaries is unknown and the volume of liquid flowing through them is not measurable. The distribution of the times of penetration of transformer oil through 2 mm thick electrotechnical pressboard was determined, the values of which range from about 220 min to about 550 min. It was found that the radii of capillaries through which the insulating oil penetrates are within the range from about 45 nm to about 70 nm. Due to the structure of the pressboard, which consists of cellulose fibres, arranged more or less tightly, there are capillaries in the structure of the board, each of which has sections of varying lengths of radii. This means that short sections of a single capillary can have radii both smaller than 45 nm and larger than 70 nm.

The developed stand and the new analysis method can be used for testing various porous materials for penetration by various liquids.

Keywords: electrotechnical pressboard, insulating oil, impregnation, capillary.

DOI: 10.21122/2220-9506-2020-11-2-140-147

Адрес для переписки:

C. Kozak
Lublin University of Technology,
Nadbystrzycka str., 38A, Lublin 20-618, Poland
e-mail: c.kozak@pollub.pl

Address for correspondence:

C. Kozak
Lublin University of Technology,
Nadbystrzycka str., 38A, Lublin 20-618, Poland
e-mail: c.kozak@pollub.pl

Для цитирования:

C. Kozak.
Tests of Impregnation Speed of Electrotechnical Pressboard with Insulating Oil.
Приборы и методы измерений.
2020. – Т. 11, № 2. – С. 140–147.
DOI: 10.21122/2220-9506-2020-11-2-140-147

For citation:

C. Kozak.
Tests of Impregnation Speed of Electrotechnical Pressboard with Insulating Oil.
Devices and Methods of Measurements.
2020, vol. 11, no. 2, pp. 140–147.
DOI: 10.21122/2220-9506-2020-11-2-140-147

Измерение скорости просачивания трансформаторного масла через электротехнический картон

Ч. Козак

Люблинский технологический университет,
ул. Надбыстрицкая, 38А, Люблин 20-618, Польша

Поступила 04.03.2020

Принята к печати 21.04.2020

В работе представлена новая установка для исследования скорости просачивания трансформаторного масла через электротехнический картон. Установка состоит из прозрачной трубы, к нижнему концу которой приклеена пластинка электротехнического картона. Затем в трубу вливается трансформаторное масло. Под пластинкой находится зеркало, направляющее её изображение в объектив фотоаппарата, который регистрирует серию изображений пластинки с заданным временным интервалом. Электротехнический картон, смоченный трансформаторным маслом, изменяет свой цвет со светло-жёлтого на тёмно-жёлтый. Время просачивания трансформаторного масла через электротехнический картон определяется по появлению на изображении поверхности картона тёмно-жёлтого пятнышка, свидетельствующего о просачивании трансформаторного масла через пластинку.

Разработан способ расчёта среднего диаметра капилляров, через которые трансформаторное масло просачивается через электротехнический картон в случае, когда их число является неизвестным, в связи с чем объём вытекающей через один капилляр жидкости невозможно измерить. Установлено, что в разных местах пластинки картона с толщиной 1 мм времена просачивания различаются. На основании проведённых измерений определено распределение времён просачивания, которые изменяются от 224 мин до 556 мин. Рассчитаны радиусы капилляров, через которые трансформаторное масло просачивается через электротехнический картон. Их величины изменяются от 47 нм до 75 нм. Структура картона представляет собой волокна целлюлозы, упакованные достаточно плотно. В связи с этим между волокнами существуют капилляры, каждый из которых состоит из участков с изменяющимися по длине радиусами. Таким образом, в картоне имеются короткие участки капилляров с радиусами как меньшими 47 нм, так и большими 75 нм.

Разработанная установка и способ расчёта размеров капилляров могут быть использованы для исследования протекания различных жидкостей через пористые материалы.

Ключевые слова: электротехнический картон, трансформаторное масло, импрегнация, капилляры.

DOI: 10.21122/2220-9506-2020-11-2-140-147

Адрес для переписки:
С. Козак
Lublin University of Technology,
Nadbystrzycka str., 38A, Lublin 20-618, Poland
e-mail: c.kozak@pollub.pl

Address for correspondence:
С. Kozak
Lublin University of Technology,
Nadbystrzycka str., 38A, Lublin 20-618, Poland
e-mail: c.kozak@pollub.pl

Для цитирования:
С. Козак.
Tests of Impregnation Speed of Electrotechnical Pressboard with Insulating Oil.
Приборы и методы измерений.
2020. – Т. 11, № 2. – С. 140–147.
DOI: 10.21122/2220-9506-2020-11-2-140-147

For citation:
С. Kozak.
Tests of Impregnation Speed of Electrotechnical Pressboard with Insulating Oil.
Devices and Methods of Measurements.
2020, vol. 11, no. 2, pp. 140–147.
DOI: 10.21122/2220-9506-2020-11-2-140-147

Introduction

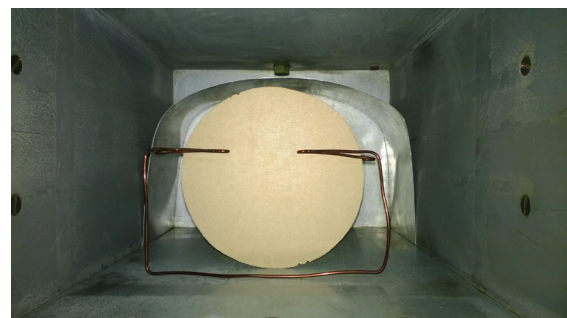
The most popular type of electrical insulation used in power transformers is the so-called liquid-solid insulation. Among many technical solutions, the most commonly used is the use of cellulose materials in the form of paper and pressboard as solid elements of insulation. Its popularity is mainly due to its good insulation parameters, ease of manufacture and shaping, and low price. Cellulose is a naturally occurring biopolymer derived from wood. It is composed of repeating glucose groups forming monomers, from which fibres are eventually formed. The number of repeated monomers in a single fiber is an important material parameter and is referred to as the degree of polymerisation (DP). The degree of polymerisation for newly made insulating paper takes the values of about 1200 [1]. During many years of operation, the cellulose fibres disintegrate to the level of 200 DP [2], which is considered to be the end of insulation life. As the cellulose depolymerisation progresses, it gradually loses its electrical and mechanical properties, which may result in catastrophic transformer failure. One of the main factors in accelerating the depolymerisation of paper insulation is the presence of water in it. In order to protect the cellulose insulation from the ingress of water molecules, it is impregnated with insulating liquid. Since the beginning of the 20th century, the commonly used insulating liquid is petroleum-derived mineral transformer oil, which is characterised by low viscosity, good ageing strength, excellent insulating parameters and low price [3]. Another task of the insulating oil is to ensure cooling of the insulation and active elements of the transformer [4]. Moreover, due to their fibrous structure, cellulose materials have free spaces between the fibres in the form of capillaries, in which there is a noticeable amount of air, which during the impregnation process is replaced by oil, increasing the dielectric strength of the insulation. The remaining air in cellulose after improper impregnation, due to its low dielectric permittivity ($\epsilon \approx 1$), compared to cellulose ($\epsilon \approx 4.4$) and applied insulating liquid ($\epsilon \approx 2.2\text{--}3.2$), causes local electric field intensity which may lead to partial discharges [5]. Important parameters of cellulose materials are their absorbability – the volume of oil which is absorbed by a unit of material volume, and the rate of impregnation – the impregnation time. Such parameters also include capillary dimensions and distribution of their diameters.

The properly performed impregnation process is crucial for failure-free transformer operation [6]. In atmospheric conditions, impregnation of the pressboard with transformer oil takes over 46 days [7]. The use of vacuum impregnation, in which the pressboard is treated with oil under reduced pressure, allows to shorten the impregnation time to even several dozen minutes [8]. Previous studies revealed the presence of statistical distribution of capillaries present in the pressboard [9, 10].

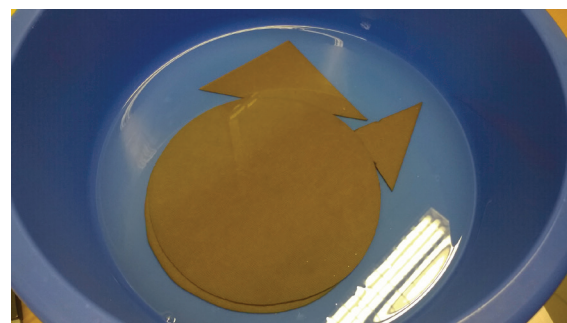
The aim of the present study is to present the position for testing the rate of transformer oil impregnation through the electrotechnical pressboard and the method of determining the dimensions of capillaries when their number is unknown and the volume of liquid flowing through them is impossible to record.

The oil-impregnation test stand

In order to test the process of penetration of insulating oil through the pressboard, a measuring stand and the method of optical recording of the time of penetration of oil through the pressboard sample were prepared. The basis of the new method is that after moistening its surface with insulating oil, the pressboard is changing its colour from light to dark yellow (Figure 1).



a



b

Figure 1 – Dry (a) and transformer oil moistened (b) pressboard samples

Figure 2 shows a diagram and basic elements of the measuring stand. The main element of the stand is a 2 m long polycarbonate pipe. A plate made of pressboard is tightly glued to the lower end of the pipe. Under the vertically positioned pipe, a vessel is placed to catch oil in case the pipe and plate should get unsealed. A mirror is placed in the vessel at a 45° angle, directing the image of the pressboard plate to the camera lens. By using a concave mirror, the sample image was magnified approximately 1.5 times its actual size, which improved the image resolution. After starting the cyclic operation of the camera, the tube is filled with transformer oil so that the height of its column is (1000 ± 1) mm. In the research, electrotechnical pressboard and transformer oil intended for the production of power transformers were used, obtained from the world's leading manufacturers of insulating materials. It was important to use a suitable adhesive that did not impregnate the pressboard, but was resistant to transformer oil and allowed the samples to be glued to the pipe. For this purpose, experimental tests were carried out to glue the pressboard to the polycarbonate pipe with contact, polymer, acrylic and epoxy adhesives. The epoxy adhesive proved to be the most suitable both in terms of density, adhesion to the glued surfaces and oil resistance.

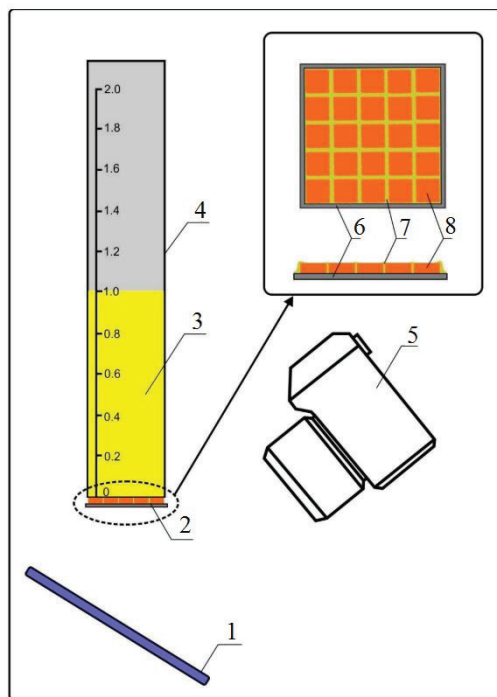


Figure 2 – Outline of the measuring stand: 1 – mirror; 2 – sample matrix; 3 – insulation oil; 4 – polycarbonate pipe; 5 – camera; 6 – perforated iron sheet; 7 – adhesive layer; 8 – pressboard sample

A high resolution digital camera was used to record the image. To control the operation of the camera, an intervalometer was used, allowing for cyclic release of the camera shutter in the time range of 1 s to 99 min. The camera is capable of a reduction of wobble during the shooting process thanks to image stabilisation and the possibility of initial mirror lift. After a series of tests, the optimum time between shooting was determined to be 15 s, ensuring an accuracy of approximately 0.5 %.

The exposure time was adjusted to the ISO200 sensitivity so that the images had the lowest noise level. The lens aperture was selected on the basis of MTF50 [lp/mm] charts for maximum focal length resolution of the camera lens. White LEDs were used as the illumination of the tested sample, placed in such a way as to make the surface of the tested sample evenly illuminated. The use of a digital camera in comparison with visual observation gives the possibility to take measurements without the participation of the observer and allows for re-analysis of the set of images in order to verify the correctness of the setting of oil permeation times.

Initially, the measuring station consisted of a pipe with an internal diameter of 40 mm and a length of 1.5 m, to which a $50 \times 50 \text{ mm}^2$ pressboard plate was glued. The measurement of percolation time consisted in the analysis of obtained photographs and determination of colour changes on the surface of the tested sample. Then, knowing the number of photos taken until the first dark point appeared on the lower surface of the sample and the length of the time interval, the impregnation time of the oil through the pressboard sample was determined. Images of the sample obtained after successively increasing times are shown in Figure 3. Figure 3 shows that on the initially bright lower surface of the pressboard plate (Figure 3a) a dark point appears after some time (Figure 3b). The time after which this point appears is the time of the fastest penetration. This probably corresponds to the capillary of the largest diameter. Then the dark area around this point gradually expands (Figure 3c). This indicates that there are capillaries with longer penetration times, i. e. with smaller diameters than the first capillary. The analysis of the images presented in Figure 3 shows the presence of capillaries of significantly different diameters in the structure of the electrotechnical pressboard.

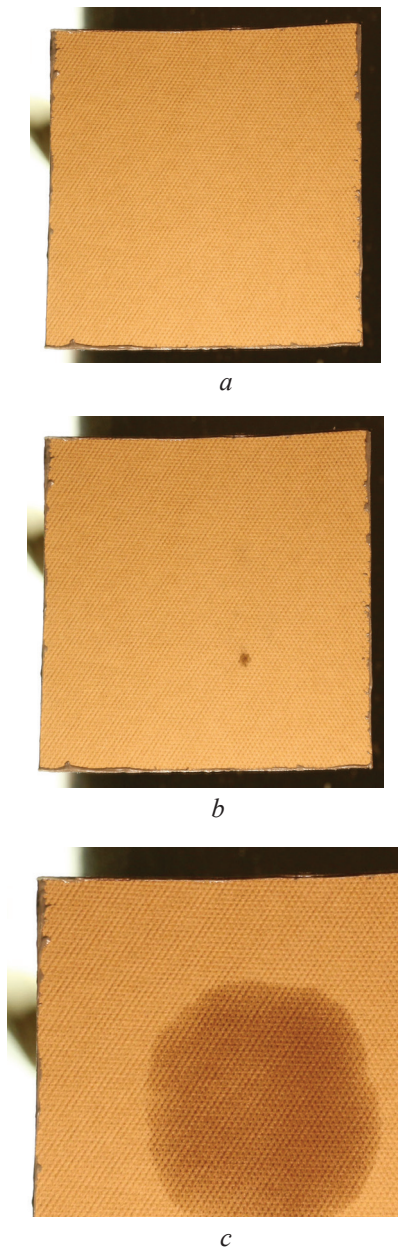


Figure 3 – Images of the pressboard sample during permeation time measurements

This means that the oil permeation times differ at different points in the pressboard sample. By analysing the subsequent images it is possible to determine the moment of oil permeation at a given point. Unfortunately, in a number of cases the time differences were small, so that the surface of the sample quickly became completely dark, making it impossible to determine the individual times. By analysing a single sample, one or rarely two permeation times could be determined. In order to determine the statistical distribution of permeation times at least several dozen times had to be determined.

For this purpose, the size of the seepage area of a single sample was limited to 15×15 mm in order to make a matrix from such samples as shown in Figure 4. The samples were glued to a perforated galvanised sheet with 10×10 mm holes. The next step was to apply the adhesive to the cutting edges of the samples in order to eliminate the penetration of oil through the side edges of the sample. The matrix consisted of 25 samples, but after taking into account the dimensions of the 90 mm diameter polycarbonate pipe used in this case and the adhesive area, only 9 centrally located samples were analysed.

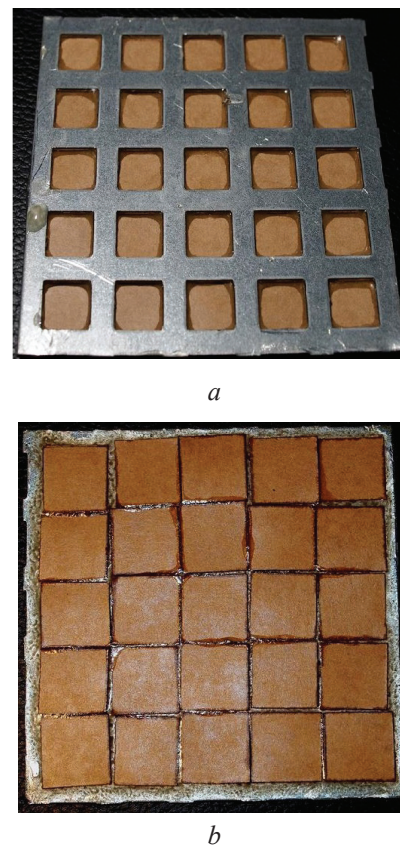


Figure 4 – View of the matrix with prepared samples of pressboard: 1 – matrix view from the bottom side; 2 – from the oil side

In this way 20 matrices were made for 2 mm thick samples, on the basis of which 180 values of the penetration times were obtained. The distribution of the obtained permeation times is shown in Figure 5, containing the histogram of time intervals, which differ in values with a step of 30 min. As can be seen from this figure, there are more than twofold differences in permeation times, the smallest one about 220 min, the largest about 550 min.

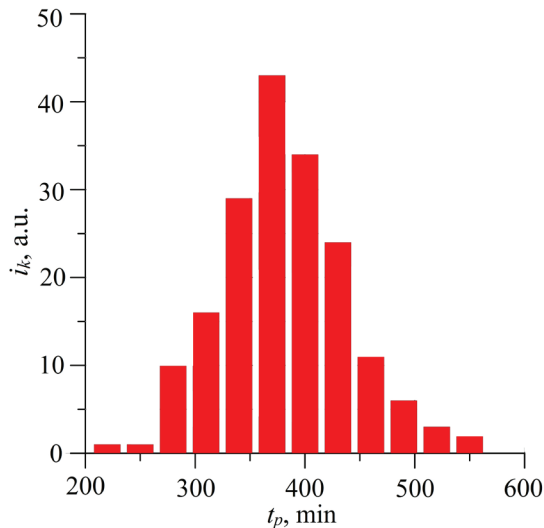


Figure 5 – Histogram of the number of occurrences of individual permeation times

Penetration of oil through the pressboard is done by capillaries between the cellulose fibres. The distribution of penetration times shown in Figure 5 means that the capillaries in the pressboard are different in their rays. To determine the values of capillary rays, the Hagen–Poiseuille's law was applied:

$$\frac{dV}{dt} = \frac{\pi r^2 \Delta p}{8\eta L}, \quad (1)$$

where dV – volume of oil flowing through the capillary in time dt ; Δp – pressure inducing liquid flow in the capillary; η – dynamic oil viscosity; L – length of the capillary; r – radius of the capillary.

Assuming that the oil flow in the capillaries is caused by the pressure of the oil column, we obtain:

$$\Delta p = \rho gh, \quad (2)$$

where ρ – oil density; g – standard gravity; h – oil column height.

By substituting formula (2) with formula (1) and integrating, we obtain the expression for the volume of liquid flowing through a single capillary:

$$V = \frac{\pi r^4 \rho gh}{8\eta L} t. \quad (3)$$

In the study of the phenomenon of capillarity by traditional methods, formula (3) is used to determine the dynamic viscosity of a liquid, in the case of known radius and length of the capillary. When the radius of the capillary is not known, its value can be determined by observing the flow of a

liquid of known viscosity. In both cases, the volume of liquid V , which for time t will flow out through the capillary, is determined. In our case, an unknown number of capillaries of different unknown radii pass through the sample of the pressboard. Therefore, it is not possible to use the standard interpretation of formula (3) consisting in measuring the volume of oil leaking from the capillary at time t . In order to solve this problem, an approach has been taken to determine the time t_p after which the oil fills the entire capillary, i.e. from the moment the pipe is filled with oil to the moment the oil permeates the sample. Such a moment is recorded when a dark point appears on one of the subsequent pictures shown in Figure 3. At t_p , the volume of oil in the capillary will be:

$$V = \pi \cdot r^2 \cdot L, \quad (4)$$

where r – radius of the capillary; L – thickness of the pressboard.

By substituting the permeation time t_p and formula (4) to formula (3) we obtain:

$$\pi \cdot r^2 \cdot L = \frac{\pi r^4 \rho gh}{8\eta L} t_p. \quad (5)$$

From here:

$$r = L \sqrt{\frac{8 \cdot \eta \cdot L}{\rho \cdot g \cdot h \cdot t_p}}. \quad (6)$$

By substituting to formula (6) physical constants and the permeation times obtained from measurements, as shown in Figure 5, the distribution of capillary radius values was calculated, as shown in Figure 6. From Figure 6 it follows that the capillary radii are in the range from about 45 to about 70 nm. According to the data presented by the employees of Weidmann, one of the leading manufacturers of cellulose products intended for the construction of insulation of electrical transformers, the dimensions of capillaries in the pressboard range from 10 nm to several micrometers [11]. Formula (6) shows that the radius of the capillary, calculated on the basis of the measured permeation time t_p depends linearly on the capillary length. When calculating the radii of capillaries, the values of which are shown in Figure 6, it was assumed that the length of each capillary is equal to the thickness of the pressboard. This means that the capillary is in the form of a cylinder connecting two surfaces of the pressboard plate. The real shape of the capillary may look like a broken line. It can increase the length of the capillary by several

times. However, taking into account that the shortest seepage times were used to calculate the radii of the capillaries, it should be assumed that the seepage was made by capillaries of lengths similar to the thickness of the pressboard. Besides, in such heterogeneous materials as cellulose fibre clusters, the capillary is unlikely to be cylinder-shaped with a constant radius. It should be assumed that the capillary consists rather of short sections of variable thickness close to the length of the cellulose fibres. This means that the achieved capillary radii are average values. Real short sections of the capillary may have radii both shorter than 45 nm and longer than 70 nm. Paper [11] argues that the upper limit of capillary diameter is several μm . If in the plates tested in the study there were capillaries of such diameter connecting both surfaces of the pressboard plate, according to formula (6) the time of oil permeation would be very short and would be about 20 s. The permeation times we observed, as shown in Figure 5, are about two orders larger. This means that such large diameters concern rather short and rare sections of the capillary.

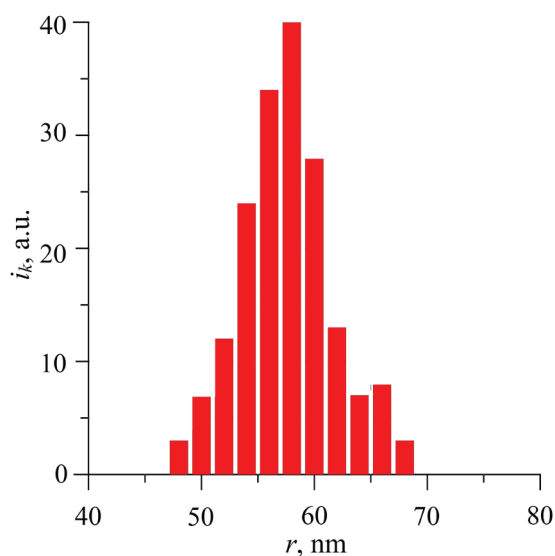


Figure 6 – The graph of the number of occurrences of particular radii of capillaries

The structure of the pressboard consists of cellulose fibres, arranged more or less tightly, between which are capillaries with radii of up to several hundred nanometres. The research shows that there are capillaries in the pressboard structure, each of which has sections of varying lengths of radii. Average values of capillary radii range from 130 to 200 nm. Impregnation of the pressboard causes that the capillaries are filled with insulating oil. This means that the paper-oil insulation

of power transformers should be considered as a composite of cellulose and nano-capillaries filled with insulating oil.

Conclusion

The paper presents a developed and constructed stand for testing the rate of penetration of transformer oil through the electrotechnical pressboard, which consists of a pipe, to the lower end of which a pressboard plate is glued. A mirror is placed under the tube at a 45° angle, which directs the image of the pressboard plate to the camera lens. After flooding the tube with transformer oil, the camera takes a series of photos with a given time interval. The principle of the station is that after moistening its surface with insulating oil, the pressboard changes its colour from light to dark yellow. The soaking time is defined as the time in which, after filling the pipe with oil, a dark yellow spot appears on the lower light surface of the pressboard, recorded in subsequent pictures. On the basis of the Hagen–Poiseuille law describing capillary phenomena, a new way of determining capillary diameters has been developed, where the number of capillaries is unknown and the volume of liquid flowing through them is impossible to measure. On the basis of the tests carried out with the use of the stand, the penetration times of transformer oil through the 2 mm thick electrotechnical pressboard were determined, the values of which range from about 220 min to about 550 min. The capillary radii through which the insulating oil seeps were determined to be between approx. 45 nm and approx. 70 nm. Due to the structure of the pressboard, which consists of cellulose fibers, there are capillaries in the it, each of which has sections of varying lengths of radii. This means that the obtained capillary radii are average values. Real short sections of the capillary can have radii both smaller than 45 nm and larger than 70 nm.

The test stand for examining the rate of penetration of liquids through porous materials and the new method of analysis of test results described in the article can be successfully used for testing other porous materials and other liquids. The condition for using the test stand and the new method of analysis of results for other materials and liquids is a change in colour or reflectance of the solid material under the influence of the liquid. These phenomena are often encountered in practice. In the absence of such features, the liquid can be coloured.

References

1. Krause C. Power transformer insulation – history, technology and design. *IEEE Trans. Dielectr. Electr. Insul.*, 2012, vol. 19, no. 6, pp. 1941–1947.
DOI: 10.1109/TDEI.2012.6396951
2. Jalbert J., Rodriguez-Celis E., Duchesne S., Morin B., Ryadi M., Gilbert R. Kinetics of the production of chain-end groups and methanol from the depolymerization of cellulose during the ageing of paper/oil systems. Part 3: extension of the study under temperature conditions over 120 °C. *Cellulose*, 2015, vol. 22, no. 1, pp. 829–848.
DOI: 10.1007/s10570-014-0516-8
3. Fofana I. 50 years in the development of insulating liquids. *IEEE Electr. Insul. Mag.*, 2013, vol. 29, no. 5, pp. 13–25. **DOI:** 10.1109/MEI.2013.6585853
4. Huang M., Zhou Y., Zhou Z., Qi B. A Combined Electro-Thermal Breakdown Model for Oil-Impregnated Paper. *Energies*, 2017, vol. 10, no. 12, p. 2160.
DOI: 10.3390/en10122160
5. CIGRE A2.35. Experiences in service with new insulating liquids CIGRE Working Group A2.35, 2010, no. 436, pp. 1–95. **DOI:** ISBN:978-2-85873-124-4
6. Rogalski P., Opielak M. The effect of reduced pressure on the bubble effect in the composite cellulose-insulation oil-water nanodrops. *In Proceedings Advanced Topics in Optoelectronics, Microelectronics, and Nanotechnologies IX*, 2019, vol. 10977, 130 p.
DOI: 10.1117/12.2324860
7. Rogalski P. Optical registration of transformer oil absorption processes in electrical pressboard nanocapillaries. *In Proc. Spie 10010, Advanced Topics in Optoelectronics, Microelectronics, and Nanotechnologies VIII*, 2016, vol. 10010, pp. 100101R-1-100101R-8.
DOI: 10.1117/12.2243269
8. Rogalski P., Okal P. Optical registration of the vacuum impregnation process of electrotechnical pressboard by transformer oil. *In Proc. Spie 10445, Photonics Applications in Astronomy, Communications, Industry, and High Energy Physics Experiments*, 2017, vol. 10445, pp. 104455E-1-104455E-7.
DOI: 10.1117/12.2281033
9. Rogalski P., Kozak C., Lebedynskyi I. Statistical analysis of transformer oil penetration speed through electrotechnical pressboard. *In Proc. IEEE 7th International Conference Nanomaterials: Application & Properties (NAP)*, 2017, pp. 02MAN11-1-02MAN11-4.
DOI: 10.1109/NAP.2017.8190356
10. Rogalski P., Zukowski P., Korenciak D. Determination of nanocapillaries radii statistical distribution in electrotechnical pressboard. *In Proceedings of SPIE – The International Society for Optical Engineering*, 2018, vol. 10808.
DOI: 10.1117/12.2501462
11. Moser H.P., Dahinden V., Brechna H. Transformerboard II: properties and application of Transformerboard of different fibres. Zürich: Weidmann AG, 1987.

About Possibility of Remote Diagnostics of the Respiratory System by Auscultation

E.G. Zaitseva, M.V. Chernetsky, N.A. Shevel

Belarusian National Technical University,
Nezavisimosty Ave., 65, Minsk 220013, Belarus

Received 13.01.2020

Accepted for publication 09.04.2020

Abstract

Development of technical base, software, accumulated information on the diagnosis of the respiratory system provided the prerequisites for creating remote diagnostics of the human respiratory system through auscultation. The known methods do not solve the problem of determining auscultation points at patient's housing without a diagnostic specialist. The purpose of this study is to develop a method for remote diagnostics of the respiratory system which provides ability to determine the points of auscultation without presence of a diagnostic specialist.

The definition of auscultation points is provided using a computer program that allows to calculate the points' coordinates based on the coordinates of points that determine the anatomical structure of the patient's torso. The patient or his assistant places the recording device at the auscultation points combining their images on the display with the image of the location of the recording device. The signal recorded at the auscultation point is remotely transmitted to a specialist for direct analysis and/or computer processing. The diagnostic module consists of two main units. The first unit contains a stethoscope, microphone, and amplifier connected to a mobile phone or other similar device containing an accelerometer. The patient or his assistant at the housing uses the unit. The second unit is a mobile phone with a mechanical marker or a computer with the ability to access the network in conjunction with the necessary software and is used remotely by a diagnostic specialist. The layout of the unit for recording and transmitting breath sounds was made. To avoid discrepancies in the diagnostic results the technical characteristics of the module elements must be normalized. Unified software is required for the module to function. The organizational tasks that need to be solved for the implementation of diagnostics are formulated.

Use of the method of remote diagnostics of the respiratory system, providing the ability to determine points of auscultation without the direct presence of a diagnostic specialist and the module will allow increasing efficiency of treatment of pulmonary diseases reduce infection risks and economic costs.

Keywords: remote medical diagnostics, human respiratory system, auscultation points, diagnostic module.

DOI: 10.21122/2220-9506-2020-11-2-148-154

Адрес для переписки:

Е.Г. Зайцева
Белорусский национальный технический университет,
пр-т Независимости, 65, г. Минск 220013, Беларусь
e-mail: egzaytseva@bntu.by

Address for correspondence:

E. G. Zaitseva
Belarusian National Technical University,
Nezavisimosty Ave., 65, Minsk 220013, Belarus
e-mail: egzaytseva@bntu.by

Для цитирования:

E.G. Zaitseva, M.V. Chernetsky, N.A. Shevel.
About Possibility of Remote Diagnostics of the Respiratory System by Auscultation.
Приборы и методы измерений.
2020. – Т. 11, № 2. – С. 148–154.
DOI: 10.21122/2220-9506-2020-11-2-148-154

For citation:

E.G. Zaitseva, M.V. Chernetsky, N.A. Shevel.
About Possibility of Remote Diagnostics of the Respiratory System by Auscultation.
Devices and Methods of Measurements.
2020, vol. 11, no. 2, pp. 148–154.
DOI: 10.21122/2220-9506-2020-11-2-148-154

УДК 616.24-008.4

О возможности дистанционной диагностики дыхательной системы человека методом аускультации

Е.Г. Зайцева, М.В. Чернецкий, Н.А. Шевель

Белорусский национальный технический университет,
пр-т Независимости, 65, г. Минск 220013, Беларусь

Поступила 13.01.2020

Принята к печати 09.04.2020

Развитие технической базы, программного обеспечения, а также накопленная информация по диагностике дыхательной системы обеспечили предпосылки для создания дистанционной диагностики дыхательной системы человека посредством аускультации. В известных методиках не решена проблема определения точек аускультации в домашних условиях без присутствия специалиста по диагностике. Целью настоящего исследования является разработка методики дистанционной диагностики дыхательной системы, обеспечивающая возможность определения точек аускультации без присутствия специалиста по диагностике.

Для этого предусмотрено определение точек аускультации с использованием компьютерной программы, позволяющей вычислить их координаты на основе координат точек, определяющих анатомическое строение торса пациента. Пациент или его помощник устанавливают записывающее устройство в точки аускультации, совмещая на дисплее их изображения с изображением точки нахождения записывающего устройства. Записываемый в точке аускультации сигнал дистанционно передаётся специалисту для непосредственного анализа и/или компьютерной обработки. Диагностический модуль состоит из двух основных узлов. Первый содержит стетоскоп, микрофон и усилитель, соединённые с мобильным телефоном или другим аналогичным устройством, содержащим акселерометр. Узел используется пациентом или его помощником в домашних условиях. Второй узел представляет мобильный телефон с механическим маркером либо компьютер с возможностью выхода в сеть в совокупности с необходимым программным обеспечением и используется дистанционно специалистом по диагностике. Изготовлен макет узла записи и передачи звуков дыхания. Чтобы избежать расхождения результатов диагностики, технические характеристики элементов модуля необходимо нормировать. Для функционирования модуля требуется унифицированное программное обеспечение. Сформулированы организационные задачи, которые необходимо решить для внедрения диагностики.

Использование разработанной методики дистанционной диагностики дыхательной системы, обеспечивающей возможность определения точек аускультации без присутствия специалиста по диагностике и соответствующего модуля позволит увеличить эффективность лечения пульмонологических заболеваний, уменьшить риски инфицирования и экономические затраты.

Ключевые слова: дистанционная медицинская диагностика, дыхательная система человека, точки аускультации, диагностический модуль.

DOI: 10.21122/2220-9506-2020-11-2-148-154

Адрес для переписки:

Е.Г. Зайцева

Белорусский национальный технический университет,
пр-т Независимости, 65, г. Минск 220013, Беларусь
e-mail: egzaitseva@bntu.by

Address for correspondence:

E.G. Zaitseva

Belarusian National Technical University,
Nezavisimosty Ave., 65, Minsk 220013, Belarus
e-mail: egzaitseva@bntu.by

Для цитирования:

E.G. Zaitseva, M.V. Chernetsky, N.A. Shevel.

About Possibility of Remote Diagnostics of the Respiratory System by Auscultation.

Приборы и методы измерений.

2020. – Т. 11, № 2. – С. 148–154.

DOI: 10.21122/2220-9506-2020-11-2-148-154

For citation:

E.G. Zaitseva, M.V. Chernetsky, N.A. Shevel.

About Possibility of Remote Diagnostics of the Respiratory System by Auscultation.

Devices and Methods of Measurements.

2020, vol. 11, no. 2, pp. 148–154.

DOI: 10.21122/2220-9506-2020-11-2-148-154

Introduction

Traditional methods of medical diagnostics require direct contact of the patient with a specialist and, in most cases, a visit to a medical institution. In order to carry out primary diagnostics faster, an alternative strategy is the introduction of telemedicine and mobile medicine which has already been successfully used in a number of countries [1–6]. Remote diagnostics has a number of advantages over traditional methods. Firstly, increase the efficiency of the disease detection at early stage and also effective and timely treatment. There are no need to transport patients to a medical facility, contact between patients and medical personnel in a medical facility, and thus decreasing the risk of mutual infection and spread of infection with all consequences of these. In addition, there is an opportunity to save money, as the number of home visits to patients, the time of patient care, and the cost of servicing premises in medical institutions are reduced. Federal law No. 242 of July 29, 2017 "On amendments to certain legislative acts of the Russian Federation on the use of information technologies in the field of health protection" comes into force in the Russian Federation on January 1, 2018. It provides possibility of medical care using telemedicine technologies through consultations as well as remote medical monitoring of the patient's health [1].

The profile of medical module for remote diagnostics is determined by the parameters of the body system to be monitored. For example, methods of remote monitoring of the cardiovascular system are already known and widely used since the procedure for measuring blood pressure (BP) is quite simple and can be performed independently at home [6]. Remote blood Pressure monitoring is based on a computer system that automatically sends patients requests for blood Pressure levels in the form of mobile phone text messages. Data on the blood Pressure level received from patients via text messages are saved in the system, automatically processed, and the physician makes the therapy correction if necessary based on the information received.

Remote diagnostics of the respiratory system is a more complex task. Traditional non-invasive method for diagnosing the respiratory system is auscultation which on the one hand is particularly effective in the early stages of the disease, on the other hand creates prerequisites for computer processing of diagnostic results [7]. The usual auscultation procedure

requires highly qualified and experienced specialist [8]. Description of airway sounds, their classification and standardization [9, 10] created opportunities for moving to their computer analysis [11, 12]. There are technical devices that allow to directly convert the sounds of breathing into a digital signal, and it is possible to simultaneously record an acoustic signal at many points on the surface of the chest [12], and sequential recording [13]. From the above, it follows that based on the existing equipment and software it is possible to create a module for remote diagnostics of the human respiratory system. At the same time, analysis of these sources shows that the problem of determining auscultation points on the chest surface is not solved without the direct presence of a diagnostic specialist, that is, the patient or his assistant cannot find these points themselves.

The purpose of this study is to develop a method for remote diagnostics of the respiratory system, which provides the ability to determine the points of auscultation without the direct presence of a diagnostic specialist. Creating an appropriate module requires solving a number of problems. First, it is necessary to ensure that the patient or his assistant can independently determine the position of auscultation points at home. Secondly, it is necessary to ensure the availability of the appropriate technical base and software. Using the module will speed up the diagnosis process and, increase the effectiveness of treatment of pulmonological diseases due to their detection at earlier stages, prevent the risks of infection when patients contact each other and with medical staff, reduce the economic costs associated with the need to move patients and staff for their contact during the diagnosis process.

The structure of the diagnostic module and the algorithm of remote diagnostics

The developed method provides determining of the primary points of auscultation using a computer program that allows to calculate the coordinates of these points based on the coordinates of the points that determine the anatomical structure of the patient's torso (here in after – the base points). The patient or his assistant determines the coordinates of the base points by installing a coordinate detection device on them in accordance with the program instructions. Based on the processing of the coordinates of the base points images of auscultation points are generated on the display. The patient or his assistant places the recording device at the auscultation points

combining their images on the display with the image of the location of the recording device. The signal recorded at the auscultation point is remotely transmitted to a specialist for direct analysis and/or computer processing in order to establish a diagnosis. If it is necessary to clarify the diagnosis the patient or his assistant receives information from a remotely located specialist about the location of additional

auscultation points, after which the recording and analysis procedure is repeated.

The method of remote diagnostics of the respiratory system without the direct presence of a diagnostic specialist for determining the points of auscultation can be implemented on the basis of the module the scheme of which is shown in Figure.

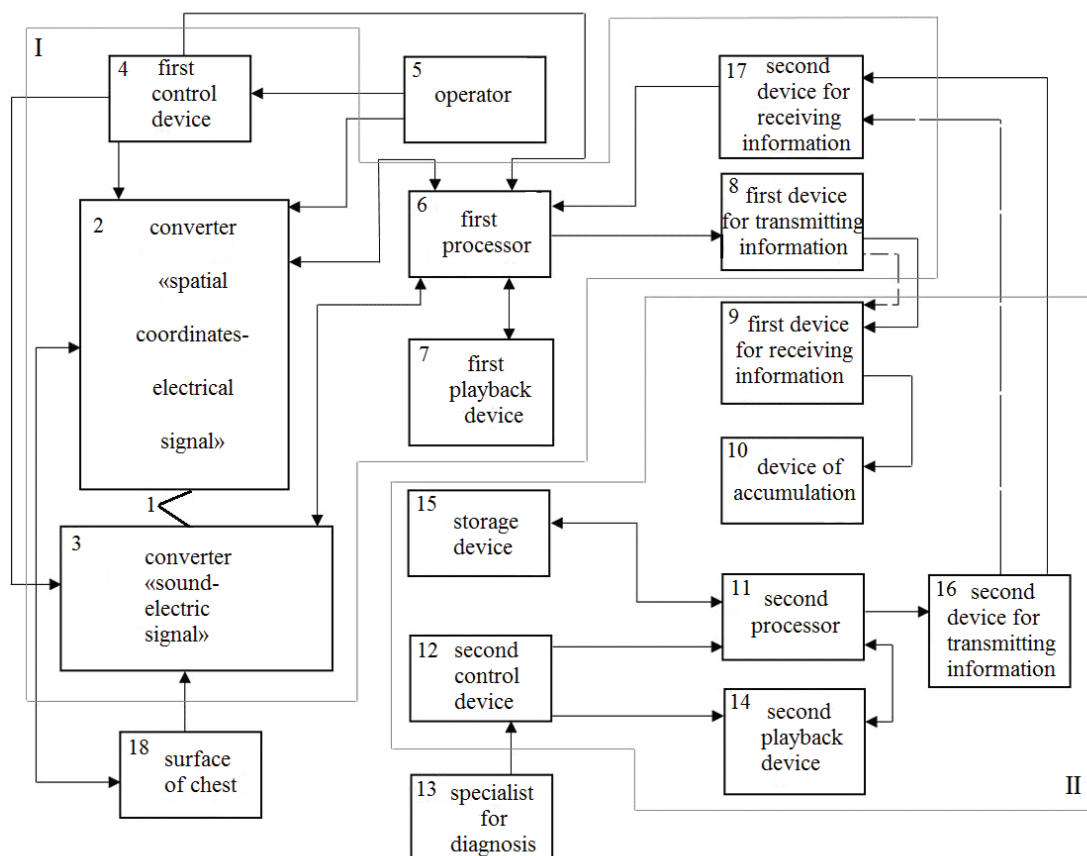


Figure – Scheme of the module for remote diagnostics of the respiratory system by auscultation method

The module contains a unit 1 consisting of two connected elements: the converter 2 "spatial coordinates of the object – an electric signal", and the converter 3 "sound – an electric signal". The first converter uses the accelerometer of a mobile phone or other device in combination with the appropriate software and the second one uses a stethoscope, microphone, and amplifier. Connection of the converters should provide an unconditional dependence between the spatial coordinates of the stethoscope and the mobile device with the accelerometer.

The presence of an accelerometer in unit 1 allows to perform the first, most problematic stage

of diagnosis – to set the position of the auscultation points on the surface of the chest in absence of a diagnostic specialist. To do this through the first control device 4 on the mobile phone, the operator 5 (the patient or his assistant) must initiate the corresponding program in the first processor 6 placed in the mobile device and determine the coordinates of the base points for a specific patient. When the program is initiated the first playback device 7 (phone display) displays an image of a person's torso with marked base points. At the same time the image of the point that determines the position of the stethoscope (hereinafter referred to as the stethoscope point) is displayed there.

When the operator 5 moves unit 1 along the torso surface the coordinates of the stethoscope point are determined based on the twice-integrated accelerometer signal and the image of the stethoscope point is moved on the display in accordance with these coordinates. Operator 5 moves the block 1 along the torso surface until the display combines the images of the stethoscope point with the image of one of the base points. This means that the coordinates of the base point on the torso coincide with the coordinates of the stethoscope point after which the coordinates of the current base point are fixed. After combining all the base points with the stethoscope point the first processor 6 calculates the coordinates of the auscultation points (points on the surface of the chest where it is necessary to record breath sounds) based on information about the coordinates of the base points of the torso that determine its geometric parameters.

The second stage of diagnostics is the primary recording of breath sounds at auscultation points by the operator 5 and their remote transmission through the first information transmission device 8 for analysis and listening. As part of this step the first processor 6 creates images of auscultation points on the phone's display, whose spatial coordinates have been calculated for a specific patient. At the same time the image of the stethoscope point is displayed on this display. The operator must move the stethoscope along the chest surface until the images on the display match the stethoscope point and one of the auscultation points. After that it initiates the recording of breath sounds at this auscultation point in different breathing modes through the first control device 4 and transmits the recorded signal for listening and analysis. The specified operation is repeated for each auscultation point.

All the elements necessary for performing the above operations can be structurally combined into one common unit I based on a stethoscope and a mobile phone. To implement the method a layout of the node for recording and transmitting breath sounds was created. The "sound – electric signal" converter used a combination of a phonendoscope with a microphone which was connected via an amplifier to a mobile phone that had a built-in accelerometer.

Listening to and analyzing recorded breath sounds are performed remotely by a specialist. Depending on the method of organization of diagnostics this function can be performed in a public or private medical institution and if possible, it is advisable to provide for the possibility of rapid communication between the patient and the spe-

cialist. For technical support of the subsequent stages of diagnostics a mobile phone with a mechanical marker or a computer with the ability to access the network in conjunction with the necessary software can be used (unit II in Figure).

During the third stage of diagnostics parameters of the recorded signal are compared with the normal values and a decision is made about further operations. The signal is sent to the first information receiving device 9 (see Figure) contained in the phone or computer then it is directed to the accumulation device 10, from there – to the second processor 11. Through the second control device 12 the diagnostics specialist 13 initiates the broadcast of the recorded breath sounds through the second playback device 14 and listens to them. Simultaneously in the processor 11 using the appropriate software the parameters of the audio signals are calculated and compared with normal values received from the storage device 15. After analyzing the audio information and the results of computer comparison of parameters with the norm the specialist can make three possible decisions:

- If the specialist makes a decision about the compliance of the breathing sounds with the norm, then through the second control device 12 he proceeds to the fourth stage of diagnostics. He remotely sends the results of listening, comparing parameters, recommendations for further actions and, if necessary, additional information via the second device 16 for transmitting information, via the second device 17 for receiving information to the operator on the first processor 6. The processor generates information on the first playback device 7 (phone display).

- In case of deviation of breath sounds from the norm based on the results of listening by a specialist and/or deviation of their parameters from the norm during computer comparison, two options for further actions are possible. If the specialist decides to formulate a decision on further necessary actions based on the information already received then the fourth stage is repeated. If the specialist needs additional information, i.e. analysis of breath sounds in additional auscultation points that have not yet been analyzed, then he initiates the fifth stage of diagnostics through the second control device 12. In this case, the second playback device 14 generates images of additional points to be analyzed selected depending on the specific nature of deviations from the norm. The position of these points can be determined by the appropriate software, if necessary, the specialist changes the position of these points on the second playback device 14 (its

display) through a device 12 for controlling of a mechanical or electronic marker. Then, through the second processor 11, the transmission device 16 and the second reception device 17, the first processor 6, the information is sent to the first playback device 7 (phone display). The operator repeats the second stage of diagnostics for the additional points indicated on the display after which the third and fourth stages are repeated for these points.

The diagnostic results at the final stage should be entered both in the patient's electronic chart and in the General statistical database.

To implement the remote diagnostics module for the human respiratory system it is necessary to solve a number of technical and organizational problems. First, experimental testing of the method is necessary for which the specialist must simultaneously perform auscultation using traditional and remote methods. Based on the expert's opinion a decision is made on the prospects and/or need to improve the method.

Since the parameters of breath sounds are determined by the technical characteristics of the nodes used they must be normalized within the framework of this technique to avoid discrepancies in the results. The same applies to software. A review of the sources showed that a large amount of information on classification, standardization and computer analysis of breath sounds has been accumulated from which it is necessary to reasonably select or additionally create a unified software for the module. Specifically, the necessary programs include: a program for determining the coordinates of base points, a program for determining the coordinates of auscultation points by base points, a program for calculating and comparing the parameters of the breath sound with normal values, a program for selecting the coordinates of additional auscultation points depending on the specific nature of deviations of breath sounds from the norm, and auxiliary programs for moving to the next stages of diagnostics. In addition, it is necessary to ensure the possibility of transmitting the received data to the patient card and statistical database.

To solve these problems a number of organizational measures are necessary. First, the use of remote diagnostics must have a legal basis. Secondly, the interaction of physicians, engineers, and programmers to create a remote diagnostics module for the respiratory system should be carried out within the framework of organized groups that have legal and material support. The effectiveness

of the introduction of remote diagnostics provides for the organization of training to work with this technique both on the part of specialists and on the part of patients and their relatives. In addition for preventive purposes, regular repetition of the diagnostic procedure is required which also requires certain organizational measures on a legal basis.

Conclusion

A method has been developed for remote diagnostics of the respiratory system, providing the ability to determine auscultation points without the presence of a diagnostic specialist. Using this technique will increase the effectiveness of treatment of pulmonological diseases; reduce the risks of infection and economic costs. The structure of the corresponding module is proposed. A part of the module was made in the form of a unit for recording and transmitting breath sounds. The technical and organizational tasks that need to be solved for the implementation of the proposed diagnostics of the respiratory system are formulated.

References

1. Lemesko V.A., Teptsova T.S. [Telemedicine: healthcare takes a step into the future]. *Meditsinskaya tehnologiya. Ocenka i otbor* [Medical technologies. Evaluation and selection], 2017, no. 4(30), pp. 30–38 (in Russian).
2. Vladzimirsky A.V., Lebedev G.S. Telemedicine. Moscow: GEOTAR-Media Publ., 2018, 576 p.
3. Le V.N. [Mechanism of output of diagnostic solution in remote medical expert system of preliminary diagnostics]. *Kibernetika i programmirovaniye* [Cybernetics and programming], 2015, no. 1, pp. 16–26 (in Russian). DOI: 10.7256/2306-4196.2015.1.13722
4. Shilko S.V., Kuzminsky Yu.G., Borisenko M.V. [Biomechanical diagnostics of hemodynamics of the cardiovascular system]. *Innovacionnye aspekty sovremennoj mediciny: Monogr. v 2-h chastyah* [Innovative aspects of modern medicine: Monogr. in 2 parts. SibAK]; edited by Volkov V.P. Novosibirsk, 2014. Part II, pp. 11–41 (in Russian).
5. Boytsov S.A. [Realities and prospects of remote monitoring of arterial pressure in patients with arterial hypertension]. *Terapevticheskij arhiv* [Therapeutic archive], 2018, no. 1, pp. 4–8 (in Russian).
6. Posnenkova O.M., Korotin A.S., Kiselev A.R., Gridnev V.I. [Evaluation of the effectiveness of remote monitoring of blood pressure in patients with arterial hypertension on the basis of indicators of implementation of clinical recommendations]. *Kachestvo v kardiologii*

[Quality in cardiology], 2015, no. 2, pp 1–5 (in Russian).
DOI: 10.15275/cardioit.2015.0203

7. Dyachenko A.I., Mikhailovskaya A.N. [Respiratory acoustics (review)]. *Trudy Instituta obshhej fiziki RAN. A.M. Prokhorov, Rossijskaya akademiya nauk* [Proceedings of the Institute of General physics. A.M. Prokhorov, Russian Academy of Sciences], 2012, vol. 68, pp. 136–181 (in Russian).

8. Cottin V., Cordier J.-F. Velcro crackles: the key for early diagnosis of idiopathic pulmonary fibrosis? *European Respiratory Journal*, 2012, vol. 40, no. 3, pp. 519–521. **DOI:** 10.1183/09031936.00001612

9. Melbye H., Garcia-Marcos L., Brand P., Everard M., Priftis K., Pasterkamp H. Wheezes, crackles, rhonchi: agreement among members of the ERS task force on lung sounds. *European Respiratory Journal*, 2014, vol. 44: Suppl. 58, pp. 4004. **DOI:** 10.13140/2.1.3359.8405

10. Pasterkamp H., Brand P., Everard M., Garcia-Marcos L., Melbye H., Priftis K. Towards the stan-

dardisation of lung sound nomenclature. *European Respiratory Journal*, 2016, vol. 47, pp. 724–732.

DOI: 10.1183/13993003.01132-2015

11. Gorbachev S.V. [Improving the accuracy of recognition of bronchopulmonary diseases based on phase-time analysis of bronchophonograms]. *Trudy vysshih uchebnyh zavedenij. Fizika* [Proceedings of higher educational institutions. Physics], 2013, vol. 56, no. 10/2, pp. 18–24 (in Russian).

12. Kushnir I., Botbol M. System for analysis and imaging of airway noise: patent RU 2 314 751, IPC A 61 B 5/08, 10/00, 7/00, 7/02; applicant DILBRIZ LTD (IL). No. 2004124247/14, declared. 12.01.2003, publ. 20.01.2008, buell. no. 7 (in Russian).

13. Uskov A.I., Yampolsky I.I. Electronic stethoscope: patent RU 182368, IPC A61B 7/04; applicant Public joint Stock company plant "Red banner" (RU). No. 2017145290, application. 22.12.2017, publ. 15.08.2018, buell. no. 23 (in Russian).

УДК 536.51:681.5.015.3

Реализация спектрального метода определения динамических характеристик средств измерений

А.Ф. Сабитов, И.А. Сафина

Казанский национальный исследовательский технический университет
имени А.Н. Туполева – КАИ,
ул. К. Маркса, 10, г. Казань 420111, Россия

Поступила 13.01.2020

Принята к печати 25.05.2020

Основным требованием спектрального метода определения динамических характеристик средств измерений (СИ) является установление амплитудного спектра сигнала в его информативной части, включающей значение амплитудного спектра на нулевой частоте. Существующие низкочастотные анализаторы спектра имеют рабочий диапазон частот, лежащий выше нулевой частоты, что приводит к погрешности определения динамических характеристик СИ спектральным методом. Целью данной работы являлась разработка программы вычисления амплитудного спектра сигналов, начиная от нулевой частоты, для реализации спектрального метода определения динамических характеристик СИ на компьютерах, оснащённых математическим пакетом *MatLab*.

Для реализации спектрального метода определения динамических характеристик средств измерений разработана программа в среде *MatLab* 2013b, позволяющая определять амплитудный спектр сигнала от нуля герц. В программе заложено считывание исходных данных из таблиц в формате *Excel* и представление вычисленного амплитудного спектра в виде диаграммы и таблицы отчётов.

Показано, что разработанная программа вычисляет амплитудный спектр сигналов со средним квадратическим отклонением не более 3,4 % на интервале частот от 0 до 10 рад/с. Вычисленный амплитудный спектр позволяет определять постоянную времени апериодических средств измерений первого порядка с погрешностью не более 0,166 % при любом уровне помех, если их частоты находятся за пределами информационной части спектра.

На примере высокочастотной помехи в переходной характеристике некоторых средств измерений продемонстрировано заявляемое преимущество спектрального метода определения динамических характеристик с использованием разработанной программы.

Ключевые слова: амплитудный спектр, динамические характеристики, средства измерений.

DOI: 10.21122/2220-9506-2020-11-2-155-162

Адрес для переписки:

А.Ф. Сабитов
Казанский национальный исследовательский технический
университет им. А.Н. Туполева – КАИ,
ул. К. Маркса, 10, г. Казань 420111, Россия
e-mail: alfir-sabitov@yandex.ru

Address for correspondence:

A.F. Sabitov
A.N. Tupolev Kazan National Research Technical University,
K. Marx str., 10, Kazan 420111, Tatarstan, Russia
e-mail: alfir-sabitov@yandex.ru

Для цитирования:

А.Ф. Сабитов, И.А. Сафина.
Реализация спектрального метода определения динамических
характеристик средств измерений.
Приборы и методы измерений.
2020. – Т. 11, № 2. – С. 155–162.
DOI: 10.21122/2220-9506-2020-11-2-155-162

For citation:

A.F. Sabitov, I.A. Safina.
[Implementation of the Spectral Method for Determining
of Measuring Instruments' Dynamic Characteristics].
Devices and Methods of Measurements.
2020, vol. 11, no. 2, pp. 155–162 (in Russian).
DOI: 10.21122/2220-9506-2020-11-2-155-162

Implementation of the Spectral Method for Determining of Measuring Instruments' Dynamic Characteristics

A.F. Sabitov, I.A. Safina

A.N. Tupolev Kazan National Research Technical University,
K. Marx str., 10, Kazan 420111, Russia

Received 13.01.2020

Accepted for publication 25.05.2020

Abstract

The spectral method for establishing dynamic response of measuring instruments basically requires determining the amplitude spectrum of the signal in its informative part that includes the amplitude spectrum at zero frequency. The operating frequency range of existing low-frequency spectrum analyzers is above zero frequency that leads to an uncertainty in dynamic response of measuring instruments determined by the spectral method. The purpose of this paper is to develop a program for calculating the signal amplitude spectrum, starting from zero frequency, to implement a spectral method for determining the dynamic response of measuring instruments on computers equipped with the *MatLab* package.

To implement the spectral method for determining the dynamic response of measuring instruments, we developed a program in the *MatLab* 2013b environment that determines the signal amplitude spectrum from zero Hertz. The program reads the source data from *Excel* tables and presents the calculated amplitude spectrum as a chart and a report table.

It is shown that the developed program calculates the signal amplitude spectrum with a standard deviation of not more than 3.4 % in the frequency range of 0 to 10 rad/s. The calculated amplitude spectrum allows determining the time constant of first-order aperiodic measuring instruments with an uncertainty of not more than 0.166 % at any noise level, if their frequencies are outside the information part of the spectrum.

We demonstrated the claimed advantage of the spectral method for determining dynamic response using the developed program by the example of a high-frequency noise in the transient response of some measuring instruments.

Keywords: amplitude spectrum, dynamic characteristics, measuring instruments.

DOI: 10.21122/2220-9506-2020-11-2-155-162

Адрес для переписки:

А.Ф. Сабитов
Казанский национальный исследовательский технический
университет им. А.Н. Туполева – КАИ,
ул. К. Маркса, 10, г. Казань 420111, Россия
e-mail: alfir-sabitov@yandex.ru

Address for correspondence:

A.F. Sabitov
A.N. Tupolev Kazan National Research Technical University,
K. Marx str., 10, Kazan 420111, Tatarstan, Russia
e-mail: alfir-sabitov@yandex.ru

Для цитирования:

А.Ф. Сабитов, И.А. Сафина.
Реализация спектрального метода определения динамических
характеристик средств измерений.
Приборы и методы измерений.
2020. – Т. 11, № 2. – С. 155–162.
DOI: 10.21122/2220-9506-2020-11-2-155-162

For citation:

A.F. Sabitov, I.A. Safina.
[Implementation of the Spectral Method for Determining
of Measuring Instruments' Dynamic Characteristics].
Devices and Methods of Measurements.
2020, vol. 11, no. 2, pp. 155–162 (in Russian).
DOI: 10.21122/2220-9506-2020-11-2-155-162

Введение

Несмотря на большое число известных методов определения динамических характеристик средств измерений продолжают работы по созданию новых и более совершенных алгоритмов и программ их определения [1–3].

Существует также достаточно большое число СИ, у которых динамические характеристики определяются исключительно или предпочтительно по экспериментальным переходным характеристикам. Примерами таких СИ являются погружаемые датчики температур жидких и газообразных потоков, у которых переходная характеристика регистрируется при перемещении из среды с одной температурой в подвижную среду с другой температурой [4–9]. При определении динамических характеристик по подобным экспериментальным переходным характеристикам возникают проблемы учёта содержащихся в них помех различной природы. Как известно, любая фильтрация помех с помощью различных методов и средств приводит к потере части полезного сигнала, что снижает точность определения динамических характеристик. Одним из методов определения динамических характеристик СИ по переходным характеристикам с помехами высокого уровня является спектральный метод, предложенный в работе [10]. Данный метод не направлен на уменьшение или подавление помех, а предлагает установить амплитудный спектр сигнала $s(\tau)$, сформированного из экспериментальной переходной характеристики СИ по приведённым в работе правилам. Определение же динамических характеристик предлагается производить по информативной части амплитудного спектра, лежащей в диапазоне частот от 0 рад/с до ω_b , где ω_b – верхняя частота информативной части. В работе [10] также показано, что если помехи даже высокого уровня находятся выше частоты ω_b , то они не оказывают существенного влияния на точность определения динамических характеристик СИ.

Для реализации спектрального метода требуется определить амплитудный спектр сигнала $s(\tau)$ в диапазоне частот от нуля герц (от нуля рад/с) и, по крайней мере, до ω_b . Как известно, амплитудные спектры сигналов можно определять с помощью соответствующих измерительных приборов – анализаторов спектра. Изучение существующих низкочастотных анализаторов спектра показало, их рабочий диапазон анали-

зируемых частот не начинается от нуля герц. Конкретное значение нижней границы рабочего диапазона анализируемых частот зависит от конкретного типа анализатора спектра и приводится в их технических характеристиках. Большинство низкочастотных анализаторов спектра имеют рабочий диапазон частот от 10 Гц. Небольшое число анализаторов спектра имеют более низкую границу диапазона частот. Так, например, у низкочастотного анализатора спектра типа *NF-XFR* фирмы *GOSSEN-METRAWATT* нижнее значение частотного диапазона равно 1 Гц. Использование подобных анализаторов спектра приведёт к погрешности определения динамических характеристик СИ спектральным методом, величина которой будет зависеть от их конкретного рабочего диапазона анализируемых частот.

На рисунке 1 представлен пример, когда рабочий диапазон частот анализатора спектра начинается от 0,1 Гц (от 0,628 рад/с) и частично перекрывает информационную часть амплитудного спектра некоторого СИ, у которого $\omega_b = 3$ рад/с.

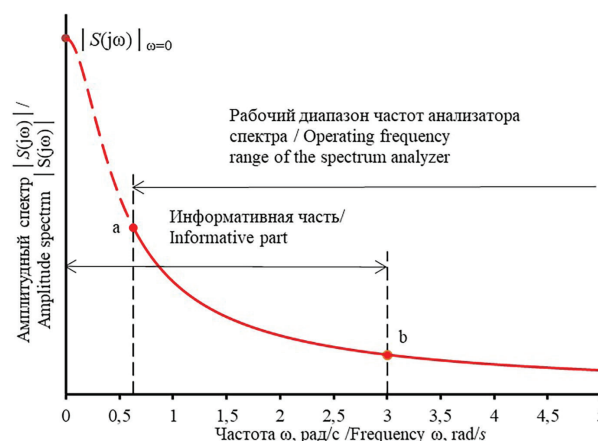


Рисунок 1 – Пример определения амплитудного спектра некоторого СИ анализатором спектра

Figure 1 – Example of determining the amplitude spectrum of a certain SI using spectrum analyzer

Как видно из рисунка 1, данный анализатор спектра определит амплитудный спектр в диапазоне частот, лежащих выше 0,628 рад/с. Таким образом, для определения динамических характеристик данного СИ спектральным методом доступен участок амплитудного спектра, лежащий между точками «а» и «b». Использование этого участка амплитудного спектра, а не всей информативной части, может привести к существенным погрешностям определения искомых динамических характеристик СИ. Следует отметить,

что величина амплитудного спектра на нулевой частоте имеет важное значение для реализации регрессионного анализа по определению иско- мых динамических характеристик СИ, поскольку она определяет постоянную составляющую ана- лизируемого сигнала.

Как следует из работы [10], значения ампли- тудных спектров на нулевой частоте для первых трёх динамических моделей СИ имеют следую- щий вид:

– для модели 1:

$$|S(j\omega)|_{\omega=0} = U_m T;$$

– для модели 2:

$$|S(j\omega)|_{\omega=0} = U_m (T_1 + T_2 - E);$$

– для модели 3:

$$|S(j\omega)|_{\omega=0} = U_m (T_1 + T_2 + T_3 - E_1 - E_2),$$

где U_m – амплитуда сигнала $s(\tau)$ при $\tau = 0$ с; $T, T_1, T_2, T_3, E, E_1, E_2$ – постоянные времени моделей в секундах.

Таким образом, исследователям при ис- пользование анализаторах спектра потребуется дополнительно оценивать влияние на точность определения динамических характеристик СИ спектральным методом результатов вычисле- ния амплитудного спектра конкретными при- борами.

Другим вариантом использования спек- трального метода определения динамических характеристик СИ может быть применение вы- числительных программ, лишённых указанно- го недостатка низкочастотных анализаторов спектра. Целью данной работы являлась раз- работка программы вычисления амплитудного спектра сигналов, начиная от нулевой частоты, для реализации спектрального метода опреде- ления динамических характеристик СИ на ком- пьютерах, оснащённых математическим паке- том *MatLab*.

Основная часть

При разработке программы вычисления ам- плитудного спектра, необходимого для реализа- ции спектрального метода определения динами- ческих характеристик СИ, ставились следующие задачи:

– разработать программу в математическом пакете *MatLab*, доступном широкому кругу ис- следователей;

– создать достаточно точную вычислитель- ную программу, обеспечивающую вычисление амплитудного спектра от 0 Гц;

– использовать исходную информацию об экспериментальной переходной характери- стике, представленной в виде таблицы отсчётов «время – сигнал», в формате таблиц *Excel*;

– в процессе работы программы наблюдать графики исходного сигнала и амплитудного спектра;

– видеть числовые значения амплитудного спектра;

– сохранять полученные значения амплитуд- ного спектра в формате таблиц *Excel*.

Реализация спектрального метода определе- ния динамических характеристик СИ с привлече- нием вычислительной программы в математиче- ском пакете *MatLab* содержит следующие основ- ные процедуры.

1. Из экспериментальной переходной ха- рактеристики исследуемого СИ формируется дискретный сигнал $s(\tau)$, состоящий из N точек, по правилам, приведённым в работе [10]. При этом время дискретных отсчётов Δt должно удовлетворять практическому применению тео- ремы Котельникова.

2. Вычисляется быстрое преобразование Фурье $S(n)$ по N точкам с использованием функ- ции *fft* в пакете *MatLab*.

3. Определяется верхняя граница времени T_{\max} дискретного сигнала $s(\tau)$.

4. Определяется нижняя граница времени T_{\min} дискретного сигнала $s(\tau)$. Для сигнала $s(\tau)$ $T_{\min} = 0$ с.

5. Вычисляется шаг частоты амплитудного спектра:

$$\Delta F = \frac{1}{T_{\max} - T_{\min}}, 1/\text{с}.$$

6. Определяется количество точек N_F на по- ложительной частоте амплитудного спектра с ис- пользованием функции *length* в пакете *MatLab*.

7. Создаётся вектор частот F с шагом ΔF из N_F точек.

8. Производится пересчёт секундной частот- ы F в угловую частоту:

$$\omega = 2 \pi F, \text{ рад/с}.$$

9. Определяется количество частот M_F в пре- образовании Фурье $S(n)$ с использованием функ- ции *length* в пакете *MatLab*.

10. Рассчитывается корректирующий коэффициент:

$$k = \frac{1}{M_F \Delta F}, \text{ с.}$$

11. Выделяется из результатов преобразования амплитудный спектр $|S(j\omega)|$ с учётом корректирующего коэффициента k и использовании функции *abs* в пакете *MatLab*.

Разработанная программа позволила вычислять амплитудный спектр сигналов от 0 Гц за счёт включения в алгоритм новых процедур № 5 – № 11 по сравнению с известными программами.

Оценка точности вычисления амплитудного спектра разработанной программой произведена путём сравнения с идеальным спектром сигнала $s(\tau)$, который описывается следующим выражением:

$$|S(j\omega)|_{id} = \frac{U_m T}{\sqrt{1 + \omega^2 T^2}}. \quad (1)$$

Сигнал $s(\tau)$ соответствует преобразованной переходной характеристике некоторого СИ с передаточной функцией аperiodического звена первого порядка и имеет вид:

$$s(\tau) = U_m e^{-\tau/T},$$

где $U_m = 100^\circ\text{C}$ – амплитуда сигнала $s(\tau)$ при $\tau = 0$ с; $T = 3$ с – постоянная времени СИ.

В качестве оценки точности использовано относительное среднее квадратическое отклонение (СКО), рассчитанное по формуле:

$$\text{СКО} = 100 \sqrt{\frac{1}{N-1} \sum_{i=1}^N \frac{[|S(j\omega_i)|_{id} - |S(j\omega_i)|]^2}{|S(j\omega_i)|_{id}^2}}, \quad \%. \quad (2)$$

В работе [10] показано, что для СИ с постоянными времени от 1 до 3 с информативная часть амплитудного спектра находится примерно в диапазоне от 0 до 3 рад/с. Для оценки СКО использован диапазон частот амплитудного спектра с гарантией до 10 рад/с с числом отсчётов $N = 51$, при этом полученное значение СКО составило 3,4 %.

Для оценки точности определения динамических характеристик по амплитудным спектрам, полученным по разработанной программе, проведены исследования по двум моделям СИ, в переходных характеристиках которой содержатся помехи различного уровня с частотами, лежащими выше ω_b .

В качестве первой модели СИ выбрана его передаточная функция, соответствующая аperiodическому звену первого порядка (модель 1), вида:

$$W(p) = \frac{1}{Tp + 1},$$

а в качестве второй модели – передаточная функция, соответствующая аperiodическому звену второго порядка (модель 2):

$$W(p) = \frac{Ep + 1}{(T_1 p + 1)(T_2 p + 1)},$$

где $T = 3$ с; $T_1 = 3$ с; $T_2 = 1$ с; $E = 2$ с – тестовые постоянные времени выбранных моделей.

Преобразованные переходные характеристики моделей с помехой рассматривались в следующем виде:

– для первой модели:

$$s(\tau) = U_m e^{-\frac{\tau}{T}} + f(\tau); \quad (2)$$

– для второй модели:

$$s(\tau) = U_m \left[\frac{T_1 - E}{T_1 - T_2} e^{-\frac{\tau}{T_1}} - \frac{T_2 - E}{T_1 - T_2} e^{-\frac{\tau}{T_2}} \right] + f(\tau),$$

где U_m – амплитуда сигнала $s(\tau)$ без помехи при $\tau = 0$ с; $f(\tau)$ – помеха в зарегистрированном сигнале.

Для реализации помехи, частоты которой лежали бы выше ω_b и уходили в бесконечность, использован пилообразный сигнал, который разлагается в следующий бесконечный гармонический ряд:

$$f(\tau) = \frac{2A}{\pi} \left[\sin\left(\frac{2\pi}{\Theta}\tau\right) - \frac{1}{2}\sin\left(\frac{2 \cdot 2\pi}{\Theta}\tau\right) + \frac{1}{3}\sin\left(\frac{3 \cdot 2\pi}{\Theta}\tau\right) - \frac{1}{4}\sin\left(\frac{4 \cdot 2\pi}{\Theta}\tau\right) + \dots \right],$$

где A – амплитуда пилообразного сигнала; τ – период пилообразного сигнала, с.

Оценка точности определения динамических характеристик выбранных моделей СИ произведена при различной амплитуде A пилообразного сигнала, которая составила 0, 5, 10, 35, 40, 45, 50, 75 и 100 % от амплитуды U_m . Предположим, что выбранные модели СИ соответствуют передаточным функциям датчиков температуры, у которых $U_m = 100^\circ\text{C}$. Значение периода пилообразного сигнала выбрано равным 0,25 с, т. е. $\tau = 0,25$ с, что соответствует частоте первой гармоники ряда 25,12 рад/с (4 Гц).

Результаты определения постоянных времени моделей СИ по амплитудному спектру, вычис-

ленному по разработанной программе, приведены в таблице.

Таблица /Table

Результаты определения постоянных времени моделей по спектральному методу при наличии в переходной характеристике помехи и использовании информативной части амплитудного спектра от 0 до 3 рад/с

Results of determination of time constants of models on spectral method in the presence of interference in the transient response and use the informative part of the amplitude spectrum from 0 to 3 rad/s

A	0 %	5 %	10 %	35 %	40 %	45 %	50 %	75 %	100 %	$\delta_{\max}, \%$
T, c	3,005	3,005	3,005	3,005	3,005	3,005	3,005	3,005	3,005	0,166
T_1, c	3,019	3,019	3,019	3,021	3,022	3,022	3,023	3,025	3,026	0,867
T_2, c	1,021	1,022	1,022	1,023	1,024	1,024	1,024	1,026	1,027	2,700
E, c	2,035	2,036	2,036	2,040	2,041	2,041	2,042	2,045	2,049	2,045

Определение постоянных времени выбранных моделей по информативной части их амплитудного спектра произведено с привлечением регрессионного анализа, реализованного модулем *User-specified regression* в системе *STATISTICA*. При этом функцией регрессии для первой модели являлось следующее выражение:

$$|S(j\omega)| = \frac{U_m T}{\sqrt{1 + \omega^2 T^2}};$$

для второй модели:

$$|S(j\omega)| = U_m \sqrt{\frac{(T_1 + T_2 - E)^2 + \omega^2 T_1^2 T_2^2}{(1 + \omega^2 T_1^2)(1 + \omega^2 T_2^2)}}.$$

Из таблицы видно, что спектральный метод определяет постоянные времени модели практически одинаковыми независимо от уровней помехи. При этом значения установленных постоянных времени при различных уровнях помехи отличаются от тестовых постоянных времени для первой модели с относительной погрешностью δ_{\max} не более чем на 0,166 %, а для второй модели – не более 2,7 %. Отличие установленных постоянных времени от тестовых объясняется погрешностью вычисления амплитудного спектра разработанной программой и погрешностью использованного регрессионного анализа.

На рисунке 2 для примера представлен сигнал вида (1) при $A = 0 \%$ и $A = 50 \%$, а на рисунке 3 – вычисленный амплитудный спектр этого сигнала при $A = 50 \%$.

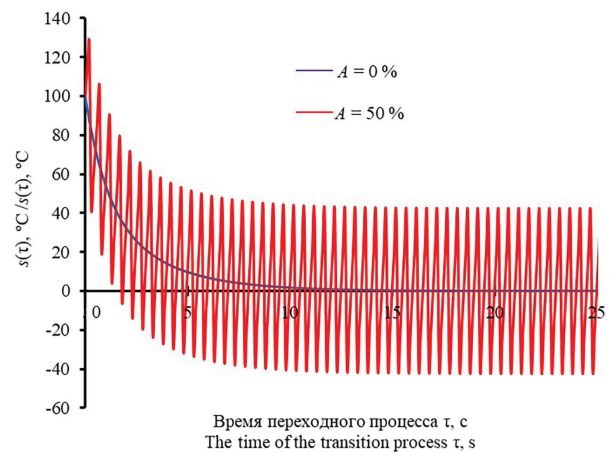


Рисунок 2 – Сигнал вида (1) при $A = 0 \%$ и $A = 50 \%$

Figure 2 – Signal of the form (1) at $A = 0 \%$ and $A = 50 \%$

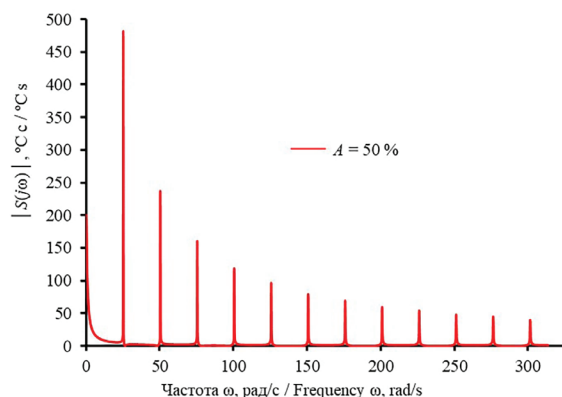


Рисунок 3 – Амплитудный спектр сигнала вида (1) при $A = 50 \%$

Figure 3 – Amplitude spectrum of the signal of the form (1) at $A = 50 \%$

Амплитудный спектр в диапазоне от 0 до 10 рад/с при $A = 50\%$ изображён на рисунке 4, где, для сравнения, изображён также график идеального амплитудного спектра без помехи, вычисленный по выражению (1).

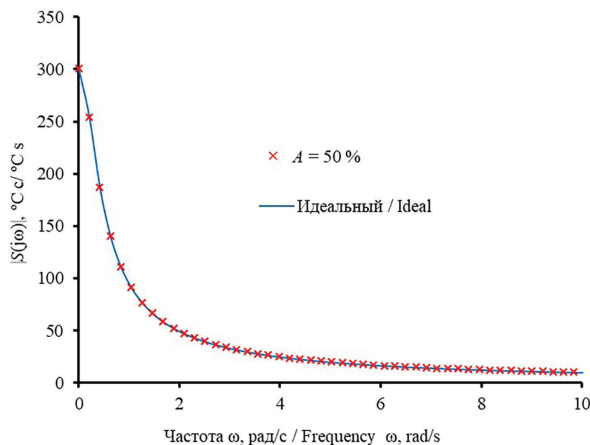


Рисунок 4 – Идеальный и вычисленный по программе амплитудные спектры сигнала $s(\tau)$ для первой модели

Figure 4 – Ideal and program-calculated amplitude spectra of signal $s(\tau)$ for the first model

Из рисунка 4 видно, что рассматриваемые амплитудные спектры практически совпадают на информативной части от 0 до 3 рад/с, что подтверждает выдвинутые в работе [10] рекомендации о её использовании для определения динамических характеристик СИ спектральным методом.

Заключение

Исследования на конкретных примерах показали, что разработанная программа позволяет вычислять амплитудные спектры сигналов с достаточно высокой точностью. Так, например, для средств измерений с постоянной времени 3 с вычисленный амплитудный спектр в диапазоне частот от 0 до 10 рад/с отличается от идеального со средним квадратическим отклонением не более чем на 3,4 %.

Вычисленные по разработанной программе амплитудные спектры также позволяют определять динамические характеристики средств измерений с вполне удовлетворительной точностью. К примеру, погрешность определения постоянной времени средств измерений, описываемого апериодическим звеном первого порядка, не превышает 0,166 %.

Разработанная программа может быть реализована на компьютерах, оснащённых математическим пакетом *MatLab*. При этом информация о сигнале, преобразованном из экспериментальной переходной характеристики, считывается программой из таблиц в формате *Excel*, что также упрощает использование данной программы.

Дальнейшие исследования будут направлены на повышение точности вычисления амплитудного спектра разработанной программой, включающей более точный алгоритм регрессионного анализа для определения искомых динамических характеристик средств измерений.

Список использованных источников

1. Бекенева, Я.А. Динамические характеристики средств измерений промышленной автоматики / Я.А. Бекенева, В.А. Комшилова, К.О. Комшилова // Известия СПбГЭТУ «ЛЭТИ». – 2013. – № 1. – С. 81–86.
2. Dubovitskii, V.F. Use of a data measurement system for studying the characteristics of temperature sensors / V.A. Dubovitskii, L.P. Sebina, M.V. Godunov, E.M. Maksimova // Fibre Chemistry. – 2011. – Vol. 42, no. 6. – P. 399–403. DOI: 10.1007/s10692-011-9297-0
3. Иосифов, В.П. Определение полных динамических характеристик средств измерений с применением рекуррентных процедур / В.П. Иосифов // Известия высших учебных заведений. Поволжский регион. Технические науки. – 2011. – № 1 (17). – С. 126–131.
4. Маршалов, Е.Д. Определение времени термической реакции термопреобразователей сопротивления / Е.Д. Маршалов, А.Н. Никоноров, И.К. Муравьев // Вестник Ивановского государственного энергетического университета. – 2017. – № 3. – С. 54–59.
5. Вавиловская, С.Л. Автоматизация определения динамических и скоростных характеристик датчиков температуры на установке воздушной УВ-010 ЦИАМ / С.Л. Вавиловская, Д.Л. Захаров, М.В. Корнеев // Автоматизация в промышленности. – 2016. – Т. 4. – С. 28–29.
6. Froehlich, T. Temperature-Dependent Dynamic Behavior of Process Temperature Sensors / T. Froehlich, S. Augustin, C. Ament // International Journal of Thermophysics. – 2015. – Vol. 36, no. 8. – P. 2115–2123. DOI: 10.1007/s10765-015-1869-4
7. Jamroz, P. Relationship between dynamic coefficients of two temperature sensors under non stationary flow conditions / P. Jamroz // IEEE Sens. J. 2011. – Vol. 11, no. 1–2. – P. 335–340. DOI: 10.1109/JSEN.2010.2073463
8. Zimmerschied, R. Nonlinear time constant estimation and dynamic compensation of temperature sensors / R. Zimmerschied, R. Isermann // Contr. Eng.

Pract. – 2010. – Vol. 18, no. 3. – P. 300–310.

DOI: 10.1016/j.conengrac.2009.11.008

9. Сафина, И.А. Идентификация номинальных динамических характеристик авиационных датчиков температуры газовых потоков / И.А. Сафина, А.Ф. Сабитов, В.И. Гаркушенко // *Авиакосмическое приборостроение*. – 2017. – № 3. – С. 3–11.

10. Сабитов, А.Ф. Идентификация динамических характеристик авиационных датчиков температуры газов / А.Ф. Сабитов, И.А. Сафина // *Приборы и методы измерений*. – 2017. – Т. 8, № 1. – С. 7–14.

DOI: 10.21122/2220-9506-2017-8-1-7-14

References

1. Bekenova Y.A., Komshilova V.A., Komshilova K.O. [Dynamic characteristics of measurements systems based on industrial automation systems]. *Izvestiya Sankt-Peterburgskogo gosudarstvennogo elektrotekhnicheskogo universiteta "LETI"*, 2013, no. 1. pp. 81–86 (in Russian).

2. Dubovitskii V.F., Sebina L.P., Godunov M.V., Maksimova E.M. Use of a data measurement system for studying the characteristics of temperature sensors. *Fibre Chemistry*, 2011, vol. 42, no. 6, pp. 399–403.

DOI: 10.1007/s10692-011-9297-0

3. Iosifov V.P. [Determination of the full dynamic characteristics of measuring instruments with the use of recurrent procedures]. *Izvestiya vysshikh uchebnykh zavdenij. Povolzhskij region. Tekhnicheskije nauki* [Proceedings of the higher educational institutions. Volga region. Technical science], 2011, no. 1 (17), pp. 126–131 (in Russian).

4. Marshalov E.D., Nikonorov A.N., Murav'ev I.K. [Determination of thermal reaction time of thermal

resistance converters]. *Vestnik Ivanovskogo gosudarstvennogo energeticheskogo universiteta* [Bulletin of Ivanovo state power engineering University], 2017, no. 3, pp. 54–59 (in Russian).

5. Vavirovskaja S.L., Zaharov D.L., Korneev M.V. [Automation determination of dynamic and high-speed characteristics of temperature sensors in the installation of air УВ-010 CIAM]. *Avtomatizacia v promyshlennosti* [Automation industry], 2016, vol. 4, pp. 28–29 (in Russian).

6. Froehlich T., Froehlich T., Augustin S., Ament C. Temperature-Dependent Dynamic Behavior of Process Temperature Sensors. *International Journal of Thermophysics*, 2015, vol. 36, no. 8, pp. 2115–2123.

DOI: 10.1007/s10765-015-1869-4

7. Jamroz P. Relationship between dynamic coefficients of two temperature sensors under non stationary flow conditions. *IEEE Sens. J.*, 2011, vol. 11, no. 1–2, pp. 335–340. **DOI:** 10.1109/JSEN.2010.2073463

8. Zimmerschied R., Isermann R. Nonlinear time constant estimation and dynamic compensation of temperature sensors. *Contr. Eng. Pract.*, 2010, vol. 18, no. 3, pp. 300–310.

DOI: 10.1016/j.conengrac.2009.11.008

9. Safina I.A., Sabitov A.F., Garkushenko V.I. [Identification of nominal dynamic characteristics gas temperature sensors of aircraft]. *Aviakosmicheskoe priborostroenie* [Aerospace instrument-making], 2017, no. 3, pp. 3–11 (in Russian).

10. Sabitov A.F., Safina I.A. [Identification of nominal dynamic characteristics gas temperature sensors]. *Pribory i metody izmerenii* [Devices and Methods of Measurements], 2016, vol. 7, no. 2, pp. 211–218 (in Russian).

DOI: 10.21122/2220-9506-2016-7-2-211-218

ПРАВИЛА ОФОРМЛЕНИЯ СТАТЕЙ

Статьи, направленные в редакцию журнала, должны удовлетворять требованиям «Инструкции о порядке оформления квалификационной научной работы (диссертации)...», утвержденной Постановлением ВАК РФ от 28.02.2014 г. № 3

1. Материал статьи должен соответствовать профилю журнала и излагаться предельно ясно.

2. Статья представляется на русском или английском языке и публикуется на языке представления.

3. Поступившие в редакцию статьи проходят двойное полуслепое рецензирование. Основные критерии целесообразности опубликования – актуальность тематики, информативность, научная новизна.

4. Статья представляется в распечатанном и в электронном виде в формате текстового редактора Word for Windows. Объем статьи не должен превышать 14 страниц, включая текст (шрифт Times New Roman, размер 12 п., интервал 1,5), таблицы, графический материал, всю необходимую информацию на английском языке.

5. На первой странице статьи указываются: индекс УДК, название статьи, фамилии авторов (фамилия автора, с которым следует вести переписку, отмечается звездочкой и указывается его адрес электронной почты), названия и почтовые адреса организаций (улица, номер дома, индекс, город, страна), в которых работают авторы, на русском и английском языках. Статья включает: аннотацию (в пределах 200–250 слов); ключевые слова (не более 5); введение, в котором делается краткий обзор сделанного в мире и конкретно формулируется цель работы; основную часть; заключение, в котором в сжатом виде сформулированы основные полученные результаты с указанием их новизны, преимуществ и возможностей применения; список использованных источников. Аннотация, ключевые слова, список использованных источников представляются на русском и английском языках.

6. Аннотация должна быть информативной (содержать «выжимку» из всех разделов статьи – введения с указанием цели работы, методики, основной части и заключения).

7. Графический материал должен быть контрастным и четким. Фотографии представляются в электронном виде (**формат tif, jpg, разрешение не менее 300 dpi**). Все рисунки нумеруются и сопровождаются подписными подписями. Фрагменты рисунка обозначаются строчными курсивными латинскими буквами – «a», «b» и т. д. Надписи на рисунках и подписи к рисункам даются на русском и английском языках. Все сокращения и обозначения на рисунках должны быть расшифрованы в подписной подписи. Рисунки желательно предоставлять в цвете.

8. Таблицы не должны дублировать графики. Каждая таблица имеет заголовок. На все таблицы и рисунки следует давать ссылки в тексте. Название и содержание таблиц представляется на русском и английском языках.

9. Обозначения и сокращения, принятые в статье, расшифровываются непосредственно в тексте.

10. Размерность всех величин, принятых в статье, должна соответствовать Международной системе единиц измерений (СИ).

11. Многострочные формулы должны быть набраны в редакторе MathType, номера формул – по правому краю. Нумеруются лишь формулы, на которые есть ссылки в тексте. Отдельные строчные буквы и специальные символы набираются в тексте гарнитурой Symbol **без использования редактора формул**. При наборе формул и буквенных обозначений необходимо учитывать следующие правила: **русский алфавит не используется**; греческие буквы, математические символы (grad, div, ln, min, max и др.), символы химических элементов (в т.ч. в индексе) набираются **прямо**; латинские буквы – переменные и символы физических величин (в т.ч. в индексе) набираются **курсивом**; векторы – жирным шрифтом (стрелки вверх не ставятся).

12. Список использованных источников составляется в порядке упоминания ссылок по тексту, должен содержать полные библиографические данные и приводится в конце статьи. Не рекомендуется давать ссылки на материалы конференций, статьи из электронных журналов без идентификатора DOI, учебные пособия, интернет-ресурсы. Ссылки на неопубликованные работы не допускаются. Желательно, чтобы количество ссылок было не менее 10; самоцитирование – не более 20 %.

13. Авторы на отдельной странице предоставляют о себе следующие сведения: фамилия, имя, отчество, ученая степень и звание, место работы и занимаемая должность, адрес электронной связи.

14. Статьи, излагающие результаты исследований, выполненных в учреждениях, должны иметь соответствующее разрешение на опубликование в открытой печати.

15. При необходимости в конце основного текста указываются наименование фонда, оказавшего финансовую поддержку, или уровень и наименование программы, в рамках которой выполнена работа, на русском и английском языках.

16. Авторы несут ответственность за направление в редакцию статей, ранее уже опубликованных или принятых к печати другими изданиями.

17. Статьи, не соответствующие перечисленным требованиям, к рассмотрению не принимаются и возвращаются авторам. Датой поступления считается день получения редакцией первоначального варианта текста.

18. Редакция предоставляет возможность первоочередного опубликования статей лицам, осуществляющим послевузовское обучение (аспирантура, докторантура, соискательство), в год завершения обучения; не взимает плату с авторов за опубликование научных статей; оставляет за собой право производить редакторские правки, не искажающие основное содержание статьи.

AUTHOR GUIDELINES

1. Article materials should correspond to the journal profile and be clearly written.

2. An article should be submitted in Russian or English and will be published in its original language.

3. Articles received by the Editorial Board will be reviewed by 2 specialists. The main criteria of acceptance are theme actuality, information value, and scientific novelty.

4. All materials should be submitted in two hard copies together with electronic file in the Word for Windows format (97/2000/2003). The paper should not exceed 14 pages of the typewritten text (Times New Roman, 12 points, 1.5-space).

5. The article should contain UDC number, Title (printed in capitals), Authors' names (the corresponding author name should be marked with asterisk), full Address of organization(s) in which the author(s) work, Abstract (200–250 words), Keywords (not more than 5 words), Introduction, the Text of the paper with tables, diagrams and figures (if there are any), Conclusion with clearly stated inferences, List of References, List of Symbols and Abbreviations (if it is necessary). Title, Authors' names and affiliation(s), Abstract, Keywords should be presented both in English and Russian languages.

6. The abstract should be informative (contain «squeeze» from all sections of the article – the introduction stating the purpose of the work, methods, main part and conclusion).

7. Figures should be black-and-white, represented in graphical formats tif, attached with Excel or MS Graph and added with captions. All symbols in figures should be described.

8. Tables should be placed directly in the article body. Diagrams and tables should not contain the same information. Each table should have the title. All tables, diagrams and figures should be referenced in the text.

9. Symbols and abbreviations which are used in articles should be deciphered directly in the text and also (if necessary) taken out on a separate page.

10. Dimensions of all quantities used in the article should correspond to International System of Units.

11. Formulas should be typed in MathType.

12. List of References is to be placed at the end of the article with full bibliographic information. Order of references should correspond to the order of their occurrence in the text. It is not recommended to refer to conference proceedings, papers from electronic journals without *DOI* number, textbooks, internet resources. References on unpublished works are prohibited. It is recommended to refer to not less than 10 references, self-citations – not more than 20 %/

13. The following information about every co-author should be presented: family name, first name, patronymic (or second) name (if there are any), scientific degree and title, organization and position, full address with the postal code for correspondence, office or mobile phone numbers, fax, e-mail.

14. Articles containing investigation results obtained in organizations should have a corresponding permission for publication.

15. Names of Foundations or Programs financially granted the research may be acknowledged in the end of the text.

16. Authors are responsible for submitting articles previously published or accepted by other publisher.

17. Articles not meeting the requirements of the Editorial Board would not be accepted and may be returned to the authors. The date of receipt is considered to be the day when the Editorial Board receives the author's original paper.

18. Authors conducting postgraduate (graduate studies, doctoral studies) have a priority in publishing their articles out of queue in the year of completion. Authors do not pay for publishing scientific articles. The Editorial Board can shorten and/or change the text if it does not strain the meaning of the article.

Индексы:
74835; 748352